

CHARACTERIZATION OF FIBER OPTIC EVANESCENT WAVE SENSOR FOR WATER QUALITY MONITORING



CHEAH WAN CHEN



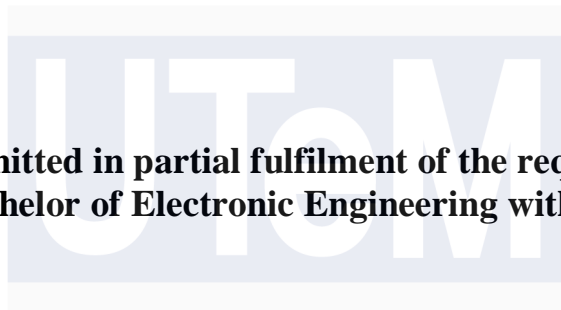
اونيورسيتي تيكنيكل مليسيا ملاك

UNIVERSITI TEKNIKAL MALAYSIA MELAKA

UNIVERSITI TEKNIKAL MALAYSIA MELAKA

CHARACTERIZATION OF FIBER OPTIC EVANESCENT WAVE SENSOR FOR WATER QUALITY MONITORING

CHEAH WAN CHEN



**This report is submitted in partial fulfilment of the requirements
for the degree of Bachelor of Electronic Engineering with Honours**

**Faculty of Electronics and Computer Technology and
Engineering
Universiti Teknikal Malaysia Melaka**

2024

BORANG PENGESAHAN STATUS LAPORAN
PROJEK SARJANA MUDA II

Tajuk Projek : **CHARACTERIZATION OF FIBER OPTIC
EVANESCENT WAVE SENSOR FOR
WATER QUALITY MONITORING**

Sesi Pengajian : 2023/2024

Saya CHEAH WAN CHEN mengaku membenarkan laporan Projek Sarjana Muda ini disimpan di Perpustakaan dengan syarat-syarat kegunaan seperti berikut:

1. Laporan adalah hakmilik Universiti Teknikal Malaysia Melaka.
2. Perpustakaan dibenarkan membuat salinan untuk tujuan pengajian sahaja.
3. Perpustakaan dibenarkan membuat salinan laporan ini sebagai bahan pertukaran antara institusi pengajian tinggi.
4. Sila tandakan (✓):

☐

SULIT*

(Mengandungi maklumat yang berdarjah keselamatan atau kepentingan Malaysia seperti yang termaktub di dalam AKTA RAHSIA RASMI 1972)

☐

TERHAD*

(Mengandungi maklumat terhad yang telah ditentukan oleh organisasi/badan di mana penyelidikan dijalankan).

☒

TIDAK TERHAD

Disahkan oleh:

(TANDATANGAN PENULIS)

(COP DAN TANDATANGAN PENYELIA)

Alamat Tetap: _____

Dr Hazura binti Haroon,
Fakulti Teknologi dan Kejuruteraan Elektronik dan Komputer (FTKEK),
Universiti Teknikal Malaysia Melaka (UTeM),
Hang Tuah Jaya,
76100, Durian Tunggal, Melaka

Tarikh : 21 June 2024

Tarikh : 21 June 2024

DECLARATION

I declare that this report entitled “**CHARACTERIZATION OF FIBER OPTIC EVANESCENT WAVE SENSOR FOR WATER QUALITY MONITORING**” is the result of my own work except for quotes as cited in the references.

اونيورسيتي تېكنيكل مليسيا ملاك
UNIVERSITI TEKNIKAL MALAYSIA MELAKA

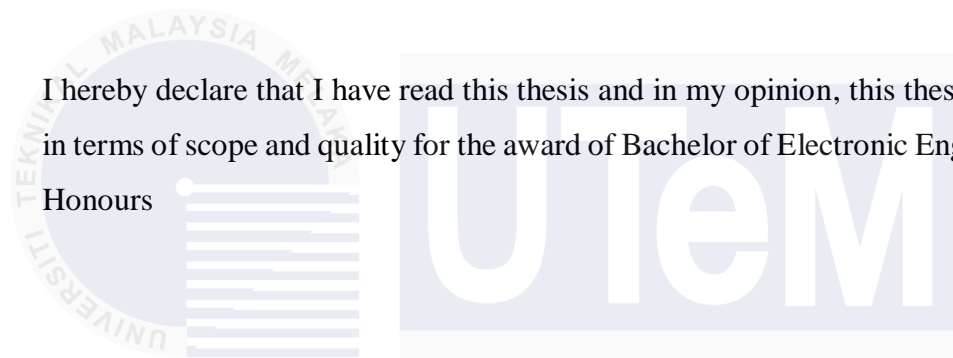
Signature :

Author :CHEAH WAN CHEN.....

Date :21 June 2024.....

APPROVAL

I hereby declare that I have read this thesis and in my opinion, this thesis is sufficient in terms of scope and quality for the award of Bachelor of Electronic Engineering with Honours



Signature :

UNIVERSITI TEKNIKAL MALAYSIA MELAKA

Supervisor Name : Dr Hazura binti Haroon,
Fakulti Teknologi dan Kejuruteraan Elektronik dan Komputer (FTKEK),
Universiti Teknikal Malaysia Melaka (UTeM),
Hang Tuah Jaya,
76100, Durian Tunggal, Melaka

Date :21 June 2024.....

DEDICATION

The completion of this thesis would not have been possible without the help and guidance of many individuals. First and foremost, I extend my heartfelt gratitude to my supervisor, Dr. Hazura binti Haroon, for her unwavering support, motivation, enthusiasm, and vast knowledge. Her dedicated involvement at every step of this project has been invaluable, and this paper would not have been accomplished without her assistance. I could not have asked for a better supervisor for my final year project.

From the bottom of my heart, I am profoundly grateful to my beloved parents and friends, for their endless support and spiritual encouragement throughout my final year project journey. This thesis stands as a testament to your unconditional love and encouragement. Lastly, I extend my sincere thanks to Universiti Teknikal Malaysia Melaka for providing me with the opportunity to pursue my studies and successfully complete my final year project.

ABSTRACT

In this project, an evanescent wave fibre-optic sensor for detecting water quality is proposed and studied experimentally. The fiber is set up by tapered manually using a polishing method to a diameter of 0.6 mm and coated with zinc oxide (ZnO) nanorods. This project technique is divided into two parts: optical characterization and electrical characterization. The light source meter, POF sensor, and Output Power Meter are used in the Optical Characterization section to evaluate the water quality by measuring the output power loss of the water sample. The receiver circuit is built for the Electrical Characterization to sense the output voltage variation to the water quality level of the water sample. From this project, the experimental results revealed that the sensor has linear relationship with ammonia concentration ranging from 1 mg/L to 1.8 mg/L and pH levels ranging from 5 to 9. It has been found that the concentration is proportionally related to its refractive index where high refractive index will experience greater loss since the light rays tend to be refracted out of the fiber instead of being internally reflected. Upon completion, the highest sensitivity and linearity was achieved by fiber optic sensor with coated ZnO, with $0.0128 \text{ V/mg L}^{-1}$ and linearity 0.9861 for concentration of ammonia measurement, with 0.0419 V/pH and linearity 0.9887 for pH level measurements.

ABSTRAK

Dalam projek ini, penderia gentian optik gelombang evanescent untuk mengesan kualiti air dicadangkan dan dikaji secara eksperimen. Gentian disediakan secara tirus secara manual menggunakan kaedah penggilap hingga diameter 0.6 mm dan disalut dengan nanorod zink oksida (ZnO). Teknik projek ini dibahagikan kepada dua bahagian: pencirian optik dan pencirian elektrik. Penderia POF dan Meter Kuasa Output digunakan dalam bahagian Pencirian Optik untuk menilai kualiti air dengan mengukur kehilangan kuasa keluaran sampel air. Litar penerima dibina untuk Pencirian Elektrik untuk mengesan variasi voltan keluaran kepada tahap kualiti air sampel air. Daripada projek ini, keputusan eksperimen mendedahkan bahawa sensor mempunyai hubungan linear dengan kepekatan ammonia antara 1 mg/L hingga 1.8 mg/L dan tahap pH antara 5 hingga 9. Telah didapati bahawa kepekatan adalah berkadar berkadar dengan biasannya. Indeks di mana indeks biasan tinggi akan mengalami kehilangan yang lebih besar kerana sinaran cahaya cenderung dibiaskan keluar daripada gentian dan bukannya dipantulkan secara dalaman. Setelah selesai, kepekaan dan kelinearan tertinggi dicapai oleh sensor gentian optik dengan ZnO bersalut, dengan $0.0128 \text{ V/mgL}^{-1}$ dan kelinearan 0.9861 untuk kepekatan pengukuran ammonia, dengan 0.0419 V/pH dan kelinearan 0.9887 untuk pengukuran tahap pH.

ACKNOWLEDGEMENTS

I would like to express my deepest gratitude to all those who supported me throughout the journey of completing my Final Year Project (FYP). First and foremost, I would like to thank my supervisor, DR HAZURA BINTI HAROON, for their invaluable guidance, continuous support, and insightful feedback. Their expertise and encouragement were crucial in shaping the direction and outcome of this project.

Without her patience and dedication, this work would not have been possible.

We also extend our appreciation to the members of Photonics Engineering Research Group for supporting me and the use of laboratory equipment and materials for this project. I am also grateful for their collaboration, constructive discussions, and for providing a stimulating environment that facilitated our research. The mutual support we shared was vital in overcoming the challenges we faced.

Finally, our heartfelt thanks go to my families and friends for their unwavering support and understanding during the demanding phases of this project. Their encouragement kept us motivated and focused, and their sacrifices did not go unnoticed. Special thanks to my parents for their emotional support and belief in our capabilities.

TABLE OF CONTENTS

Declaration	
Approval	
Dedication	
Abstract	i
Abstrak	ii
Acknowledgements	iii
Table of Contents	iv
List of Figures	xiii
List of Tables	xvii
List of Symbols and Abbreviations	xviii
List of Appendices	xviii
CHAPTER 1 INTRODUCTION	1
1.1 Research Background	2
1.2 Problem Statement	3
1.3 Objectives	5
1.4 Scope of Work	5

1.4.1	Fiber Optic Evanescent Wave Sensor	5
1.4.2	NodeMCU ESP8266	6
1.4.3	IoT Cloud Server	6
CHAPTER 2 BACKGROUND STUDY		8
2.1	Fiber Optic Sensor	9
2.2	Polymer Optical Fiber	11
2.3	Types of Fiber Optic Sensor	13
2.3.1	Intrinsic Fiber Optic Sensor	13
2.3.2	Extrinsic Fiber Optic Sensor	14
2.3.3	Comparison of Intrinsic and Extrinsic Fiber Optic Sensor	15
2.4	Total Internal Reflection	16
2.5	Refractive Index	17
2.6	Hydrothermal Zinc Oxide Process	18
2.7	Zinc Oxide Coating	20
2.8	IF-D918 Photodiode	21
2.9	Water Quality Standards	23
2.10	Significant Result of Previous Study	25

2.11	Summary of Chapter 2	35
------	----------------------	----

CHAPTER 3 METHODOLOGY	36
------------------------------	-----------

3.0	Flowchart	37
-----	-----------	----

3.1	Technical Design	38
-----	------------------	----

3.2	Component Used for Project	39
-----	----------------------------	----

3.2.1	NodeMCU Module ESP8266	39
-------	------------------------	----

3.2.2	16x2 Crystal LCD Display Monitor	42
-------	----------------------------------	----

3.2.3	I2C LCD 16x2 Module	44
-------	---------------------	----

3.2.4	POF Sensor	46
-------	------------	----

3.2.5	Receiver Circuit and Op-Amp IC LT1884	46
-------	---------------------------------------	----

3.2.6	Potentiometer Variable Resistor	47
-------	---------------------------------	----

3.3	Hardware Development	48
-----	----------------------	----

3.3.1	Receiver Circuit and Operation	53
-------	--------------------------------	----

3.4	Software Development	54
-----	----------------------	----

3.4.1	Project's Coding operating	58
-------	----------------------------	----

3.5	Prototype Design and Project Testing	61
-----	--------------------------------------	----

3.6	Fiber Optic Preparation	62
-----	-------------------------	----

3.6.1	Uncladding the POF Jacket	62
3.6.2	Tapered the POF	63
3.6.3	Hydrothermal Zinc Oxide Method	64
3.6.3.1	Seeding Process and Core Treatment	64
3.6.3.2	Dipping & Annealing Process	68
3.6.3.3	Growth Process	69
3.7	Optical Characterization	71
3.7.1	Refractive Index of Water Samples	71
3.7.2	Optic Output Power	72
3.8	Electrical Characterization	74
3.9	Summary of Chapter 3	76
CHAPTER 4 RESULTS AND DISCUSSION		77
4.0	SEM and EDX Analysis ZnO Nanorod Structure and Composition	78
4.1	Optical Characterization	79
4.1.1	Refractive Index of Water with Vary pH Levels	79
4.1.2	Refractive Index of Water with Vary Concentration Ammonia	81
4.1.3	Optical Output Power	83

4.1.4	Output Power of Water Sample with Vary Concentration of Ammonia (Uncoated and Coated POF)	83
4.1.5	Output Power of Water Sample with Vary pH Levels (Uncoated and Coated POF)	87
4.2	Electrical Characterization	90
4.2.1	Output Voltage of Water Samples with Vary Concentration of Ammonia (Uncoated and Coated POF)	90
4.2.2	Output Voltage of Water Samples with Vary pH Levels (Uncoated and Coated POF)	93
4.3	Sensitivity and Linearity between uncoated POF and coated POF	96
4.3.1	Sensitivity and Linearity of Uncoated and Coated ZnO POF with Vary Concentration of Ammonia	97
4.3.2	Sensitivity of Uncoated and Coated ZnO POF with Vary pH Levels	100
4.4	Importance of Zinc oxide in Sensitivity of POF	102
4.5	Adoptability of Glass Fiber Optic	104
4.6	Comparative with Previous Study	104
4.6.1	Comparison of Previous Developments for Detection of Concentration Ammonia in Water Samples	105

4.6.2	Comparison of Previous Developments for Detection pH Levels in Water Samples	106
-------	--	-----

4.7	Summary of Chapter 4	108
-----	----------------------	-----

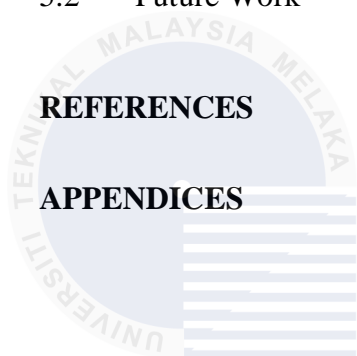
CHAPTER 5	CONCLUSION AND FUTURE WORKS	109
------------------	------------------------------------	------------

5.1	Conclusion	110
-----	------------	-----

5.2	Future Work	113
-----	-------------	-----

	REFERENCES	115
--	-------------------	------------

	APPENDICES	121
--	-------------------	------------



اونيورسيتي تېكنيكل مليسيا ملاك

UNIVERSITI TEKNIKAL MALAYSIA MELAKA

LIST OF FIGURES

Figure 1.1: Block diagram of scope of work	7
Figure 2.1: Optical Fiber Sensor	9
Figure 2.2: Fiber optic overview	12
Figure 2.3: Basic Structure of POF	12
Figure 2.4: Intrinsic FOEW sensors	13
Figure 2.5: Extrinsic FOEW sensors	14
Figure 2.6: Propagation of Light in POF	15
Figure 2.7: Hydrothermal Zinc Oxide Process	20
Figure 2.8: IF-D91B Photodiode	22
Figure 2.9: Department of Environment (DOE)	23
Figure 2.10: Water quality standards for Malaysia	24
Figure 3.0: Flowchart for overall project	37
Figure 3.1: Block diagram of project	38
Figure 3.2: NodeMCU Module ESP8266	39
Figure 3.3: GPIO of NodeMCU Module ESP 8266	40
Figure 3.4: Crystal LCD Display Monitor	43
Figure 3.5: I2C LCD 16x2 Module	44
Figure 3.6: Lcd Screen & I2C Module connection	45

Figure 3.7: POF Sensor	46
Figure 3.8: Op-Amp IC LT1884 and pin layout	47
Figure 3.9: 10M ohms Resistor	46
Figure 3.10: PCB Board	48
Figure 3.11: Schematic design	49
Figure 3.12: 3D visual of circuit design	50
Figure 3.13: Printing Bottom Layer	50
Figure 3.14: Remove copper with chloride solution	51
Figure 3.15: Check continuity with multimeter	52
Figure 3.16: Drill hole and solder all components	52
Figure 3.17: Receiver Circuit	53
Figure 3.18: IOT template selection	55
Figure 3.19: Virtual pin declaration	56
Figure 3.20: IOT web dashboard setup	56
Figure 3.21: Device's creation & information	57
Figure 3.22: IoT widget displayed on smartphone	57
Figure 3.23: Testing of circuit	62
Figure 3.24: 4cm Unclad jacket of POF	62
Figure 3.25: Digital microscope view of tapered POF	63
Figure 3.26: Measurement of tapered POF using digital micrometer screw gauge	64
Figure 3.27: Step process for Seeding process	65
Figure 3.28: Treated Core of POF	65
Figure 3.29: Zinc oxide nanoparticle solution preparation	66
Figure 3.30: pH control solution preparation	67
Figure 3.31: Seeding solution preparation	67

Figure 3.32: Dipping process for the hydrothermal method	68
Figure 3.33: Annealing process	69
Figure 3.34: 4cm expose fiber with zinc oxide coated	70
Figure 3.35: Fiber with zinc oxide coated	70
Figure 3.36: The RI measurement of water samples	72
Figure 3.37: Measurement of output power of the water samples	73
Figure 3.38: Electrical Characterization experiment	75
Figure 4.1: Scanning Electron Microscope (SEM) Image of ZnO on POF	78
Figure 4.2: EDX elemental analysis of ZnO on POF	79
Figure 4.3: The graph of Refractive Index against pH value	81
Figure 4.4: The graph of Refractive Index against Concentration of Ammonia	83
Figure 4.5: The graph of Output Power against Concentration of Ammonia (Uncoated) .	86
Figure 4.6: The graph of Output Power against Concentration of Ammonia (Coated) .	86
Figure 4.7: The graph of Output Power against PH Levels (Uncoated)	89
Figure 4.8: The graph of Output Power against PH Levels (Coated)	89
Figure 4.9: The graph of Output Voltage against Concentration of Ammonia (Uncoated)	92
Figure 4.10: The graph of Output Voltage against Concentration of Ammonia (Coated) .	93
Figure 4.11: The graph of Output Voltage against PH levels (Uncoated)	95
Figure 4.12: The graph of Output Voltage against PH levels (Coated)	96
Figure 4.13: Sensitivity and Linearity of Uncoated and Coated ZnO POF with Vary Concentration of Ammonia	99
Figure 4.14: Sensitivity and Linearity of Uncoated and Coated ZnO POF with Vary PH Levels	102
Figure 5.1: FOEW sensors based on multiple detection mechanisms	114

LIST OF TABLES

Table 2.1: Comparison of Intrinsic & Extrinsic FOEW sensors	15
Table 2.2: Example of material and refractive index measurements	18
Table 2.3: Significant result of previous study	25
Table 3.1: GPIO of NodeMCU ESP 8266	42
Table 4.1: pH values and Refractive Index	80
Table 4.2: Concentration of Ammonia and Refractive Index	82
Table 4.3: Concentration of Ammonia and Output Power (Uncoated and Coated)	84
Table 4.4: PH Levels and Output Power (Uncoated and Coated)	87
Table 4.5: Concentration of Ammonia and Output Voltage (Uncoated and Coated)	91
Table 4.6: PH Levels and Output Voltage (Uncoated and Coated)	94
Table 4.7: Sensitivity and Linearity of Uncoated and Coated ZnO POF with Vary Concentration of Ammonia	99
Table 4.8: Sensitivity and Linearity of Uncoated and Coated ZnO POF with Vary PH Levels	101
Table 4.9: Performance comparison of the Previous Developments for Detection of Concentration Ammonia in Water Samples	106
Table 4.10: Performance comparison of the Previous Developments for Detection of PH Levels in Water Samples	107

LIST OF SYMBOLS AND ABBREVIATIONS

For examples:

POF : Plastic Optical Fiber

ZnO : Zinc Oxide

UCPOF : Unclad Plastic Optical Fiber

IoT : Internet of Thing

TIR : Total Internal Reflection

OPM : Optical Power Meter

EMI : Electromagnetic Interference

LED : Light Emitting Diode

NaOH : Sodium Hydroxide

$\text{Zn}(\text{O}_2\text{CCH}_3)_2 \cdot 2\text{H}_2\text{O}$: Zinc Acetate

$\text{CH}_2)_6\text{N}_4$: Hexamethylenetetramine

PMMA : Polymethyl methacrylate

SEM : Scanning Electron Microscope Image

EDX : Energy dispersive X-ray analysis

LIST OF APPENDICES

Appendix A: LT1884 Lab Sheet

121



CHAPTER 1



This first chapter introduces the background of fiber optic displacement sensor development, particularly for the detection of water quality. It includes an introduction, a problem statement, an objective, and a description of the scope of the work.

1.1 Research Background

Water is one the most important components of any ecosystem. All living organisms need water to grow and survive. Nowadays, water pollution has become a global issue affecting most countries in the world [1]. Water quality should be monitored to alert authorities to water pollution, so that action can be taken quickly. Water quality monitoring plays a crucial role in safeguarding both the environment and public health. Traditional methods for water quality assessment often involve time-consuming and costly procedures [2]. In response to this challenge, the "Characterization of Fiber-Optic Evanescent Wave Sensor for Water Quality Monitoring" project is an innovative research initiative aimed at developing and evaluating a novel sensor technology for monitoring water quality. The project combines the advantages of fiber-optic technology and evanescent wave sensing to create a highly sensitive and versatile system for detecting a wide range of water contaminants and pollutants. Fiber-optic evanescent wave (FOEW) sensors are promising in pollutant detection and evaluation of water quality because of their high resistance to corrosion, smart structure, anti-electromagnetic interference, and low cost.

Since their early use nearly four decades ago, the world of network communication has been changed by fiber optics. The application has been rapidly increases such as in telecommunication, computer networking, medical, chemical, and so on [3]. Fiber optic is a technology that conveys a light beam along a thin fiber consisting of glass or silica core. To contain the light beam within the core, it is surrounded with cladding which has a higher refractive index thus the beam would experience total internal reflection. Then it was discovered that fiber optic has the capability to be used as a

sensor since optical properties such as transmittance, absorbance and refractive index can be manipulated to show for example, a difference in solution concentration [4].

Therefore, this project will focus on the development of a water quality monitoring system for measuring various water samples using the coated and uncoated polymer optic fiber (POF). The method is used to determine whether coating the cladding of the fiber with zinc oxide makes a difference in terms of sensitivity and accuracy. The optical properties and power output change after being dipped in various water samples are also investigated. Upon completion, it was discovered that the coated zinc oxide sensor corresponds to changes in water quality with greater sensitivity than the uncoated sensor.

1.2 Problem Statement

Water quality monitoring plays a crucial role in safeguarding both the environment and public health. However, traditional methods for assessing water quality are often labor intensive, time-consuming, and costly [9]. They frequently rely on point-sampling methods that may not accurately represent the dynamic nature of aquatic ecosystems. Furthermore, these methods can fall short in providing real-time data, impeding timely responses to water quality issues such as contamination events or the impacts of climate change [10]. Therefore, there is a pressing need for a more efficient, cost-effective, and versatile solution that can offer accurate, real-time data on multiple water quality parameters, such as organic pollutants and microbial contaminants.

Water contaminants can have various adverse effects on health. For example, exposure to bacteria and viruses in contaminated water can lead to gastrointestinal infections, causing symptoms like diarrhea and vomiting. Chemical contaminants, such as heavy metals or pesticides, may pose long-term health risks, including damage

to the nervous system, kidneys, or other organs. Consuming water with high levels of pollutants over time can contribute to a range of short-term and long-term health issues and increase the risk of diseases. Addressing these challenges is critical for effective environmental protection, sustainable resource management, and the promotion of public health. The "Characterization of Fiber-Optic Evanescent Wave Sensor for Water Quality Monitoring" project seeks to provide a solution to these pressing issues through the development and validation of an innovative sensor technology.



1.3 Objectives

The objectives of the project are as follows:

- a) To design and develop uncoated and coated Zinc Oxide polymer optical fiber (POF) sensor capable of measuring multiple water quality parameters, including PH, and Ammonia.
- b) To analyze and monitor the sensing response of the fiber-optic evanescent wave sensor towards the water quality in term of output power, output voltage and sensitivity.

1.4 Scope of Work

In this project, Fiber Optic Evanescent Wave Sensor (POF), NodeMCU ESP8266 and IoT cloud server is mainly used:

1.4.1 Fiber Optic Evanescent Wave Sensor

Fiber optic Evanescent sensor is used to measure changes in water quality. There are different light reflectance responses depending on the water quality used. The contaminant in water measured include the concentration of ammonia in water and pH level of water. The ammonia concentration in water will be monitored within the range of 1.0 to 1.8 mg/L. For pH measurement, the sensor will ensure that the water's pH value remains within the acceptable range of 5 to 9. Fiber optic cables are used for lighting and imaging and as sensors to measure and monitor a vast array of variables. It transmits a light beam along with a thin fiber. Light sensing must be done carefully by allowing no external movement or disturbance on the Polymer Optic Fiber sensor. This is because the light source is a dynamic variable which it is continuously

travelling, and it is easily to be affected by external movement which will then result in the different of refractive index. The refractive index can be determined by a refractometer. It will provide a reading that is as accurate as possible based on the light that is reflected through it. Analysis of the data and comparison to a reference value are performed. A red led will turn on and transmit an alert to the user if the water quality is hazardous. In this project, polymer optical fiber (POF) will be applied as the sensing media. The optical to electrical (O/E) converter consists of an optical amplifier and photodetector will be employed to convert the optical signal to electrical before send to the NodeMCU ESP8266.

1.4.2 NodeMCU ESP8266

NodeMCU ESP8266, which acts as microcontroller is integrated with a Wi-Fi Module, and LED to alert the nearby citizens and fiber optic sensor which detects the change of water quality. C++ language is used to code or execute algorithms. The coding for this system is compiled using the Arduino IDE software as it is very easy to build commands. NodeMCU ESP8266 is used to read data from sensors and send data to the server in real time.

1.4.3 IoT Cloud Server

IoT cloud server is an open source IoT application and API that allows to browse and compose data from devices. It enables us to collect and store sensor data in the cloud either in private or public channel and develop IoT application. The data can be analyzed and visualized by using online analytical tools. By using this IoT cloud server, may access the most recent information on the Internet via smartphone. The reading

will be measured in voltage and transform to the current water quality monitoring condition that in relation to the voltage measured.

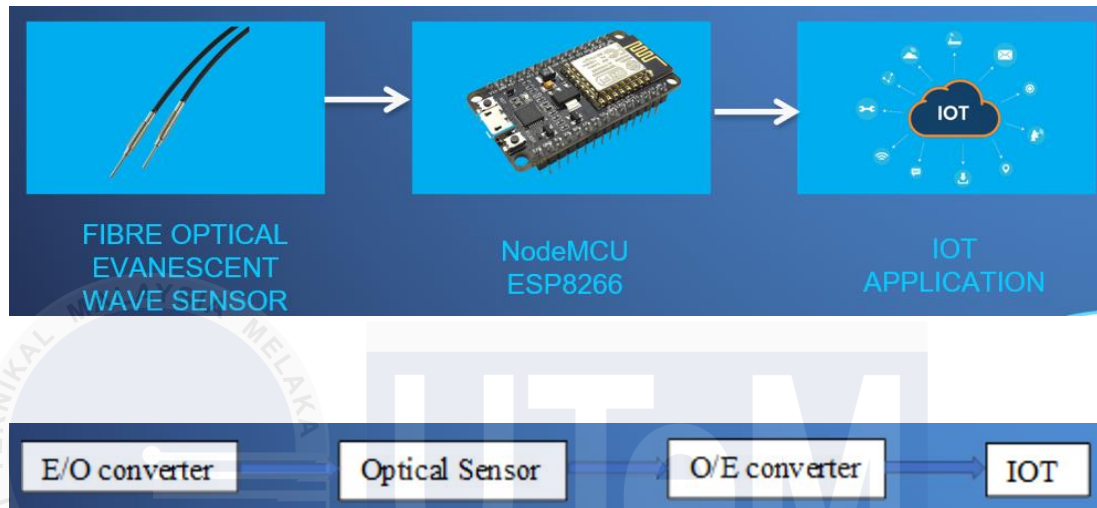


Figure 1.1: Block diagram of scope of work

CHAPTER 2

BACKGROUND STUDY



This chapter briefly describes the related research of the project. Prior study that are pertinent to this project are presented in this chapter. These studies include the theoretical underpinnings, methodology, and review of the previous studies.

2.1 Fiber Optic Sensor

Due to modern fiber optic technological advancements, the telecommunications sector has changed dramatically. The ability of optical fiber to carry gigabits of data at light speed increased their research potential. Simultaneous advances and cost savings in optoelectronic components resulted in the emergence of analogous new product categories.

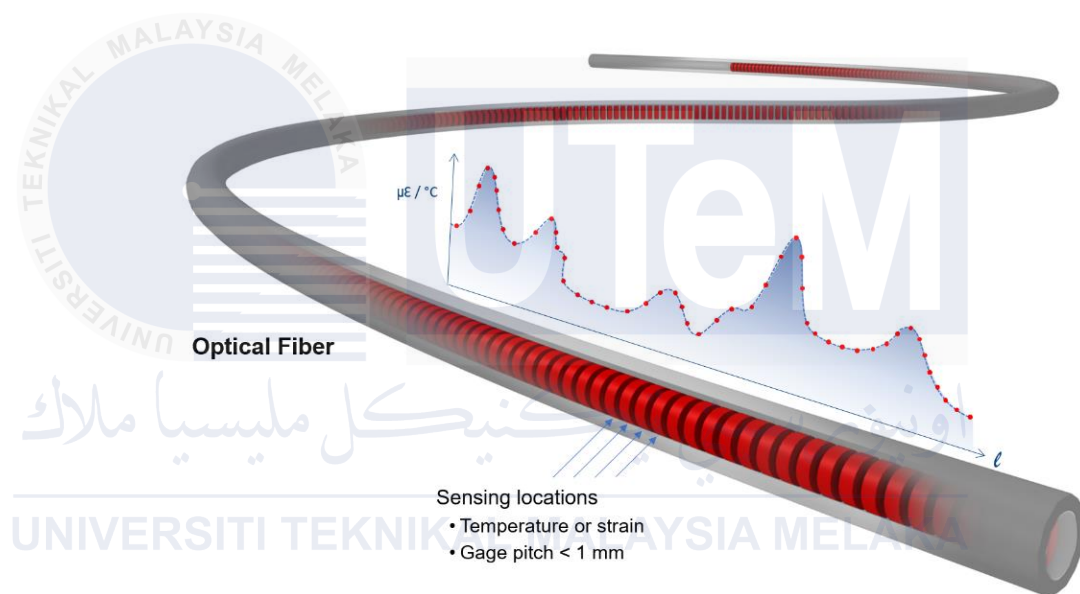


Figure 2.1: Optical Fiber Sensor

In a previous revolution, engineers combined fiber optic telecommunications product outgrowths with optoelectronic devices to create fiber optic sensors [11]. Changes in phase, intensity, and wavelength on the fiber itself could be detected as material loss decreased and sensitivity increased. As a result, a fiber optic sensor was developed.

Fiber optic technology's key advantage lies in its ability to transmit data quickly and efficiently over long distances. Higher frequency of light signal used in fiber optic facilitates substantially greater data transferring rate as compared to standard electric

signal. Fiber optic cables make it possible to transmit large amounts of information quickly due to their ability to transmit at speeds ranging from megabits to terabits per second.

Another advantage of fiber optics is its immunity to electromagnetic interference (EMI). Unlike traditional copper cables, which are susceptible to EMI, fiber optic cables are not affected by electromagnetic fields, making them highly reliable for data transmission in environments with high electrical noise or radio frequency interference.

Additionally, fiber optics offer a high level of security for data transmission. Since light signals are used instead of electrical signals, it is difficult to tap into or intercept the transmitted data. This makes fiber optic networks more secure compared to traditional copper-based networks, which are more susceptible to eavesdropping and hacking [11].

Fiber optic technology also provides a significant bandwidth advantage. The large capacity of fiber optic cables allows for the simultaneous transmission of multiple signals, including voice, video, and data, over the same fiber. This makes fiber optics ideal for multimedia applications, video conferencing, and streaming high-definition content.

In this project plastic optical fiber was used as the sensor equipment. The structure of the POF is made from plastic with the core at the center of the optical fiber. The larger core size of multimode fiber enables several light travel paths, whereas the small core size of single-mode fiber only gives a single path.

125 micrometer thick cladding retains light within the core and controls the direction of light propagation throughout the fiber. When light enters a fiber at the correct approach angle, also known as the critical angle, it reflects and remains within

the core, therefore attaining "complete internal reflection." If the angle is not quite right, the light will scatter, and the signal will be lost.

2.2 Polymer Optical Fiber

The core diameter and step-index of the commercial POF with a standard core and cladding are 1.49 and 1.41 as shown in Figure 2.3. POF is comprised of polymers, including polymethylmethacrylate (PMMA). The advantages of plastic optical fiber, commonly known as POF, are flexibility, high fracture resistance, and high sensitivity [4]. POF fiber needs to be tapered at a specified diameter in order to improve performance. Due to the tapered fiber's increased sensitivity, the evanescent wave's power inside the POF cladding will also increase. Additionally, coating the tapered portion of the POF with a sensitive substance might increase the sensor's sensitivity.

The mass market for low- priced (but tolerably less accurate) sensors is another area that POF sensor solutions are aiming towards. Due to its huge core size, high numerical aperture, flexibility, ease of handling, and reduced price, POF may also provide additional noteworthy benefits [12].



Figure 2.2: Fiber optic overview

اونيورسيتي تېكنيكل مليسيا ملاك

UNIVERSITI TEKNIKAL MALAYSIA MELAKA

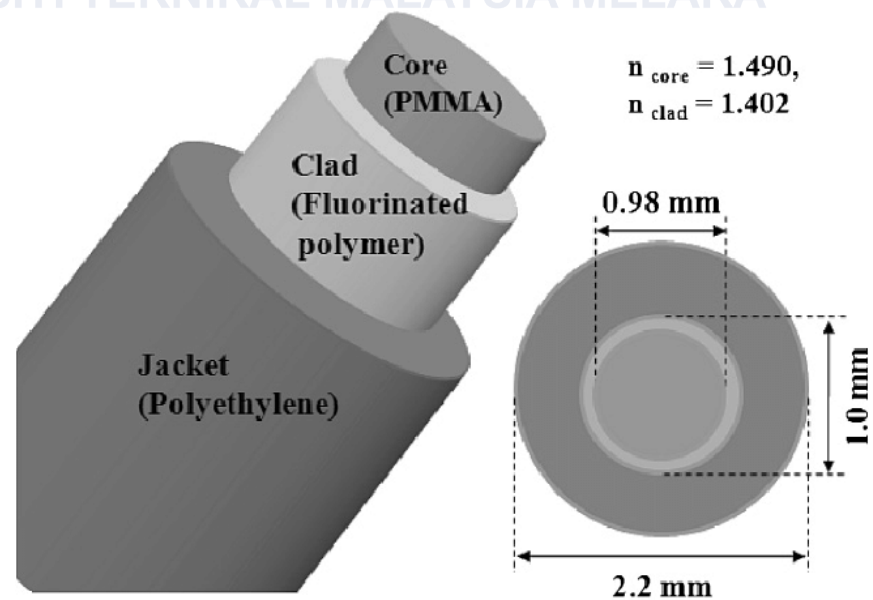


Figure 2.3: Basic Structure of POF

2.3 Types of Fiber Optic Sensor

There are two main types of fiber optic sensors: intrinsic and extrinsic:

2.3.1 Intrinsic Fiber Optic Sensor

Intrinsic FOEW sensors are based on the direct interaction of the evanescent wave with the surrounding medium. They do not require any additional coating or functional element, which makes them relatively simple to fabricate.

Intrinsic FOEW sensors are typically used to detect changes in the refractive index of the surrounding medium. The refractive index is a measure of how fast light travels through a material. Different materials have different refractive indices. For example, water has a higher refractive index than air [13].

When the refractive index of the surrounding medium changes, it affects the propagation of the evanescent wave. This change in propagation can be measured to determine the refractive index of the medium.

Intrinsic FOEW sensors are often used to measure pH, turbidity, and dissolved oxygen. They can also be used to detect specific compounds in the surrounding medium, such as heavy metals and organic pollutants.

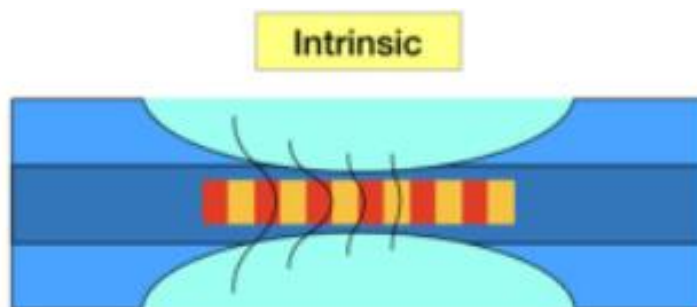


Figure 2.4: Intrinsic FOEW sensors

2.3.2 Extrinsic Fiber Optic Sensor

Extrinsic FOEW sensors use a coating or other functional element to interact with the surrounding medium and modify the evanescent wave. This coating or functional element can be used to increase the sensitivity and selectivity of the sensor.

Extrinsic FOEW sensors are typically more complex to fabricate than intrinsic sensors, but they can be more sensitive and selective. They are also more susceptible to fouling and other environmental effects [14].

Extrinsic FOEW sensors are often used to detect heavy metals, organic pollutants, and biological contaminants. They can also be used to measure pH, turbidity, and dissolved oxygen.

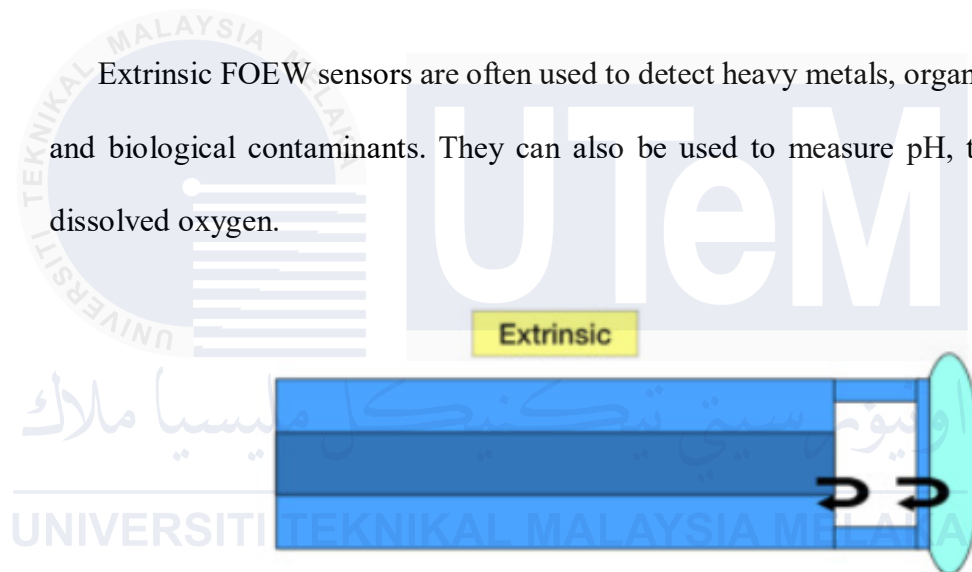


Figure 2.5: Extrinsic FOEW sensors

2.3.3 Comparison of Intrinsic and Extrinsic Fiber optic Sensors

Intrinsic and extrinsic FOEW sensors offer different advantages and disadvantages. Intrinsic sensors are simpler to fabricate and less susceptible to fouling, but they are less sensitive and selective. Extrinsic sensors are more sensitive and selective, but they are more complex to fabricate and more susceptible to fouling.

The choice of sensor type depends on the specific application. Intrinsic sensors are typically used for applications where simplicity and robustness are important. Extrinsic sensors are typically used for applications where high sensitivity and selectivity are required. The Table 2.1 compares intrinsic and extrinsic Fiber optic sensors.

Table 2.1: Comparison of Intrinsic & Extrinsic FOEW sensors

Characteristic	Intrinsic FOEW Sensors [13]	Extrinsic FOEW Sensors [14]
Fabrication	Simple	Complex
Sensitivity	Lower	Higher
Selectivity	Lower	Higher
Susceptibility to fouling	Lower	Higher
Typical applications	Measurement of pH, turbidity, and dissolved oxygen; detection of specific compounds	Detection of heavy metals, organic pollutants, and biological contaminants; measurement of pH, turbidity, and dissolved oxygen

2.4 Total Internal Reflection

Total internal reflection is used on a large scale in fiber optics. It is used to send messages in communications like the phone, the internet, and cable TV. Light can be sent through plastic or glass fibers with fiber optics.

When light moves through a thick medium and hits a boundary at a steep angle that is bigger than the boundary's critical angle, all the light is reflected as shown in Figure 2.6. The outside of the fiber must have a lower refractive index than the inside. This condition is met by coating the outside of the fiber with a substance that has a proper refractive index. So, most fibers have different refractive indices so that more light can pass through the fiber through a process called total internal reflection. This process is used to store light in the core of optical fibers. Along with the fiber, light moves in a back-and-forth rhythm against the edge. Since the light must hit the boundary at an angle greater than the critical angle, it can only go through the fiber without leaking out if it comes in at a certain range of angles. The fiber's acceptance cone is the name for this range of angles. The size of the acceptance cone is affected by the change in the refractive index between the fiber's core and its cladding. To put it simply, light enters the fiber and moves through the core when it is at its farthest point from the fiber's axis [15].

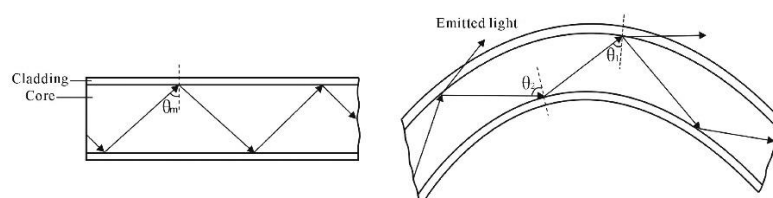


Figure 2.6: Propagation of Light in POF

Figure 2.6 shows the light flow through the fiber optic may strike a large angle on the inside surface and fully reflect between the surface and create the critical angle.

Snell's law states that the relationship between angles, θ and indices of refraction, n is given by:

$$n_1 \sin \theta_1 = n_2 \sin \theta_2 \quad Eq. (2.1)$$

When the incident angle is equal to critical angle, the angle of refraction is 90 and the Snell's Law becomes.

$$n_1 \sin \theta_1 = n_2 \quad Eq. (2.2)$$

The critical angle θ_c , for given combination of materials thus.

$$\theta_c = \sin^{-1} \left(\frac{n_2}{n_1} \right) \quad Eq. (2.3)$$

2.5 Refractive Index

The term refraction index refers to the speed at which light moves through a medium, which is dependent on the composition of the medium. The velocity of electromagnetic waves is influenced by the density of the medium in relation to light. The likelihood of atoms in a material returning absorbed electromagnetic energy is known as optical density. Objects that are less transparent tend to have slower speeds of light. The refractive index serves as an indicator of how dense light is within a given medium. Refractive indexes do not possess dimensions and measure how much slower a light wave travels through a substance compared to vacuum conditions. Symbolized by n , the refractive index is calculated by dividing the speed of light in a medium by its velocity in vacuum. n represents the refractive index, while c denotes the velocity of light in vacuum (3×10^8 m/s). v signifies the velocity of light in a substance.

$$n = \frac{c}{v} \quad Eq. (2.4)$$

The refractive index of the vacuum is 1. The equation above can be used to determine the refractive index of other materials. The optical density increases with the refractive index, slowing down the speed of light [16]. The refractive indices of various media are listed in the table below.

Table 2.2: Example of material and refractive index measurements

Material	Refractive Index
Diamond	2.417
Ethyl Alcohol	1.36
Water	1.333
Ice	1.31
Air	1.0003

2.6 Hydrothermal Zinc Oxide Process

The hydrothermal zinc oxide (ZnO) process was employed in the development of fiber optic sensors for water quality monitoring due to its distinct advantages in enhancing sensor sensitivity and reliability. ZnO's excellent optical, chemical, and physical properties make it ideal for environmental sensing applications [17]. The hydrothermal synthesis method produces high-purity, well-crystallized ZnO nanostructures at low temperatures and pressures, which is cost-effective and environmentally friendly [18]. Integrating ZnO with polymer optical fibers (POF) improves the sensor's ability to detect changes in water quality by enhancing light-water interaction and increasing sensitivity to contaminants like ammonia. The process's adaptability allows for precise control of ZnO nanostructures' properties,

optimizing sensor performance. ZnO's robustness under various conditions ensures long-term reliability, making it an ideal choice for continuous water quality monitoring and the timely detection of hazardous pollutants.

When performing this process, it is common to mix together a hydroxide and precursor solution that has compounds of Zinc Nitrate or Zinc Acetate. In order to perform mixing, one may choose between sodium and ammonium hydroxides as possible sources within a high-pressure reaction vessel. The temperature range of the mixture is increased by heating it under elevated pressures that are generally above atmospheric pressures and range from 100 to 200 degrees Celsius.

In a hydrothermal setting, where there is a lot of pressure and heat, zinc oxide crystals or nanoparticles can form and grow. The zinc precursor is broken down by water and pushed together, which starts the process and causes zinc oxide particles to form and grow.

The hydrothermal method makes it possible to control the size, form, and structure of the zinc oxide nanoparticles that are made. The characteristics of the zinc oxide that is made can be changed by changing things like the reaction temperature, reaction time, concentration of the precursors, and pH of the solution. By getting these factors just right, you can make nanoparticles with certain properties, like controlled particle size, high purity, and crystal structures.

Hydrothermal methods can be used to make nanoparticles of zinc oxide as shown in Figure 2.7. These nanoparticles can be used in many different fields, such as catalysis, sensing, optoelectronics, energy storage, and medical uses. Their unique qualities, like a high surface area, a bandgap that can be changed, and good photocatalytic activity, make them good for a wide range of technological uses. Overall, hydrothermal synthesis is a flexible and effective way to make zinc oxide

nanoparticles with qualities that can be changed. This lets them be used in many different areas of science and technology [19].

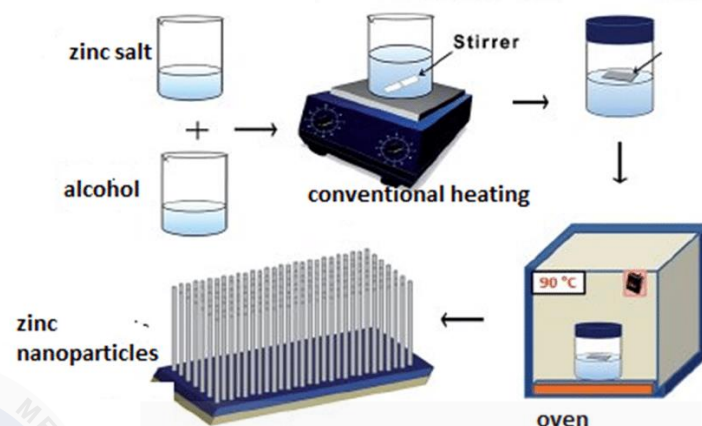


Figure 2.7: Hydrothermal Zinc Oxide Process

2.7 Zinc Oxide Coating

For centuries, zinc oxide has been utilized in traditional medicine and skin care products due to its antimicrobial and soothing qualities. Nevertheless, its usage goes beyond these applications. With advancements in technology and increased scientific knowledge, zinc oxide has made its way into various industries such as cosmetics, pharmaceuticals, electronics, textiles, and more.

One of the key characteristics of zinc oxide is its ability to function as both a semiconductor and a transparent conductor. This property has made it a crucial component in the development of optoelectronic devices such as solar cells, light-emitting diodes (LEDs), and sensors. The unique combination of transparency and electrical conductivity makes zinc oxide an ideal material for these applications.

The use of Zinc Oxide (ZnO) for the coating fiber optic is approaching in optical fiber sensors using the side coupling of light into the core modes of plastic optical fiber. The characterization of zinc oxide is crystallized. The crystallize helps to

maintain the structure of the exposed optical fiber from broken. The zinc oxide is also able to change its optical nature to the plastic optical fiber sensor to increase the sensitivity of sensing the edible oil sample characterization. To perform the zinc oxide, there is a need to use binding and seeding agents to increase the durability of ZnO coatings is expressed. In addition to functional properties, the cytotoxicity of ZnO coatings is also discussed [21]. Future directions in the use of ZnO for fiber optic sensor sensitivity are identified as well, so that in this experiment ZnO will be the best selective catalyzer to increase the sensitivity to sense the water quality [23].

2.8 IF-D91B Photodiode

In the realm of fiber optic sensing for water quality monitoring, converting the optical signals into electrical signals is a crucial step for data analysis and transmission. This conversion is achieved using an optical-to-electrical (O/E) converter, which typically consists of an optical amplifier and a photodetector. The optical amplifier boosts the light signal to ensure it can be accurately detected, while the photodetector transforms the amplified light into an electrical signal that can be processed by electronic components such as microcontrollers and data loggers. The O/E converter plays a vital role in maintaining the integrity and accuracy of the measurements, enabling the seamless integration of optical sensing technology with digital data processing systems. One of the key components in this conversion process is the photodetector, specifically the IF-D91B Photodiode as shown in Figure 2.8.

The IF-D91B is a high-speed fiber optic photodiode detector housed in a "connector-less" style plastic fiber optic package. The IF-D91B photodiode is a small but mighty marvel of optoelectronics. This unassuming device, housed in a simple plastic package, packs a powerful punch when it comes to converting light into

electrical signals. It is a general-purpose photodiode that can be used in a variety of applications, including fiber optic communications, industrial sensing, and medical diagnostics.

The IF-D91B has a wide optical response of 450 to 1100 nm, making it compatible with a wide range of visible and near-infrared LED and laser diode sources. It has a high responsivity of 0.6 A/W, which means that it produces a large electrical current for a given amount of light. The IF-D91B is also a very fast photodiode, with a rise time of less than 1 ns. This makes it suitable for use in high-speed data transmission applications [24].

One of the advantages of the IF-D91B is its low cost. It is a very affordable photodiode, making it a good choice for a wide range of applications. Another advantage of the IF-D91B is its ease of use. It is a very simple to use photodiode, and it does not require any special circuitry.

The IF-D91B is a versatile photodiode that can be used in a variety of applications. It is a good choice for fiber optic communications, industrial sensing, and medical diagnostics.



Figure 2.8: IF-D91B Photodiode

2.9 Water Quality Standard

Malaysia's water quality standards, administered by the Department of Environment (DOE) under the Ministry of Environment and Water, are vital regulatory measures aimed at maintaining the integrity of water resources. The Environmental Quality (Sewage and Industrial Effluents) Regulations 1979 and the Environmental Quality (Control of Pollution from Solid Waste Transfer Stations) Regulations 2009 establish comprehensive guidelines to address diverse environmental challenges. The standards encompass a range of physical, chemical, and biological parameters, reflecting a holistic approach to water quality management.

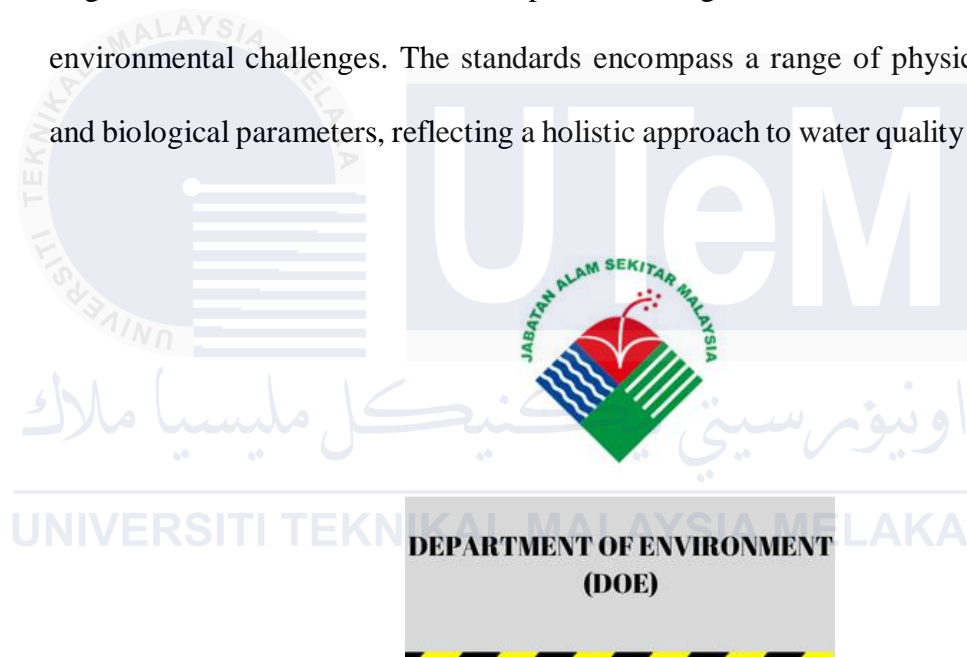


Figure 2.9: Department of Environment (DOE)

In addition to the specified limits for temperature, pH, Biochemical Oxygen Demand (BOD), Chemical Oxygen Demand (COD), Ammoniacal Nitrogen ($\text{NH}_3\text{-N}$), Total Suspended Solids (TSS), and Oil and Grease, the regulations provide stringent criteria for heavy metals. This includes maximum allowable concentrations for lead, cadmium, chromium, copper, and mercury, acknowledging the potential ecological and health risks associated with these elements. Furthermore, attention is given to

specific pollutants such as phenol and cyanide, with clearly defined limits to prevent their adverse impact on water quality.

By setting these standards, Malaysia aims to safeguard water bodies from pollution originating from industrial and sewage sources. Compliance with these regulations is essential for industries to ensure responsible environmental stewardship and to mitigate the potential consequences of water pollution on ecosystems and human health. Periodic monitoring and assessment of effluents against these standards contribute to the sustainable use and preservation of Malaysia's water resources, aligning with broader environmental conservation goals. It is imperative for stakeholders to remain informed about any updates or revisions to these standards, as part of a dynamic and adaptive approach to environmental protection and sustainable development. Figure 2.10 shown the water quality standards for Malaysia.

NATIONAL WATER QUALITY STANDARDS FOR MALAYSIA (cont.)

PARAMETER	UNIT	CLASS					
		I	IIA	IIB	III	IV	V
Ammoniacal Nitrogen	mg/l	0.1	0.3	0.3	0.9	2.7	> 2.7
Biochemical Oxygen Demand	mg/l	1	3	3	6	12	> 12
Chemical Oxygen Demand	mg/l	10	25	25	50	100	> 100
Dissolved Oxygen	mg/l	7	5 - 7	5 - 7	3 - 5	< 3	< 1
pH	-	6.5 - 8.5	6 - 9	6 - 9	5 - 9	5 - 9	-
Colour	TCU	15	150	150	-	-	-
Electrical Conductivity*	μS/cm	1000	1000	-	-	6000	-
Floatables	-	N	N	N	-	-	-
Odour	-	N	N	N	-	-	-
Salinity	ppt	0.5	1	-	-	2	-
Taste	-	N	N	N	-	-	-
Total Dissolved Solid	mg/l	500	1000	-	-	4000	-
Total Suspended Solid	mg/l	25	50	50	150	300	300
Temperature	°C	-	Normal + 2 °C	-	Normal + 2 °C	-	-
Turbidity	NTU	5	50	50	-	-	-
Faecal Coliform**	count/100 ml	10	100	400	5000 (20000) ^a	5000 (20000) ^a	-
Total Coliform	count/100 ml	100	5000	5000	50000	50000	> 50000

Notes :

N : No visible floatable materials or debris, no objectional odour or no objectional taste

* : Related parameters, only one recommended for use

** : Geometric mean

a : Maximum not to be exceeded

Figure 2.10: Water quality standards for Malaysia

2.10 Significant Result of Previous Study

Numerous types of research on the fiber-optic evanescent wave sensors for water quality monitoring system are studied and the findings of the studies are tabulated and discussed. Table 2.3 shows the significant result of the findings of the fiber-optic evanescent wave sensors for water quality monitoring system.

Table 2.3: Significant result of previous study.

Reference	Author	Title	Source	Aim of Study	Findings
[4]	Leizi Jiao, Nianbing Zhong, Xiande Zhao, Shixiang Ma, Fu Xinglan, Daming Dong (2020)	Recent advances in fiber-optic evanescent wave sensors for monitoring organic and inorganic pollutants in water	Trends in Analytical Chemistry	This paper reviews the different types of fiber-optic evanescent wave sensors used for water quality monitoring and discusses methods to enhance their performance.	<p>Significant Result:</p> <ul style="list-style-type: none"> - The review discusses challenges and methods to enhance the performance of FOEW sensors. - The future outlook of FOEW sensors in water quality monitoring is discussed. <p>Method used:</p> <ul style="list-style-type: none"> - Review of fiber-optic evanescent wave sensors for water quality monitoring.

					- Introduction of four types of fiber-optic sensors for pollutant detection in water
[11]	Yasser Chiniforooshan, Jianjun Ma, Wojtek J. Bock (2018)	Evanescent-Wave Fiber-Optic Sensor: On Power Transfer From Core-Cladding Interface to Fiber End-Face	Journal of Lightwave Technology	To study the enhancement of collection efficiency in fiber-optic evanescent-wave sensors.	<p>Significant Results:</p> <ul style="list-style-type: none"> - The roughened end-face of a large-core fiber enhances the collection of fluorescence. - Scattering from a rough end-face enhances the collection of evanescent-wave light. <p>Method used:</p> <ul style="list-style-type: none"> - A different excitation method than the traditional one is used. - The method involves perpendicular and off-axis illumination and receiving fibers.

[12]	Zubia, J., & Arrue, J. (2021).	Plastic Optical Fibers: An Introduction to Their Technological Processes and Applications	Optical fiber technology	The paper provides a comprehensive introduction to plastic optical fibers (POFs), including their manufacture, properties, and various applications.	<p>Significant Results:</p> <ul style="list-style-type: none"> - The paper reviews the features and manufacture of plastic optical fibers. - It discusses the applications and properties of plastic optical fibers. <p>Method used:</p> <ul style="list-style-type: none"> - The paper reviews the main types of plastic optical fibers (POFs) and their manufacture. - The paper discusses the properties of POFs and their applications.
[13]	M. López-López, J. C. Alonso-Álvarez, L. M. Mateos-Gil, L. M. Lechuga, and C. López-Higuera (2019)	Characterization of a Fiber-Optic Evanescent Wave Absorbance Sensor for Nonpolar Organic Compounds	IEEE Sensors Journal	This paper describes the fabrication and characterization of a FOEW sensor for the detection of nonpolar organic compounds	<p>Significant result:</p> <ul style="list-style-type: none"> - The limit of detection for benzene was found to be 10 ppb. - They found that the sensor was selective for nonpolar organic

				in water. The authors also characterized the selectivity, sensitivity, and response time of the sensor.	compounds and had a response time of less than 1 second Methods used: - The sensor is based on a claddless optical fiber coated with a thin layer of a sensitive material. - The sensor was shown to be sensitive to a variety of nonpolar organic compounds, including benzene, toluene, and ethylbenzene
[14]	M. López-López, J. C. Alonso-Álvarez, L. M. Mateos-Gil, L. M. Lechuga, and C. López-Higuera (2021)	Fiber-optic sensor based on evanescent wave absorbance around 2.7 μm for determining water content in polar organic solvents	Optics Express	This paper describes the fabrication and characterization of a FOEW sensor for the determination of water content in polar organic solvents. The	Significant result: - They found that the sensor had a sensitivity of 0.1 wt% and a selectivity ratio of 100:1. The response time of the sensor was less than 5 seconds.

				authors characterized the sensitivity, selectivity, and response time of the sensor	Methods used: <ul style="list-style-type: none"> - The sensor is based on a silica optical fiber coated with a thin layer of a water-sensitive polymer. - The sensor was shown to be sensitive and selective to water, even in the presence of other organic solvents.
[22]	Hazli Rafis Abdul Rahim, Hazli Rafis Abdul Rahim, Siddharth Thokchom, Waleed S. Mohammed, Joydeep Dutta, Sulaiman Wadi Harun (2020)	Optical fiber coated with zinc oxide nanorods toward light side coupling for sensing application	Journal of IEEE	The provided paper does not mention anything about tapered plastic optical fiber coated with ZnO nanostructures.	Significant Result: <ul style="list-style-type: none"> - The paper presents a new approach in optical fiber sensors using side coupling of light into the core modes of plastic optical fiber coated with zinc oxide nanorods. - The approach allows for scattering of light along the fiber to enhance the total coupled

					<p>power, enabling various sensing applications.</p> <p>Method used:</p> <ul style="list-style-type: none"> - Side coupling of light into the core modes of plastic optical fiber (POF) coated with zinc oxide (ZnO) nanorods. - Structuring the growth of ZnO to specific regions to enhance scattering.
[23]	A. S. Prasanth, Sukadev Meher, Z. C. Alex (2022)	Zinc Oxide Thin films coated Evanescent Wave based Fiber Optic sensor	Journal Article	The paper reports on the characterization of zinc oxide thin films coated evanescent wave-based fiber optic sensor	<p>Significant Result:</p> <ul style="list-style-type: none"> - ZnO coated sensor probe shows maximum response of 21.2% towards 250 ppm IPA. - ZnO coated sensor probe shows maximum wavelength shift of 2.4% towards 250 ppm IPA.

					Method Used: <ul style="list-style-type: none"> - Clad modification technique for fiber optic sensor - Radiofrequency magnetron sputtering for deposition of zinc oxide thin films
[25]	Kenza Azil, Kouider Ferria, Said Bouzid (2020)	Cladless optical fiber sensor based on evanescent wave absorption for monitoring methylene blue induced water pollution	Journal of The Optical Society of America B-optical Physics	The paper presents a cladless optical fiber sensor based on evanescent wave absorption for monitoring water pollution caused by methylene blue.	Significant Result: <ul style="list-style-type: none"> - The designed sensor provides a significant response to the concentration range of 6–50 mg/L. - The response of the optical fiber sensor is mainly related to the MB concentration as well as its refractive index. Methods used: <ul style="list-style-type: none"> - Fabrication of cladless optical fiber sensor - Investigation of sensitivity of the proposed sensor

[26]	Mohamad Afi Abdul Hisam (2022)	Tapered plastic optical fiber loop coated with ZnO nanorods using multiple channels for relative water quality sensing	Journal Article	The paper discusses the fabrication of a water quality sensor using a tapered plastic optical fiber (POF) coated with zinc oxide (ZnO) nanorods.	<p>Significant Result:</p> <ul style="list-style-type: none"> - Tapered POF loop coated with ZnO nanorods showed excellent sensing performance. - Increase in length of the loop improved sensitivity and repeatability properties. <p>Method used:</p> <ul style="list-style-type: none"> - Tapering of plastic optical fiber using the polishing method - Synthesis of zinc oxide (ZnO) nanorods using the hydrothermal method
[27]	Tiago B. Marinho, Victor G. M. Almeida, Waleska F. de Oliveira, Joao I. S. Miranda, Marcos E. R. da Silva, Auzuir R. de Alexandriak, Glendo de F. Guimaraes (2021)	Development of evanescent field optical fiber sensor for pH measurement using sol-gel technology	IEEE Sensors Journal	This work proposes developing a fiber optic sensor to measure pH by absorbing light in the evanescent field using sol-gel	<p>Significant Result:</p> <ul style="list-style-type: none"> - The sensor obtained a good linear behavior between values from 4 to 7 of standard pH calibration solutions with a coefficient of linear regression

				technology with the purple bromocresol indicator.	of 0.95439 and an adjusted R-squared of 0.93159. Method used: - Applied the evanescent field with sol-gel technology with the bromocresol purple indicator.
[28]	A Arifin, Hardianti, M Yunus and S Dewang (2020)	Application of plastic optical fiber material as pH measurement sensor using loop configuration	Journal of Physics	Design and manufacture of pH sensor based on POF has been done by using loop configurations in sensor type of with cladding and sensor type of without cladding sensor for number of loop variation.	Significant Result: - The best measurement result is shown in sensor type of without cladding 4 loops, i.e. sensitivity 0.035 V/pH and resolution 0.029 pH. Method used: - Applied in pH measurement using loop configuration

[30]	A.S. Rajamani, D. M, V.V.R. Sai (2022)	Plastic fiber optic sensor for continuous ammonia liquid monitoring using U-bent shape	Journal of Physics	The study demonstrates the development of a novel low-cost plastic optical fiber (POF) based sensor for ammonia liquid measurement using U-bent shape	<p>Significant Result:</p> <ul style="list-style-type: none"> - The overall sensor performance shows the sensor has sensitivity of 0.002 mg/L⁻¹, linearity of 0.9099, and LOD of 1.4 mg/L. <p>Method used:</p> <ul style="list-style-type: none"> - Applied U-bent shape plastic optical fiber (POF) based sensor for ammonia liquid measurement
[31]	Nurfatihah Che Abd Rashid, Noran Azizan Cholan, Kim Gaik Tay, Azra Munirah Mat Daud, Nurul Atika Nabila Jaharudin, Nazrah Ilyana Sulaiman, Nor Hafizah Ngajikin (2024)	Ammonia detection in water using balloon-like fiber optic sensor	Journal for Light and Electron Optics	This paper presents the detection of ammonia in water using a balloon-like fiber optic sensor coated with Oxazine 170 perchlorate and polydimethylsiloxane (PDMS).	<p>Significant Result:</p> <ul style="list-style-type: none"> - The overall sensor performance shows the sensor has sensitivity of 0.006 mg/L⁻¹, linearity of 0.9154, resolution of 1.6667 mg/L, LOD of 2.9556 mg/L, stability precision of 99.8 % and RSD of 0.0308 %.

					Method used: - Applied a balloon-like fiber optic sensor coated with Oxazine 170 perchlorate and polydimethylsiloxane (PDMS).
--	--	--	--	--	---

2.11 Summary of Chapter 2

In this chapter, the related research of the project titled "Characterization of Fiber-Optic Evanescent Wave Sensor for Water Quality Monitoring" is briefly described. The chapter encompasses a literature review, which delves into prior studies relevant to the project's objectives. The literature review entails a comprehensive examination of findings from previous research endeavors, encompassing theoretical frameworks, methodologies employed, and insights gleaned from past studies. Through this review, the chapter aims to provide a robust foundation for the project by drawing upon existing knowledge and insights in the field of fiber-optic evanescent wave sensors and water quality monitoring. By synthesizing and analyzing previous studies, the chapter contributes to supporting the information and methodologies utilized in the current project, thereby enhancing its credibility and relevance within the broader context of scientific research in the field.

CHAPTER 3



The decision-making process and overall implementation of the aim are covered in this chapter. The precise tools and supplies used for this project, as well as its functions, were covered. Besides, the project's outlines implementation for both software and hardware designs are also included. In this chapter, the experiment's procedure was explained. This chapter goes into great detail on the experiment that measured the water quality by using plastic optical fiber uncoated and coated with ZnO.

3.0 Flowchart

Figure 3.0 shows the flowchart for the overall process of this project to achieve the objective mentioned. The flows show the designing of circuit, preparation of POF, preparation of water samples and the analyses of data measured.

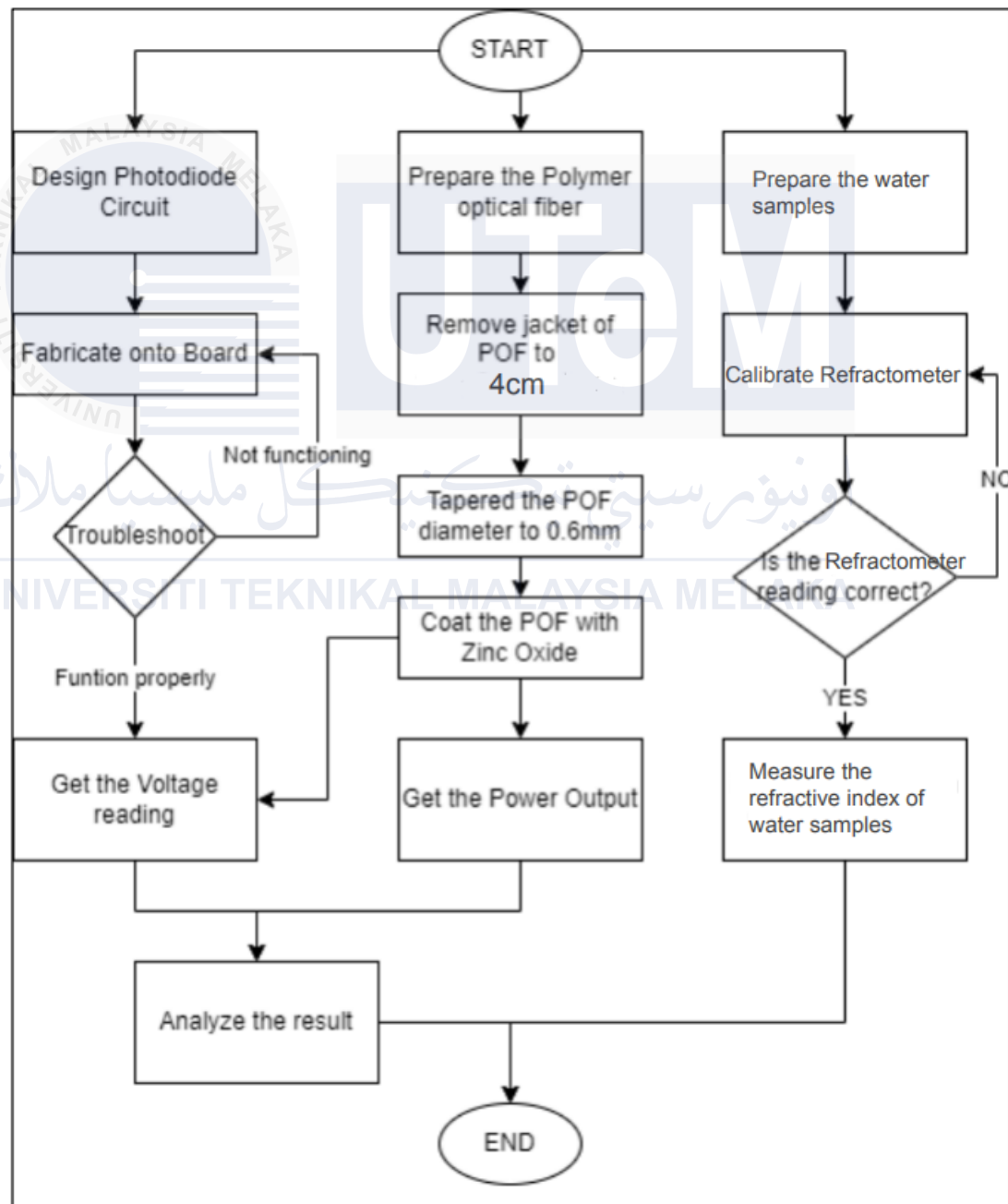


Figure 3.0 Flowchart for overall project

3.1 TECHNICAL DESIGN

The purpose of the Water Quality Monitoring System in this project is to measure the water quality level of the water samples and display the voltage of light source change through the water samples. Furthermore, the result of reading will be synchronized on to IoT system so the users could monitor the test with long distance.

It consists of some different parts as shown in Figure 3.1, which is:

- a) Light source to analog voltage converting system (receiver circuit)
- b) Physical Crystal LCD displays system.
- c) IoT displays system.

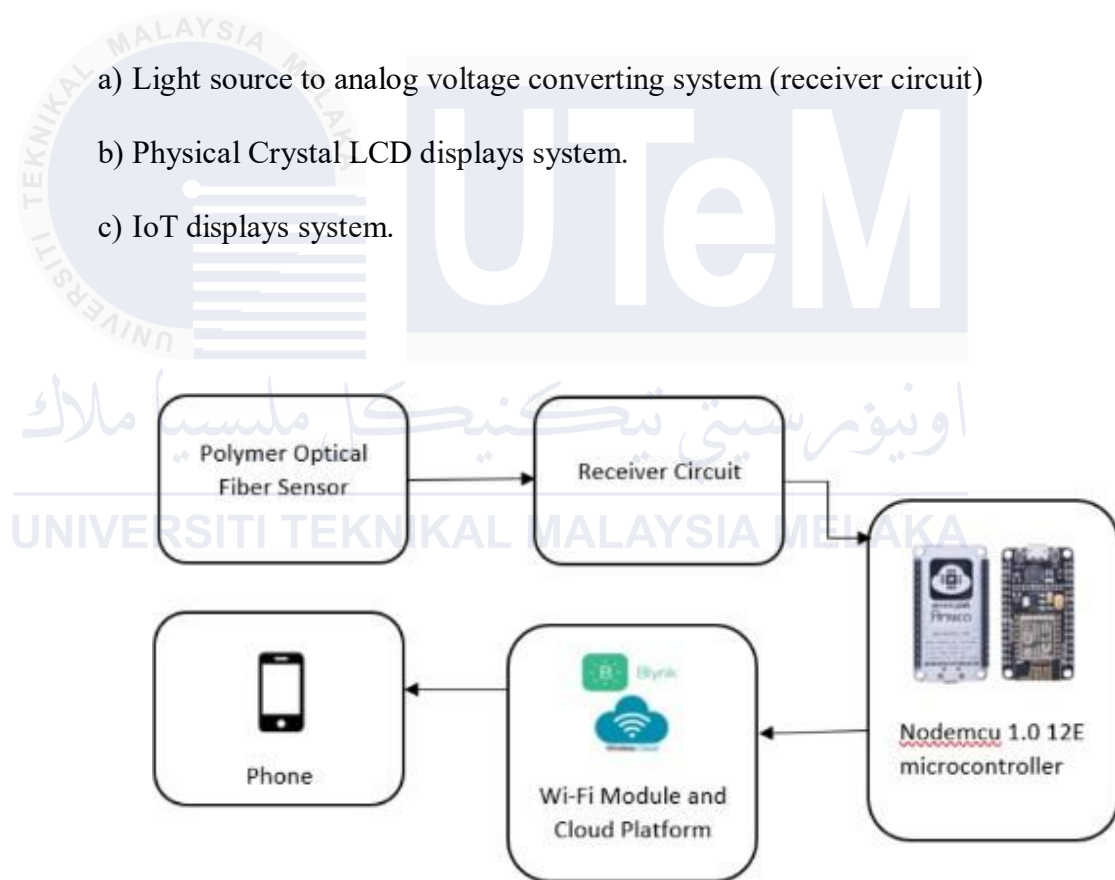


Figure 3.1: Block diagram of project

At the very beginning part of the project, a receiver circuit with phototransistor sensor will be connected to the microcontroller that known as the Nodemcu ESP8266. This PoF sensor will always receive the light sources which transmitted by Optical fiber cable. The signal will be stepped up through the Op-Amp in the receiver circuit.

Then finally an analogue voltage between 0-3.3V will be send transmit into analogue port of the microcontroller. Besides, the voltage reading and the comparison for water quality level will be displayed on a 16x2 LCD. Based on the result could trigger the different colours of led diode as alert or notifications. Furthermore, the project will develop into an Internet of Things system. The Nodemcu ESP8266 has an advantage as it has its own Wi-Fi module. Blynk platform used to link devices to IoT. The values for system parameters and detail such as output voltage, water quality level will indicate and can be viewed on the web page or smartphone by adding Internet of Things in the programming.

3.2 COMPONENT USED FOR PROJECT

3.2.1 NodeMCU Module ESP8266



Figure 3.2: ESP8266 NodeMCU ESP-8266 module

The ESP8266 NodeMCU ESP-8266 module is the newest iteration of this common module which can be used as an Arduino-enabled Wi-Fi replacement for several applications. This module can act as an access point (can create an access point) and a station (can connect to Wi-Fi), thus helping the Internet of Things to collect and download data from the Internet as easy as possible. In fact, it can be designed to have pull-up or pull-down resistors. While there are 11 physical I / O pins, 2 are usually reserved for use as TX / RX lines while serial communications are used leaving 9 physical I/O s as shown in Figure 3.3.

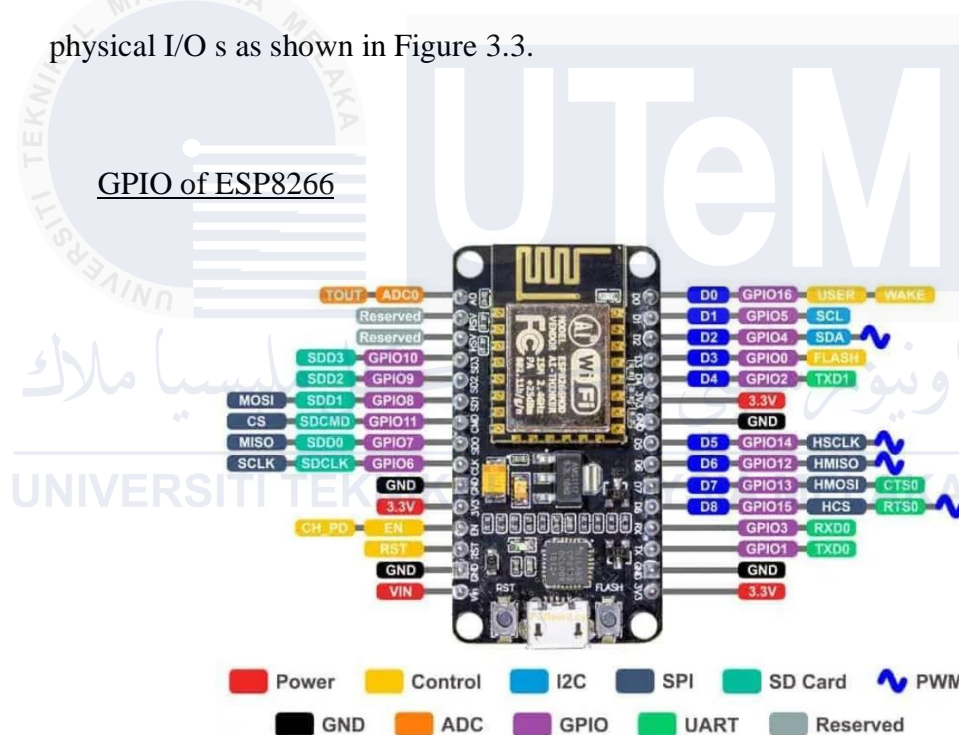


Figure 3.3: GPIO of NodeMCU Module ESP8266

One important thing to notice about ESP8266 is that the GPIO number doesn't match the label on the board silkscreen. For example, D0 corresponds to GPIO16 and D1 corresponds to GPIO5. student must study about it before starting the programming to usual the pin declaration for all I/O component is correctly. The following table shows the correspondence between the labels on the silkscreen and the GPIO number as well as what pins are the best to use in the projects, and which ones need to be

cautious.

In the project, various pins of the NodeMCU are designated for specific functions as shown in Table 3.1. The A0 pin serves as the input analog for the receiver circuit, where the NodeMCU reads the voltage of the light source, which can range from 0V to a maximum of 3.3V. The D1 and D2 pins are dedicated to the I2C communication, connecting to the SCL (Serial Clock Line) and SDA (Serial Data Line) pins of the I2C module, respectively. The D5 pin is used for the green LED component, functioning as the anode leg and indicating the system's output. Similarly, the D6 pin is utilized for the red LED component, also serving as the anode leg and indicating another aspect of the system's output. The VIN pin provides a 5V input power supply to the 16x2 LCD display, ensuring it operates correctly. The VCC pin supplies a 3.3V DC power to the entire system, ensuring proper voltage levels for the NodeMCU and other components. Lastly, the GND pin is used to ground all the ground connections from the circuit, ensuring a common reference point for the electrical components.

Table 3.1: GPIO of NodeMCU ESP8266

Label	GPIO	Input	Output	Notes
D0	GPIO16	no interrupt	no PWM or I2C support	HIGH at boot used to wake up from deep sleep
D1	GPIO5	OK	OK	often used as SCL (I2C)
D2	GPIO4	OK	OK	often used as SDA (I2C)
D3	GPIO0	pulled up	OK	connected to FLASH button, boot fails if pulled LOW
D4	GPIO2	pulled up	OK	HIGH at boot connected to on-board LED, boot fails if pulled LOW
D5	GPIO14	OK	OK	SPI (SCLK)
D6	GPIO12	OK	OK	SPI (MISO)
D7	GPIO13	OK	OK	SPI (MOSI)
D8	GPIO15	pulled to GND	OK	SPI (CS) Boot fails if pulled HIGH
RX	GPIO3	OK	RX pin	HIGH at boot
TX	GPIO1	TX pin	OK	HIGH at boot debug output at boot, boot fails if pulled LOW
A0	ADC0	Analog input	X	

3.2.2 16x2 Crystal LCD Display Monitor

An LCD (Liquid Crystal Display) screen is an electronic display module, and it was commonly used in various devices and circuits. it can display 16 characters per line and there are 2 such lines. The 16 x 2 intelligent alphanumeric dot matrix display can display 224 different characters and symbols.

The LCDs have a parallel interface, meaning that the microcontroller must manipulate several interface pins at once to control the display. The interface consists of the following pins:

- Pin RS-A register select pin that controls where in the LCD's data memory.
- Pin R/W -A Read/Write pin that selects reading mode or writing mode.
- Enable pin -a pin that enables writing to the registers.
- Pin D0-D7.- The states of these pins (high or low) are the bits that you're writing to a register when you write, or the values you're reading when you read.
- pin Vo, +5V and GND-power supply pins use to power the LCD and control the display contrast.
- (Bklt+ and Bklt-)- LED Backlight pins that turn on and off the LED backlight.
- The process of controlling the display involves putting the data that form the image of what want to display into the data registers, then putting instructions in the instruction register. The process can be simplified by using Liquid Crystal Library.

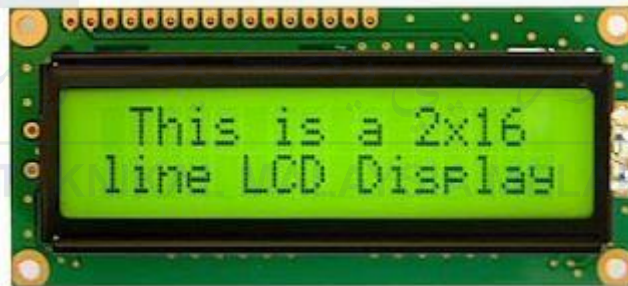


Figure 3.4: Crystal LCD Display Monitor

3.2.3 I2C LCD 16x2 Module

Controlling an LCD board might be repetitive due to limited stick assets in a microcontroller/microprocessor as shown in Figure 3.5. I2C serial interface connection modules using PCF8574 chips, for example, make the work simple when used as serial to parallel connectors. The 16x2 LCD can be connected to the serial interface connection, which also provides two flag yield pins (SDA and SCL) that can be used to communicate with an MCU or MPU. It means that only needs 4 pins for the LCD display: VCC, GND, SDA, SCL after connecting with I2C module. It will save at least 4 digital/analog pins on microcontroller.

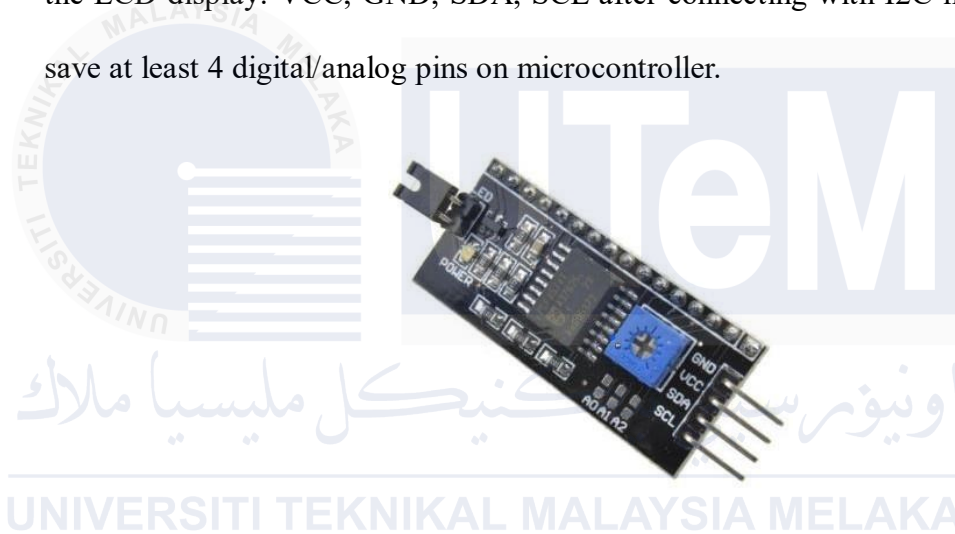


Figure 3.5: I2C LCD 16x2 Module

As the I2C Module was designed for the 16x2 Lcd Screen, two components are connected in a straight line as simple as Figure 3.6 showed. However, as needs a minimum 5volt of Vcc and Gnd to make the Lcd clearly display the words, the pin Vcc of I2C module must connect to the pin(Vin) of the Nodemcu ESP8266 Module instead of 3.3V pin. The (Vin) pin has a bit special because the value of voltage in pin (Vin) was depends on the value of input voltage of the NodeMCU. Fortunately, the power supply given to the Nodemcu ESP8266 is around 5V, it's exactly fulfilled the re-equipment to function the LCD screen.

16x2 Lcd Screen with I2C Module

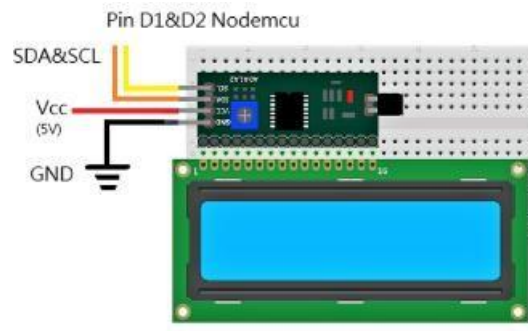


Figure 3.6: Lcd Screen & I2C Module connection

Moreover, serial data pin (SDA) and serial clock pin (SCL) convert and transmit all the data and information to lcd. It has been connected to pin D1 and D2 in this project. At the last a program library must be installed to Arduino software for starting the program, LED to NodeMCU ESP8266. For additional functions, 2 different colors of LED were used to alert the user for situation of water quality level. Table 3.2 shows the pin connection between these two parts.

Table 3.2: Pin connection for LED

Components	Module pin
Green led	D5
	Gnd
Red led	D6
	Gnd

3.2.4 POF Sensor

The PoF sensor was a type of phototransistor which received the light source from the port which connects with optical fiber. It can attract the change of light source and convert it into voltage value. However, it needs Op-amp receiver circuit to step up the voltage as the voltage produced by itself was very tiny.



Figure 3.7: POF Sensor

3.2.5 Receiver Circuit and Op-Amp IC LT1884

The POF receiver circuit consists of the photodiode that was convert the energy of light to electricity as shown in Figure 3.8. The receiver circuit was employs to read the optical signal and convert it to the voltage value. It needs Op-amp receiver circuit to step up the voltage as the voltage produced by itself was very tiny. LT1884 Op-Amp is utilized to amplify the tiny current into a suitable output voltage. The Op-amp output voltage can be represented as follows:

$$V_{out} = R_f \times I_d$$

R_f is the feedback resistor and I_d is the photocurrent. In this circuit, the feedback capacitor, C_f has no effect on the measurement as it is at low frequencies. The current, I_d is supposed to flow entirely through R_f . The Op-Amp shall give an output at least yielded up until 4.7V. Therefore, R_f was set to $7.8\text{M}\Omega$ for the output to be obtained at

1.9V at 50% of the RH level at a room condition.

The LT1884 op amps IC provides faster response than other precision amplifiers while delivering high accuracy input performance to amplifiers with rail-to-rail output swing. The dual LT1884 is offered in 8-pin SO and PDIP packages with common pinouts.

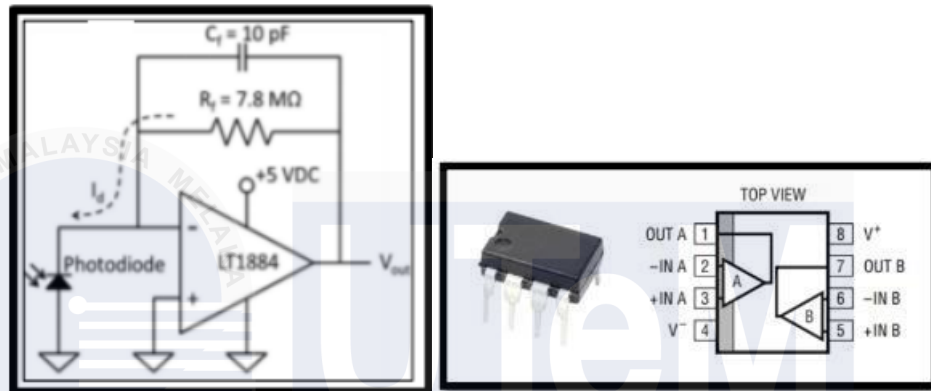


Figure 3.8: Receiver circuit and Op-Amp IC LT1884 pin layout

3.2.6 Potentiometer variable Resistor

The Variable Resistor was one of the components in the receiver circuit. In this project, 10M ohm was used. Due to their resistance can be set to a specific value, variable resistors are widely used in electric circuits to modify the value of current or voltage.



Figure 3.9: 10M ohms Potentiometer variable Resistor

3.3 Hardware Development

The project utilized PCBs (Printed Circuit Boards) to form a crucial part of the hardware as shown in Figure 3.10. PCBs, being the fundamental building blocks of electronic systems, are composed of boards with copper traces and other components attached to conduct current through the circuit. There are two types of PCBs based on design: Dotted PCBs and Layout PCBs. For designing the PCB, Proteus software was used. Proteus is an electrical design automation program primarily used for creating schematics and designing PCBs. It includes several tools that are not only simple to use but also valuable for PCB design and learning about PCB design. Proteus features an integrated autorouter, full schematic capture, adjustable design rules, power plane support, an interactive circuit simulator, industry standard CAD/CAM and ODB++ output, and 3D viewing. Components were selected and added to the device list, and then all components were placed in the workspace.

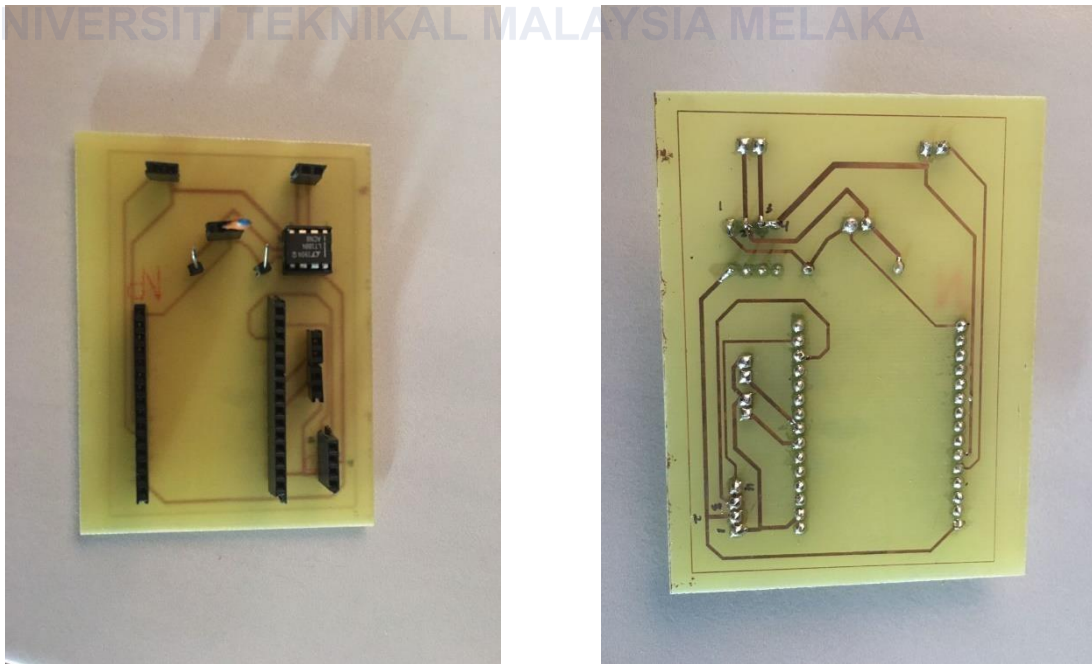


Figure 3.10: PCB Board

The design is based on schematic design in Figure 3.11.

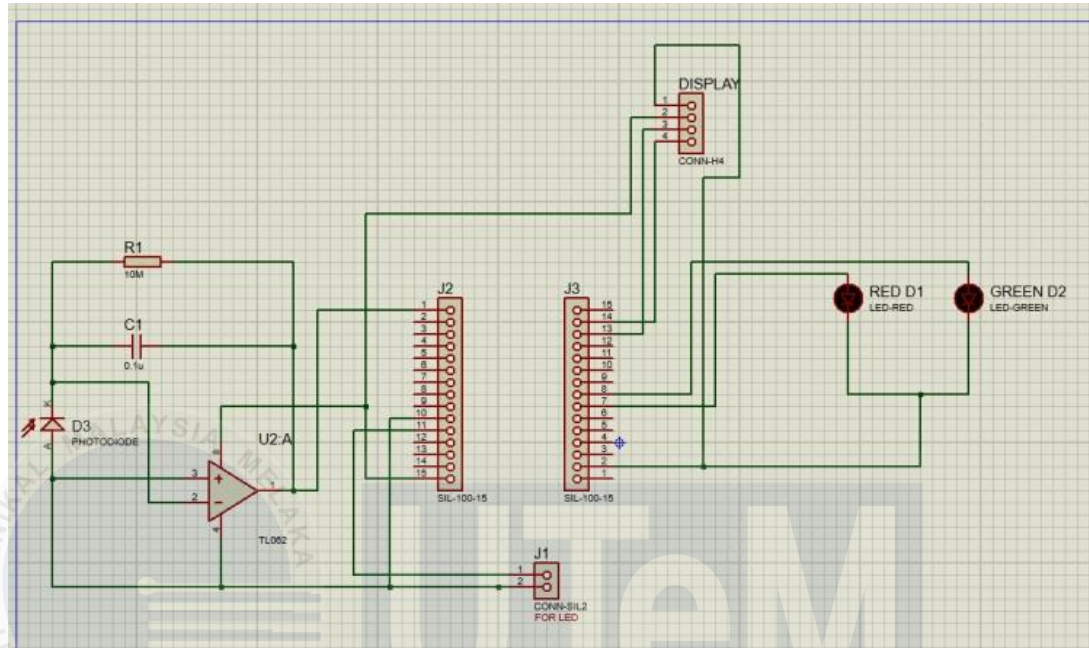


Figure 3.11: Schematic design

Next, the '2D Graphics Box Mode' was used to construct the board edge as shown in Figure 3.12. The 'board edge' option was selected from the 'select layer' menu. A box was then drawn in the workspace. Each component was clicked on and, if necessary, rotated using the rotate buttons before being placed in the workspace. The components were arranged properly, and all of them were added. To connect the components, the component end was clicked with a pen, following the green line. Once finished, the green line was removed. When creating the single-layered PCB, components were placed on one side, and connections were formed on the other. After completing the tracking, 3D visualization was chosen to view the final circuit. All angles, components, the board without components, and front and rear views were examined.



Figure 3.12: 3D visual of circuit design

When printing the layer, only 'bottom copper' and 'board edge' were selected in 'layer/artwork'. The scale was set to 100%, 'X Horizontal' was chosen in Rotation, and 'Mirror' was selected in the 'reflection' choice. The 'mirror' option was chosen because the printed side would face the copper layer in the other direction as shown in Figure

3.13.

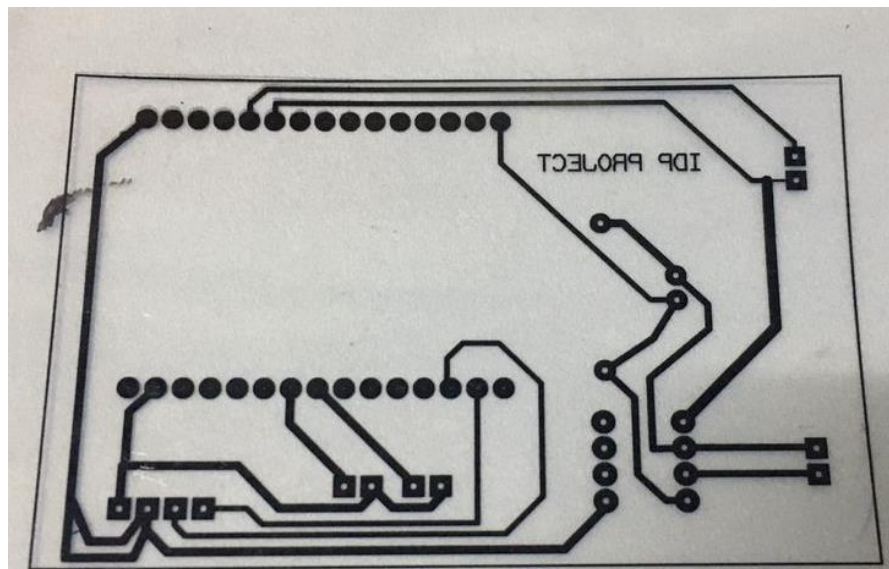


Figure 3.13: Printing bottom layer

The subsequent step was the etching process. The copper rails were designed primarily through copper layer printing. The copper layer board was taken and trimmed to the specified dimensions. The bottom copper layer print was then inserted into the copper PCB board, with the print facing the copper layer. The paper and board were carefully adjusted. Next, heat was applied to the printed paper using an iron box or another heat source. This step integrated the paper print with the board. Afterward, the board was dipped in water, and the paper was removed, preserving the carbon print on the board. Then, the board was dipped in ferric chloride solution. The copper reacted with ferric chloride, dissolving the copper without a carbon coating.



Figure 3.14: Remove copper with ferric chloride solution.

After finishing its etching process, check the continuity on PCB board with multimeter as shown in Figure 3.15 and if have any short, sandpaper will used to clean board and remove any remaining carbon layer.

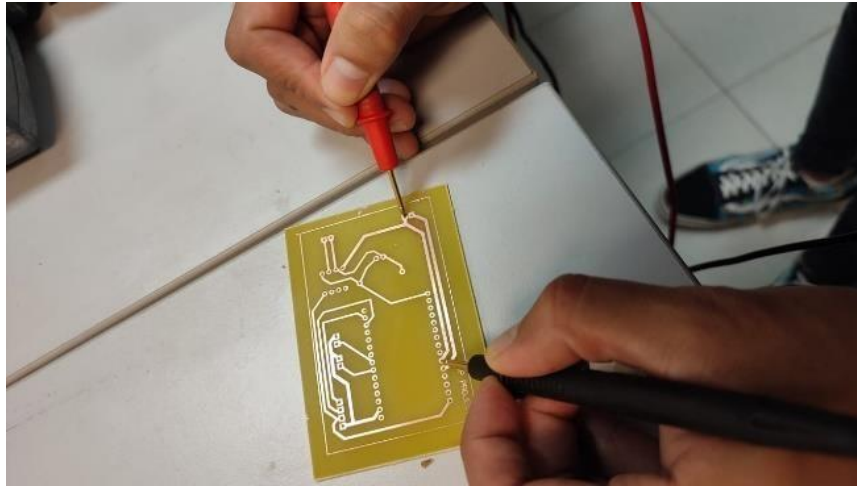


Figure 3.15: Check continuity with multimeter

Drill holes in accordance with the drill position layer we created. Next, place components and solder them into position using a soldering kit as shown in Figure 3.16.

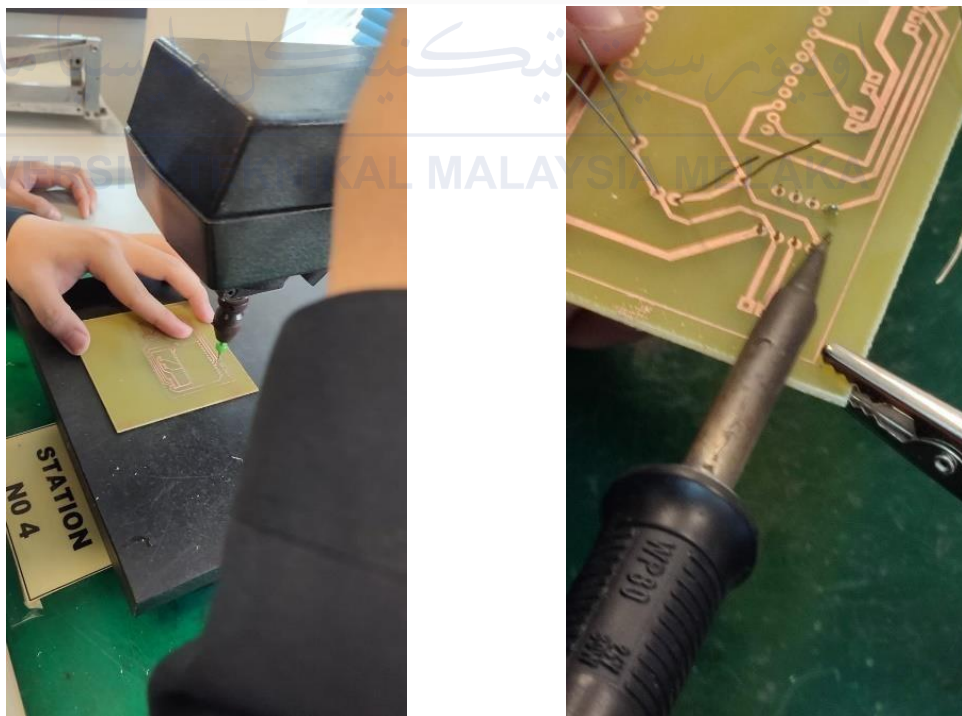


Figure 3.16: Drill hole and solder all components.

3.3.1 Receiver Circuit and Operation

As depicted in Figure 3.17, the receiver circuit is constructed using an Op-Amp connected to a POF sensor and Ground respectively at pin 2 and 3. Simultaneously, a $10\text{M}\Omega$ variable resistor and a 10pF capacitor were connected in parallel at pin 1 and 2 to serve as feedback functions. This configuration allowed the circuit to compare and adjust the input/output values to produce the analog reading. Lastly, the output, which pin 1 was connected to, was linked to the analog pin (A0) of the microcontroller.

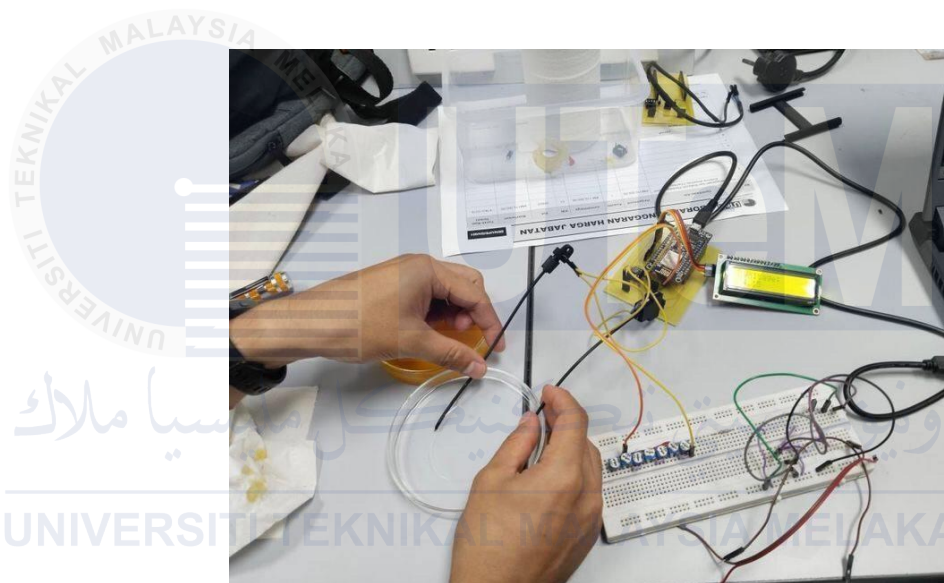


Figure 3.17: Receiver Circuit

3.4 Software Development

In the software development part, the project was carried out in 2 phases. The first phase, the project was carried out by complete offline system functions, which target to make the NodeMCU ESP8266 module be functions as well as taking reading of analog voltage and display it onto the LCD screen. For the second phase, the IoT system was develop into the primary offline system structure to evaluate it on online platform. Arduino Software (IDE) software was used to write and upload the program to the NodeMCU ESP8266 microcontroller in order to execute the task required. The Blynk app was used to interface the other codes on Internet of Things (IoT). NodeMCU ESP8266 was mounted with a receiver circuit, POF sensor, Lcd screen and LED diode for device operation and serve as the receiver component. The circuit will upload the codes to collect input then calculate and display the output.

The Blynk platform was chosen to interface the project with the Internet of Things (IoT). To ensure the system could connect with Blynk and synchronize the output results to the IoT cloud, several steps needed to be followed. Firstly, an account was created and logged into the Blynk cloud website. Before proceeding to programming, a new template had to be created as shown in Figure 3.18. In this stage, the ESP8266 hardware was selected, and the connection was configured as Wi-Fi. The template's name was entered, setting the stage for further integration with the Blynk platform.

Create New Template

NAME

FYP Water Quality Monitoring

HARDWARE

ESP8266

CONNECTION TYPE

WiFi

DESCRIPTION

Description

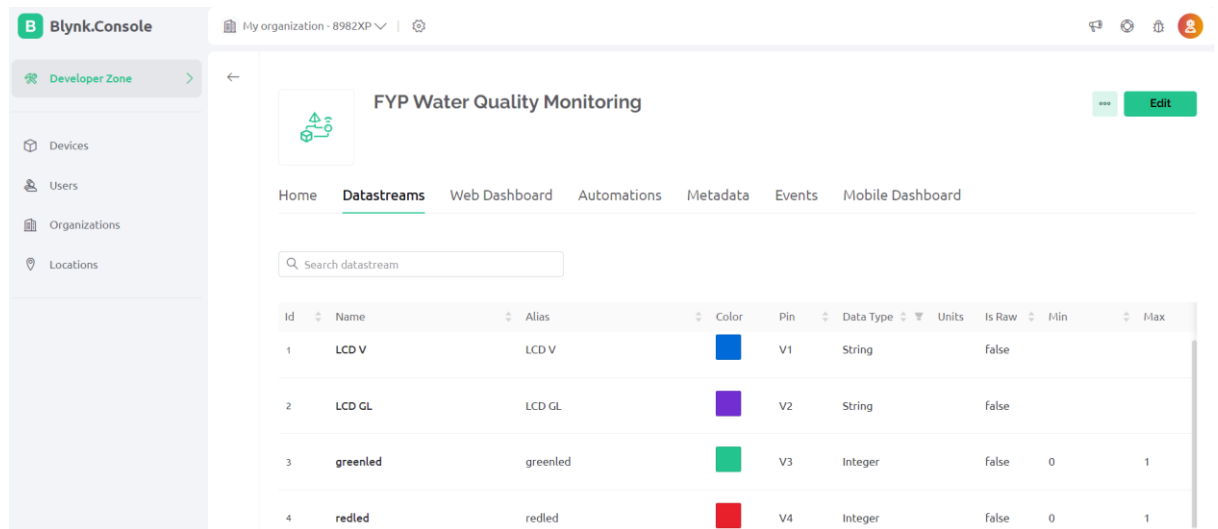
0 / 128

Cancel

Done

Figure 3.18: IOT template selection

After creating the project template, the next step involves adding virtual pins for the project's components in the DataStream inside the template as shown in Figure 3.19. In this case, two virtual pins are set as string data types for the LCD display, while another two virtual pins are configured as integer data types for controlling the on and off states of the LED. This configuration allows for efficient communication and control between the hardware components and the Blynk platform, ensuring seamless integration into the IOT system.



ID	Name	Alias	Color	Pin	Data Type	Units	Is Raw	Min	Max
1	LCD V	LCD V	Blue	V1	String		False		
2	LCD GL	LCD GL	Purple	V2	String		False		
3	greenled	greenled	Green	V3	Integer		False	0	1
4	redled	redled	Red	V4	Integer		False	0	1

Figure 3.19: Virtual pin declaration

Once the virtual pin been done, there could select the online widget that want at web dashboard. Insetting that can select the virtual pin for each widget as shown in Figure 3.20.

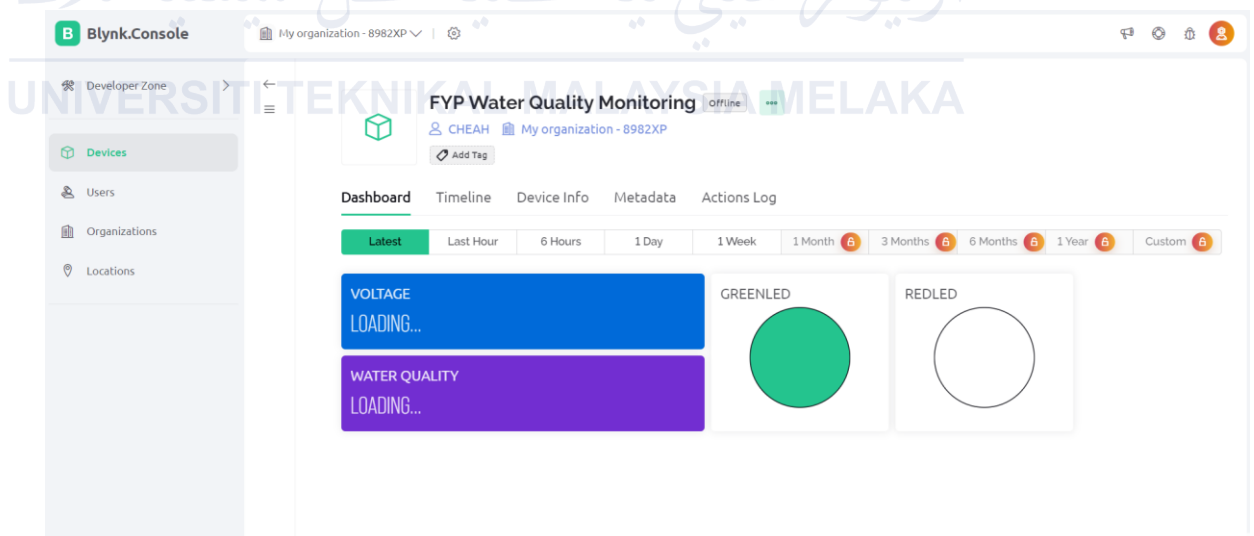


Figure 3.20: IOT web dashboard setup

Lastly, a new device has been created, the info Template ID, Device Name, and AUTH Token can get the device info. These 3 things are declared at the very top of the firmware code later shown in Figure 3.21.

FIRMWARE CONFIGURATION

```
#define BLYNK_TEMPLATE_ID "TMPL67XKn3XNS"
#define BLYNK_TEMPLATE_NAME "FYP Water Quality Monitoring"
#define BLYNK_AUTH_TOKEN "VukX1Qgay25td6fvIcY3qkaskfwrsS0t"
```

Template ID, Template Name, and AuthToken should be declared at the very top of the firmware code.

Figure 3.21: Device's creation & information.

For the Blynk Apps on smartphone, the things will be repeat on creating new device only as it is using the same project template as shown in Figure 3.22. So now the project was ready for IoT programming.



Figure 3.22: IoT widget displayed on smartphone.

3.4.1 Project's Coding operating

Table 3.3: Coding explanations

<pre>#include <LiquidCrystal_I2C.h> #include <Blynk.h> #define BLYNK_TEMPLATE_ID "TMPL67XKn3XNS" #define BLYNK_TEMPLATE_NAME "FYP Water Quality Monitoring" #define BLYNK_AUTH_TOKEN "VukXlQgay25td6fvIcY3qkaskfwrs8Ot"</pre>	<p>The 3 IoT ID and Token are taken from Blynk to link it.</p>
<pre>#define BLYNK_PRINT Serial #include <ESP8266WiFi.h> #include <BlynkSimpleEsp8266.h> #include <Wire.h> #include <LiquidCrystal_I2C.h> LiquidCrystal_I2C lcd(0x3F, 16, 2);</pre>	<p>Declaration of coding for Blynk, ESP8266 module Driver and, another library item such as Lcd, I2C</p>
<pre>char auth[] = BLYNK_AUTH_TOKEN; char ssid[] = "vivo Y35"; char pass[] = "12345678QWA";</pre>	<p>Id Wi-Fi and password used by module.</p>
<pre>int value; WidgetLED greenled (V3); WidgetLED redled (V4); int okled = 14; int xled = 12; int analogPin = A0;</pre>	<p>Declaration of coding for I/O pin of components for Hardware part and the online widget's virtualpin</p>
<pre>void setup() { Serial.begin (9600); Blynk.begin (auth, ssid, pass); pinMode (okled, OUTPUT); pinMode (xled, OUTPUT); lcd.init(); lcd.backlight(); delay (2000); lcd.setCursor(0,0); lcd.print("*FYP_PROJECT*"); lcd.setCursor(0,1); lcd.print("WATER_QUALITY_LEVEL"); delay(2000); lcd.clear(); }</pre>	<p>Void setup: The function needs to run once when switch on device.</p> <p>In this case, start up the Blynk systems, lcd screen and its backlight, display the title for 4 seconds, then clear the displays and go through the next part.</p>

<pre> void loop() { Blynk.run(); int lightLevel = analogRead (analogPin); float voltage = lightLevel * (3.3/1024.0); Blynk.virtualWrite (V1, voltage, "V"); lcd.setCursor(0,0); lcd.print("Voltage:"); lcd.setCursor(8,0); lcd.print(voltage); </pre>	<p>Void loop: Looping sequence of programming.</p> <p>Virtual Write: Instruction of IoT display</p> <p>Before displaying sentences at Lcd, cursor which the column and row must set.</p>
<pre> if(voltage<=1.5) { digitalWrite(xled, HIGH); digitalWrite(okled, LOW); greenled.off(); redled.on(); Blynk.virtualWrite(V2, "Low_Quality"); lcd.setCursor(0,1); lcd.print("Low_Quality"); delay(2000); Blynk.virtualWrite(V2, "LOADING..."); Blynk.virtualWrite(V1, "LOADING..."); lcd.clear(); lcd.setCursor(0,0); lcd.print("LOADING..."); lcd.setCursor(0,1); lcd.print("Reading"); delay(2000); } </pre>	<p>If functions. When voltage over the limit value</p> <p>Turn on both the physical and online red led.</p> <p>Turn off both the physical and online green led. Lcd display the situation.</p> <p>For let the program retake sample value, delay the time and display the “loading” on screen.</p>

<pre> else { digitalWrite(xled, LOW); digitalWrite(okled, HIGH); greenled.on(); redled.off(); Blynk.virtualWrite(V2, "High_Quality"); lcd.setCursor(0,1); lcd.print("High_Quality"); delay(2000); Blynk.virtualWrite(V2, "LOADING..."); Blynk.virtualWrite(V1, "LOADING..."); lcd.clear(); lcd.setCursor(0,0); lcd.print("LOADING..."); lcd.setCursor(0,1); lcd.print("Reading"); delay(2000); } </pre>	<p>Else function. When voltage not over the limit value.</p> <p>Trigger another looping</p>
---	---

اونیورسیتی تکنیکل ملیسیا ملاک

UNIVERSITI TEKNIKAL MALAYSIA MELAKA

3.5 Prototype Design and Project Testing

After the prototype has been designed, the power supply from the laptop was generated to the sensors circuit, Arduino circuit and the NodeMCU. Then all the circuit jumper wires are connected to one another. After this, the system should then be tested to ensure the circuit is working in the required condition. All electronic components are again tested so that the components function in prototype form. NodeMCU board, variable resistor, LEDs, POF sensor and phototransistor are placed in one breadboard. The circuit operates once the light source from LED is passing through the POF sensor. Then the variable resistor is adjusted until getting the appropriate reference voltage before starting the measurement. Then the water samples with variation of ammonia concentration and pH levels are dipped on the POF sensor sensing probe which this process will produce an output voltage from the water sample. If the voltage exceeds the threshold, indicating a high-quality condition, the actual voltage value is displayed, and a good quality is shown on an LCD screen. Simultaneously, a physical green LED is triggered to alert users visually, and the result is synchronized with the Blynk IoT platform for remote monitoring. Conversely, if the voltage is within a low quality range, the voltage value is still displayed, but a low quality status message is shown on the LCD, and a red LED is activated to signify that water is low quality. This result is also synchronized with the Blynk IoT platform. Figures 3.23 below show the testing of the project. The experiment continues by changing the POF sensor with another POF which coated by the ZnO and the result was recorded.

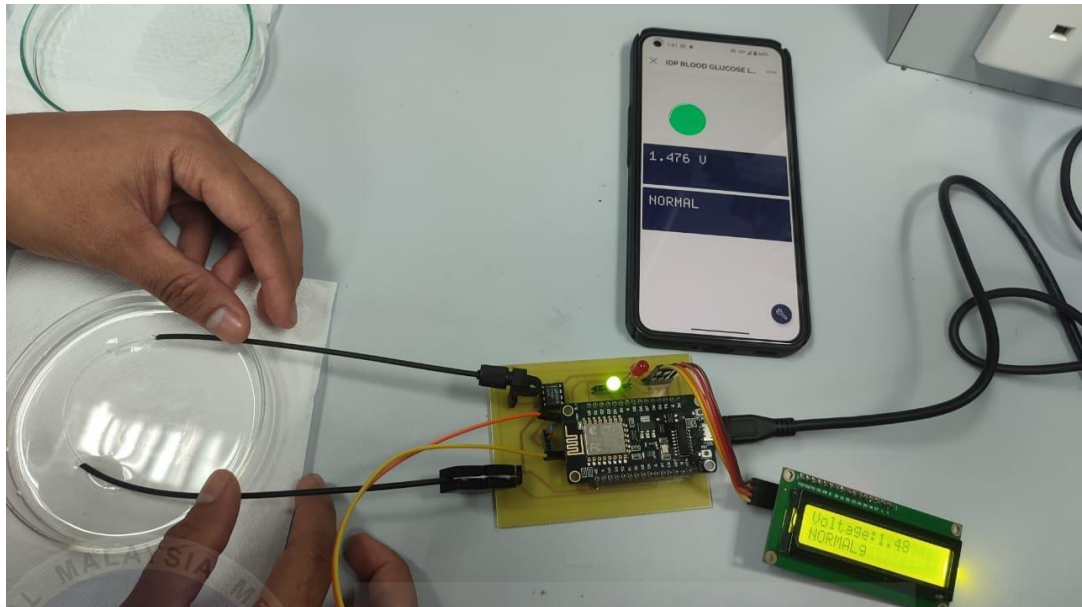


Figure 3.23: Testing of circuit

3.6 Fiber Optic Preparation

3.6.1 Uncladding the POF jacket

The POF jackets was striped using knife to expose the fiber that will be used for sensing region. The exposed length of the fiber was fixed to 4cm as shown in Figure 3.24 respectively.



Figure 3.24: 4cm Unclad jacket of POF

3.6.2 Tapered the POF

Each of the fiber was tapered to 0.6mm to further enhance the sensitivity of the POF. To ensure that the POF has a diameter of 0.6, digital micrometer gauge was used. The changes in size can be seen in the image of digital microscope as it becomes thinner. The process of tapering is by using only sandpaper with 1000 grit roughness. Figure 3.25 shows the 1.0mm not tapered fiber and 0.6mm after tapered fiber.

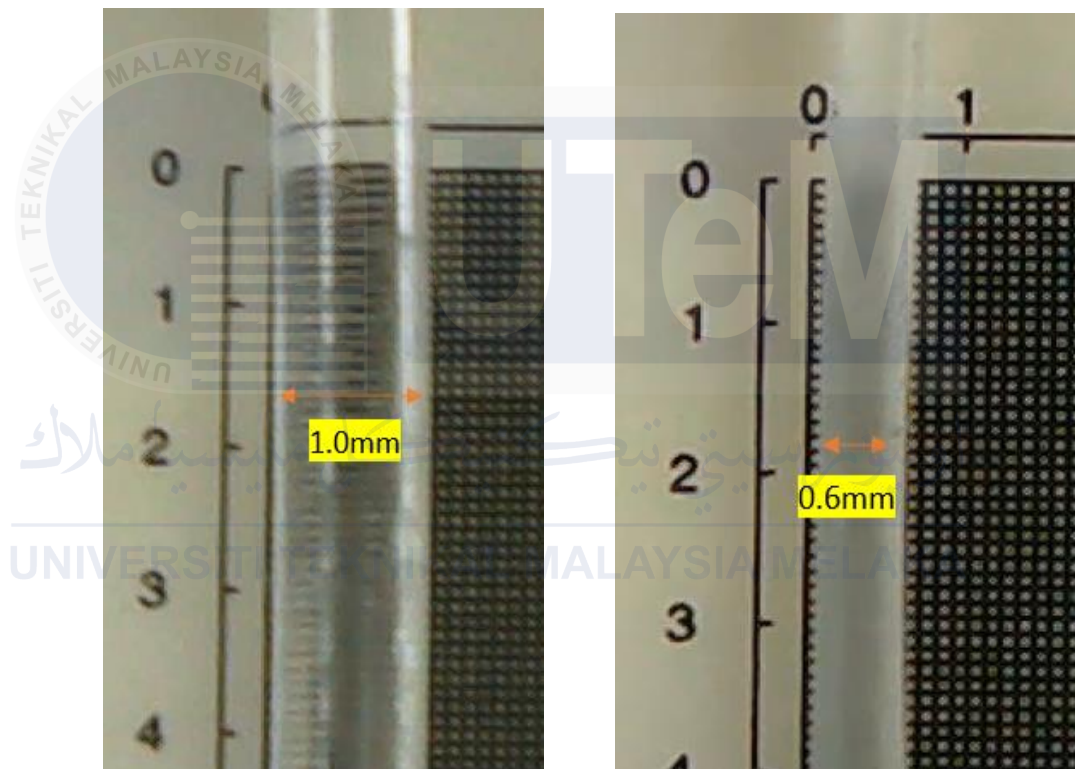


Figure 3.25: Digital microscope view of tapered POF

Depending on the diameter of the desired parameter, the etching operation took between 5 and 7 minutes. Because the brittleness of the fiber increases with decreasing fiber diameter, this technique has the drawback that it must be handled carefully.

Figure 3.26 shows the waist diameter of the tapered fiber using digital micrometer screw gauge.



Figure 3.26: Measurement of tapered POF using digital micrometer screw gauge

3.6.3 Hydrothermal Zinc Oxide method

3.6.3.1 Seeding Process and Core Treatment

After preparing the fiber to the desired exposed length and diameter, first it needs to undergo seeding process to grow the ZnO nanorods. The number of times spent can bring different results in growing of ZnO such as the length, uniformity, density, and its diameter. It has been identified four crucial steps in seeding process alone which are preparing the seeding solution, core treatment of POF, forming the nucleation center on POF and annealing. Figure 3.27 shows the block diagram for the seeding process. Figure 3.28 shows the treated core of POF with polysorbate 80.

Core Treatment & Seeding Solution preparation



Dipping in Seeding solution



Annealing

Figure 3.27: Step process for Seeding process.



Figure 3.28: Treated Core of POF

First for a good uniformity of ZnO growth the tapered fiber is treated with 50 ml polysorbate 80 mixed with 500ml deionized water. The POF are submerged for 10 minutes and dry for two hours. Simultaneously during the core treatment, the seeding solution is prepped by combining two solutions made up of Zinc Acetate and Sodium Hydroxide. For the first solution, 0.088g of Zinc Acetate Dihydrate was dissolved in 80ml of ethanol for 30 minutes at 50°C to produce 5mM solution. Extra 80ml of ethanol are poured into the solution to cooled it down. This process can be seen in Figure 3.29 below.

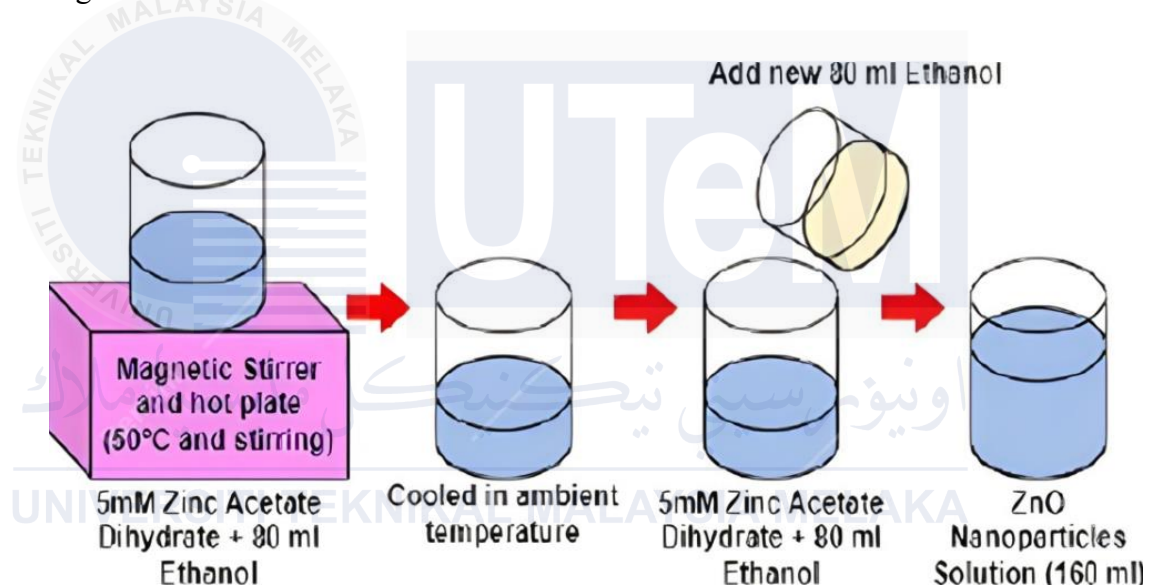


Figure 3.29: Zinc oxide nanoparticle solution preparation

Next, the second solution is prepared for the purpose of pH control which is 0.016g of Sodium Hydroxide dissolved in 80ml ethanol for 30 minutes at 50°C. Result of the stirring produces 5mM solution. This process is illustrated as in Figure 3.30.

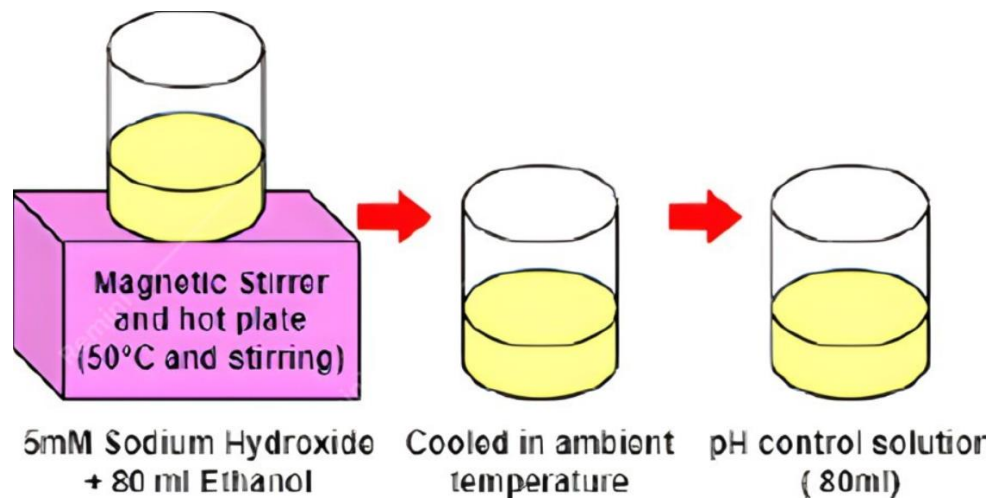


Figure 3.30: pH control solution preparation

Lastly for the preparation of seeding solutions, pH control solutions are gradually mixed into the zinc oxide nanoparticles seeding solutions using 1 ml pipette every one minute. The mixing process is repeated until all of the pH control solutions are finished. This process increases the amount of hydroxyl ions in the seeding solutions. Then the mixed solution is placed inside the water bath at a temperature of 60°C for 3 hours.

The final product of the solution is colour changes from clear to clouded solution. The process is shown in Figure 3.31.

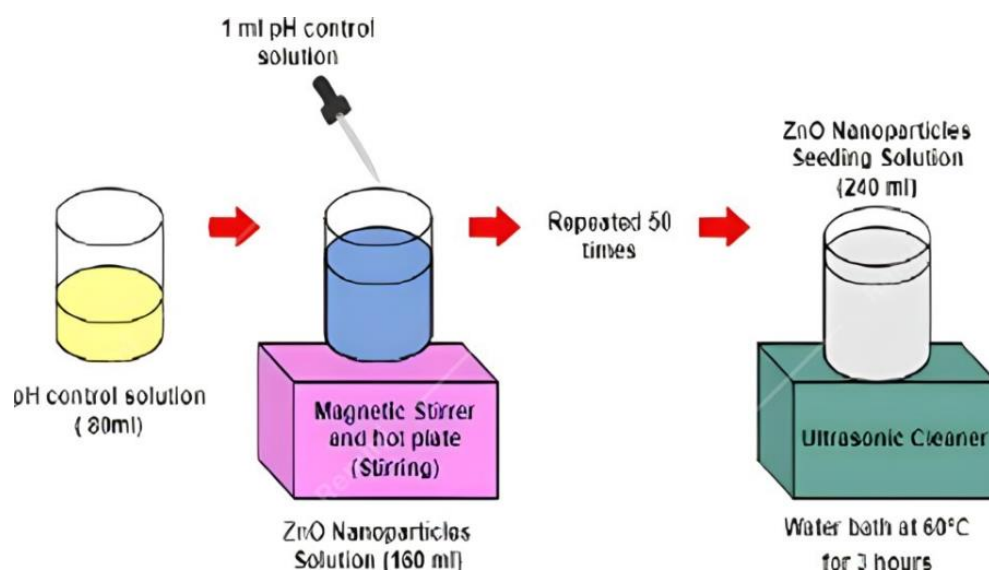


Figure 3.31: Seeding solution preparation.

3.6.3.2 Dipping & Annealing process

Figure 3.32 shows the dipping process. After preparing the seeding solutions. The last process is to dip and dry the fiber. The purpose is to develop a nucleation site on the POF. All the POF samples were submerged into the seeding solution for 1 minute and dried for 1 minute in a chamber with ambient temperature of 70°C. This process is repeated 10 times and lastly the POF is annealed in oven for three hours at 70°C, which can be seen in Figure 3.33.



Figure 3.32: Dipping process for the hydrothermal method

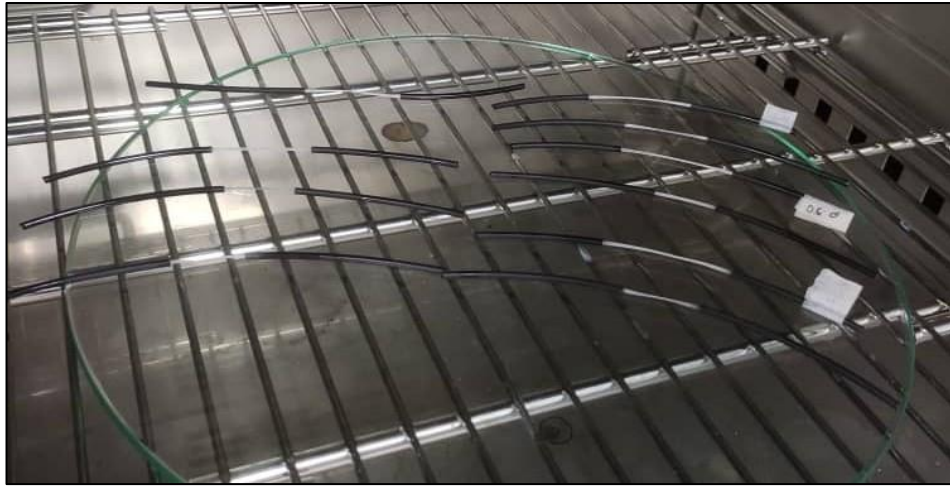


Figure 3.33: Annealing process

3.6.3.3 Growth Process

The last process for the coating of the hydrothermal method was the growth process. This process began with dissolving 2.97g of Zinc Nitrate Hexahydrate and 1.40g of Hexamethylenetetramine in 1000ml of deionized water to produce 10mM solution. All the seeded POF are submerged vertically into the synthesis solution and heated at a temperature of 90 degrees C inside the oven for a total of 10 hours. However, after the 5 hours mark, the solution is replaced with a new solution in order to maintain the growth process condition. After synthesized, the POF is rinsed with DI water several times. Figure 3.34 shows the after result of growth process for 4cm, while Figure 3.35 shows all the fiber after the growth process.



Figure 3.34: 4cm expose fiber with zinc oxide coated.



Figure 3.35: Fiber with zinc oxide coated.

3.7 OPTICAL CHARACTERIZATION

3.7.1 Refractive Index of Water Sample

Before furthering the experiment, the refractive index of each of the water samples was tested and analyzed using the refractometer. The reason for measuring the Refractive Index (RI) of every water sample is because it provides insights into their optical characteristics and how they interact with light.

To initiate the refractometer procedure, the sensing surface is delicately cleansed using ethanol to optimize its sensitivity to the water sample. Subsequently, the functionality of the refractometer is verified by activating the read button on the meter. A proper functioning refractometer should return the meter's reading to a dash line in the absence of any substance on the sensing surface, indicating its readiness for use.

Following the initial checks, the first water sample is carefully pipetted onto the sensing surface, and the read button is pressed. The refractive index (RI) data of the water sample is promptly displayed on the meter and is meticulously recorded in a dedicated table. Subsequently, the sensing surface is once again cleansed with ethanol to ensure the integrity of subsequent readings.

This process is reiterated to determine the refractive indices of the second and third water samples. Once all the requisite data is tabulated, the next step involves plotting a graph of refractive index against each water sample. This graphical representation serves as a crucial tool for further analysis and interpretation of the refractometer readings. The Figure 3.36 shows the measuring of RI for various water samples using the refractometer.



Figure 3.36: The RI measurement of water samples

3.7.2 Optical Output Power

When the refractive index of the water samples was determined and analyzed, the output power of the water is tested by using the light source meter and output power meter. The output power of every water sample is different due to the different water quality in the water sample. By measuring and analyzing the output power of every water sample, this will enable us to know the relationship between output power produced in different water quality levels.

To commence the measurement process, the container is meticulously cleansed using ethanol, along with the careful cleaning of the sensing probe of the Plastic Optical Fiber (POF). Subsequently, the first water sample is poured into the container, ensuring complete filling. The POF sensor is then cautiously connected to both the light source meter and the output power meter, with a specific input of wavelength (850nm) and frequency (0 Hz). It is crucial to verify that both the light source meter and the output power meter are set to the same wavelength and frequency (850nm, 0

Hz) to eliminate any potential errors during the measurement.

The unit of the output power meter is configured to dBm/nW to ensure consistency in measurement units. Following the setup, the POF is gently inserted to make contact with the water sample in the container, ensuring that it is securely held during the sensing process. The data reflecting the output power of the water sample is promptly displayed on the meter and methodically recorded in a designated table.

This series of steps is iterated with different water samples and coated ZnO POF to collect comprehensive data for analysis and comparison. The repetition of the procedure allows for a thorough examination of the optical characteristics of various water samples using the Plastic Optical Fiber sensing technology. Figures 3.37 show the measurement of output power of the water samples.



Figure 3.37: Measurement of output power of the water samples

3.8 ELECTRICAL CHARACTERIZATION

The second part of the experimental work is the electrical characterization. In this experiment, the receiver circuit of the system is connected with the LED light source, the phototransistor sensor and with the Polymer Optic Fiber sensor. The water samples are tested in the electrical characterization to obtain for the output voltage (V_o). The output voltage of every water sample is different due to the different water quality levels present in the water sample. By measuring and analyzing the output power of every water sample, this will enable us to know the relationship between output voltage produced in different water quality levels.

The procedure began with the compilation of the system programming into the NodeMCU. Subsequently, the receiver circuit undergoes an initial test without a light source to establish the reference voltage, which is set at 1985mV. The variable resistor was then adjusted by turning the knob clockwise to achieve the appropriate range for the initial reference voltage.

Following the calibration, the receiver circuit was connected to the LED light source (wavelength: 850nm) and the Plastic Optical Fiber (POF) sensor, and the output voltage was meticulously recorded and configured. Once the setup was complete, the first water sample was pipetted and immersed onto the POF sensor, generating an output voltage that was simultaneously displayed on the LCD screen. The LED indicators are then used to determine the status of water quality.

After the measurement, the sensing part of the POF sensor was gently cleaned using a tissue to ensure accurate subsequent readings. The process was iterated for the remaining water samples and coated ZnO POF, generating a comprehensive dataset for analysis. Finally, the output voltage readings of the various water samples were tabulated and compared, enabling a detailed assessment of their respective optical characteristics and overall water quality. Figure 3.38 shows the process of conducting the electrical characterization experiment.



Figure 3.38: Electrical Characterization experiment

3.9 Summary of Chapter 3

In this chapter, the decision-making process and the overall implementation of the project's aim are meticulously outlined. It encompasses a detailed discussion on the tools and supplies employed for the project, along with their functions and significance. Both the software and hardware designs are elaborated upon, providing insight into the project's implementation process. Additionally, the chapter elucidates the experiment's procedure, which focused on measuring water quality using plastic optical fiber (POF), both uncoated and coated with ZnO. The experimental setup and methodology are described in depth, offering a comprehensive understanding of the procedures undertaken. By delving into the experiment's intricacies, including the choice of materials and the measurement techniques employed, the chapter provides a robust foundation for interpreting the experimental results and drawing conclusions regarding the effectiveness of the proposed approach for water quality monitoring.

CHAPTER 4

RESULTS AND DISCUSSION



— This chapter assembles the project's findings and discussions. It involves acquiring data on samples containing varying proportions of water quality samples, as well as their respective refractive index values. The water quality was based on the concentration of ammonia and pH levels in water samples. Moreover, this chapter also discusses the data analysis that has been collected from the project which is output power, output voltage and from that the sensitivity and linearity have been analyzed. The characterization process is divided into two parts: Optical Characterization and Electrical Characterization.

4.0 SEM and EDX Analysis Confirming ZnO Nanorod Structure and Composition

The ZnO nanorods on the POF were then characterized. Figure 4.1 shows the scanning electron microscope (SEM) image. It confirmed that the structure of ZnO is nanorods based on the rod structure and consists of many superfine nanorods on the POF which would make the coated optical fiber interact with water samples better and faster. The magnification was set at 2.39 KX to observe the ZnO structures coated on the POF. Energy dispersive X-ray (EDX) analysis with an operating voltage of 10 keV was carried out on the ZnO POF to identify the chemical elements as shown in Figure 4.2. The analysis revealed that the topcoat layer on the POF consisted of zinc (78.99%) and oxygen (21.01%), which verified the sensing material for water quality sensing is ZnO.

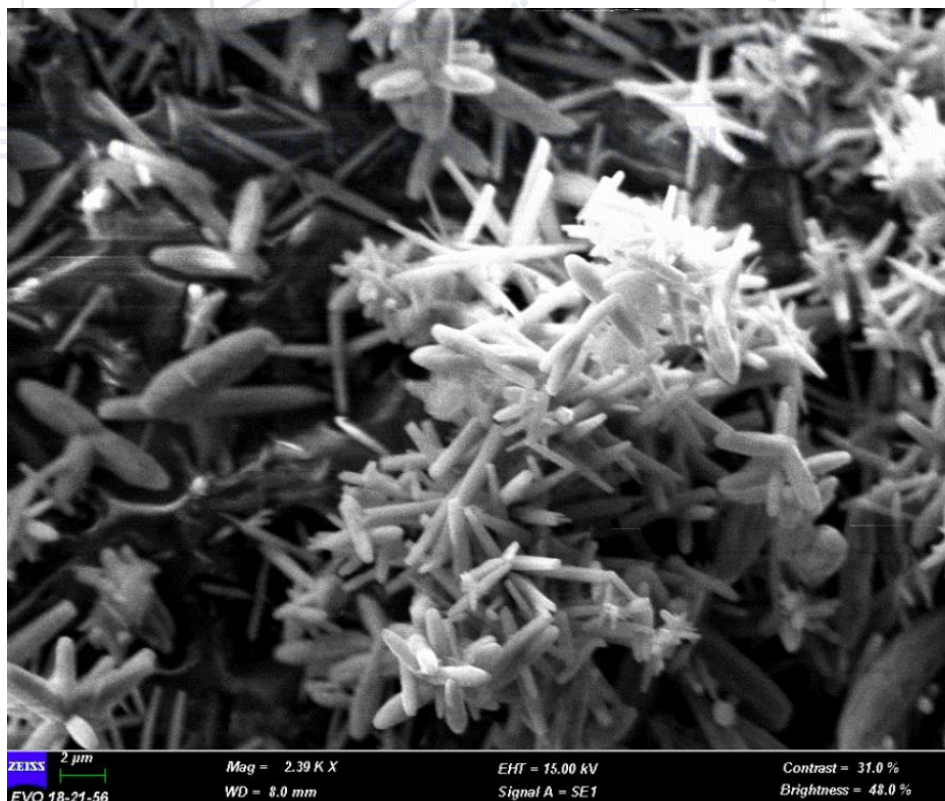


Figure 4.1: Scanning Electron Microscope (SEM) Image of ZnO on POF

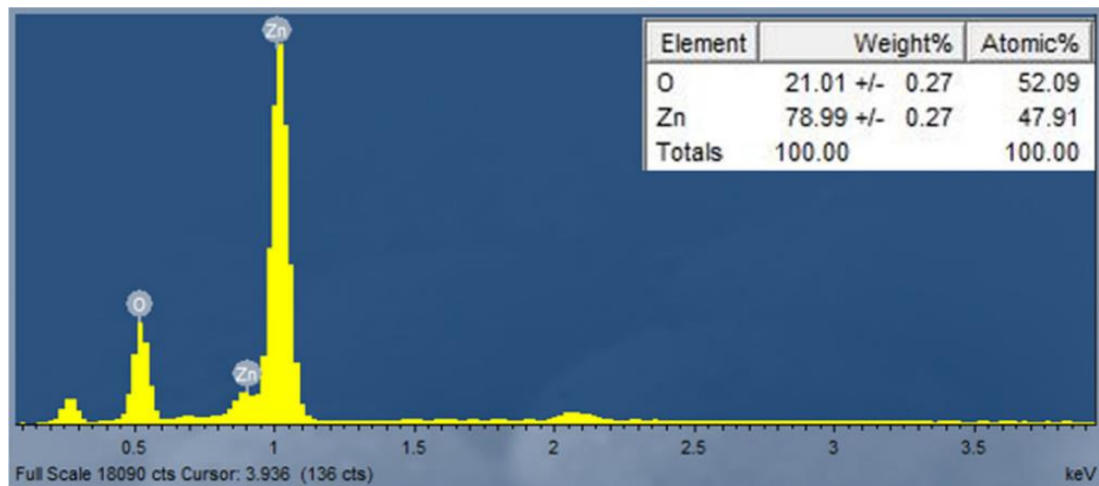


Figure 4.2: EDX elemental analysis of ZnO on POF

4.1 OPTICAL CHARACTERIZATION

For the Optical Characterization part, the results of refractive index of water samples due to the variation of pH level and concentration of Ammonia were observed.

The results of output power produced by the water samples was then analyzed.

4.1.1 Refractive Index of Water Samples with the Variation of PH Levels

Different levels of pH in water samples were used in order to study its effect sensor to the refractive index change of the water samples. Table 4.1 shows the refractive index measured on each of pH values using the digital refractometer. The results show that as the pH of the solution increases from 5pH to 9pH, the RI gradually increases from 1.3329 to 1.3347. Refractive indexes of samples will influence how much light travels through the water samples, which will change the readings from the refractometer. This information holds practical value in various applications, such as ensuring quality control during the production of drinking water and analyzing the composition of drinking water in laboratory environments.

Table 4.1: pH values and Refractive Index

Water Sample No	PH Levels	Refractive Index
1	5	1.3329
2	6	1.3348
3	7	1.3383
4	8	1.3406
5	9	1.3447

Figure 4.3 depicts the refractive index changes as the pH levels in water sample varies. The rising trendline in the graph indicates that the increase the PH levels raises the refractive index of the water samples. Refractometry relies on the principle that the speed of light changes as it passes through different mediums. In the context of pH measurement, the refractive index of a solution alters with changes in the concentration of hydrogen ions (H^+) or hydroxide ions (OH^-), which are the constituents of acidity and alkalinity, respectively. As the pH level increases, indicating a shift towards alkalinity or basicity, the concentration of hydroxide ions (OH^-) in the solution rises. This increase in hydroxide ions leads to a decrease in the concentration of hydrogen ions (H^+), resulting in a higher pH level.

The change in pH level also affects the density and composition of the solution. Alkaline solutions have a lower density compared to acidic solutions due to the presence of fewer hydrogen ions. As a result, the refractive index of the solution increases with increasing pH levels. It can be concluded that the pH levels directly proportional to the refractive indexes.

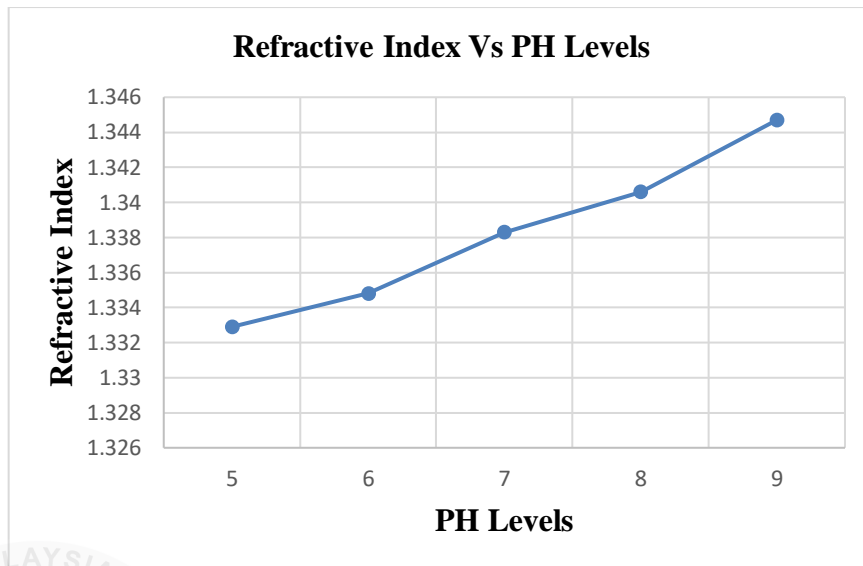


Figure 4.3: The graph of Refractive Index against pH value

4.1.2 Refractive Index of Water Samples with the Variation of Ammonia Concentration

The concentration of ammonia in water samples was gradually increased by 0.2mg/L, range from 1mg/L to 1.8 mg/L. The initial sample consists of 1.0 mg/L of ammonia, resulting in a refractive index of 1.4811. Other four water samples were prepared, with 1.2mg/L, 1.4mg/L, 1.6mg/L and 1.8mg/L of ammonia. For instance, in the second sample, there is 1.2mg/L of ammonia, resulting in a slightly higher refractive index of 1.4831. Table 4.2 summarized the refractive index observed for each mixture sample. The refractive index for the second to fifth samples were 1.4831, 1.4883, 1.4916 and 1.4947, respectively. From Table 4.2, the refractive index of can be influenced by varying concentration of ammonia. Hence, the refractive index is an important optical property that describes the behavior of light as it travels through a water samples. This information holds practical value in various applications, such as ensuring quality control during the production of drinking water and analyzing the composition of drinking water in laboratory environments.

Table 4.2: Concentration of Ammonia and Refractive Index

Water Sample No	Concentration of Ammonia (mg/L)	Refractive Index
1	1	1.4811
2	1.2	1.4831
3	1.4	1.4883
4	1.6	1.4916
5	1.8	1.4947

Figure 4.4 depicts the refractive changes as the concentration of the ammonia sample varies. The rising trendline in the graph indicates that the increase the concentration of ammonia raises the refractive index of the water samples. Preventing an increase in ammonia concentration is crucial for maintaining good water quality because changes in ammonia levels can significantly affect the refractive index of water. The refractive index is a measure of how much light bends when passing through a substance. It is directly proportional to the concentration of ammonia particles in water samples. Therefore, when more ammonia molecules are present in the solution, there are more particles for the light to interact with, leading to a greater bending of light and consequently, a higher refractive index.

High ammonia levels alter the refractive index, potentially leading to incorrect assessments of water quality. Accurate refractive index measurements are essential for ensuring the reliability of water quality monitoring systems. It can be concluded that the concentration of ammonia directly proportional to the refractive indexes.

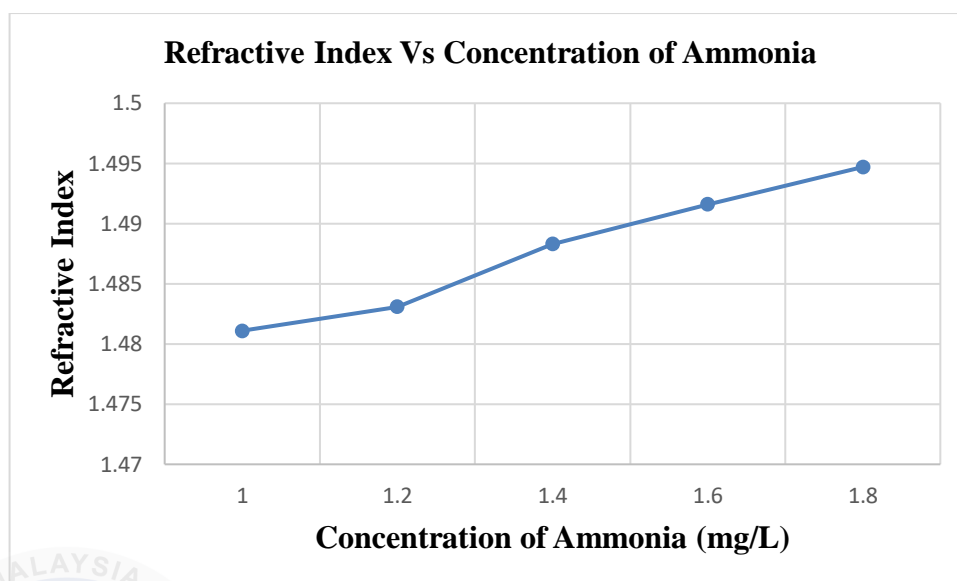


Figure 4.4: The graph of Refractive Index against Concentration of Ammonia

4.1.3 Optical Output Power

The output power for the five samples was measured and recorded for both uncoated and ZnO coated POF. The POF sensor was connected to a light source of a red light-emitting diode (LED) whilst another tip end was connected to the optical power meter (OPM) to measure the output power. In this experiment, the light source of a red LED of wavelength 650 nm was used. From the experiment, both ZnO coated and uncoated plastic optical fiber were used to measure the output power. The output power was calculated in μW .

4.1.4 Output Power of water sample with the Variation of Ammonia Concentration (Uncoated and Coated POF)

Table 4.3 shows the power output measured in μW for uncoated and zinc oxide coated POF respectively. From Table 4.3, It can be examined that as the concentration

of ammonia increases, the output power is decreased. Subsequently, 5 water samples were prepared as in previous measurement, containing 1 mg/L, 1.2 mg/L, 1.4 mg/L, 1.6 mg/L and 1.8 mg/L of ammonia. The output power of Uncoated POF decreases from 4.6983 μ W to 4.3698 μ W while Coated zinc oxide POF decreases from 4.7885 μ W to 4.3598 μ W, as the refractive index increases, as plotted in Figure 4.5 and Figure 4.6.

Table 4.3: Concentration of Ammonia and Output Power (Uncoated and Coated)

Water Sample No	Concentration of Ammonia (mg/L)	Output Power (μ W)	
		Uncoated	Coated
1	1	4.6983	4.7885
2	1.2	4.6324	4.6621
3	1.4	4.5493	4.5692
4	1.6	4.4264	4.4354
5	1.8	4.3698	4.3598

According to both Figures 4.5 and 4.6, the amount of output power produced steadily decreases as the concentration of ammonia that is present in the water sample increases. The results can be related to previous research by [30], showing similar trends where the power value decreased as the concentration of ammonia raised. As the concentration of ammonia increases, it introduces additional molecules into the environment surrounding the fiber optic sensor. These ammonia molecules can interact with the light propagating through optical fiber, causing changes in its properties.

One of the primary mechanisms through which this occurs is through absorption. Ammonia molecules have specific absorption bands in the infrared region of the electromagnetic spectrum. When light interacts with these molecules, it can be absorbed, leading to a decrease in the intensity of light reaching the sensor's detector. This absorption phenomenon becomes more pronounced as the concentration of ammonia increases, resulting in a decrease in output power.

Furthermore, the interaction between light and ammonia can also lead to scattering phenomena. Ammonia molecules may scatter light as it propagates through the optical fiber, leading to deviations in its path and ultimately reducing the intensity of light reaching the detector.

As a result of this analysis, the output power measured by the coated POF was higher than uncoated POF. It is possible to deduce that the coated ZnO POF sensor will have a higher degree of sensitivity in situations in which there is less energy being lost to the water sample. Other than that, ZnO was able to increase the sensitivity of the optical sensor. In a nutshell, the output power produced by the water sample will be lower in proportion to the concentration of ammonia that is present in the sample.

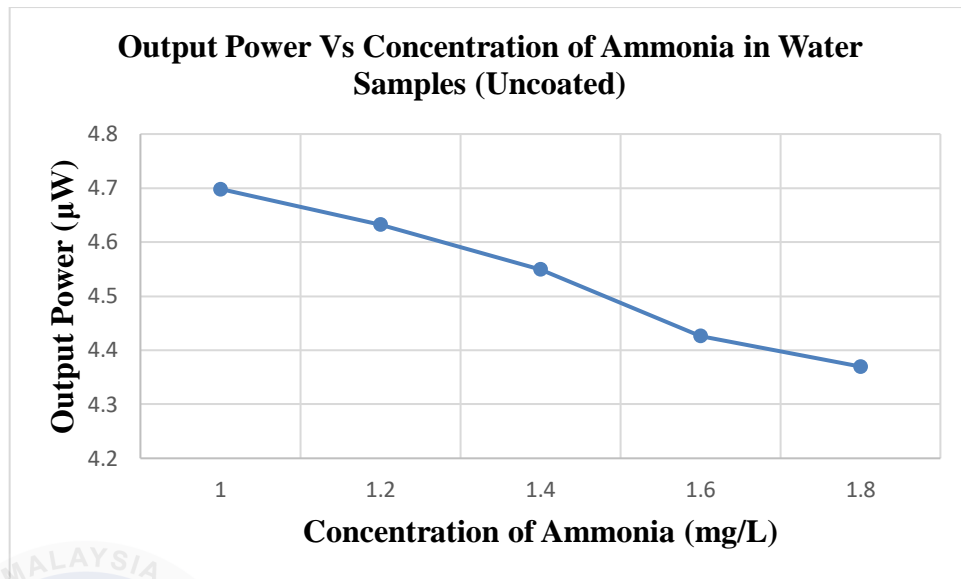


Figure 4.5: The graph of Output Power against Concentration of Ammonia (Uncoated)

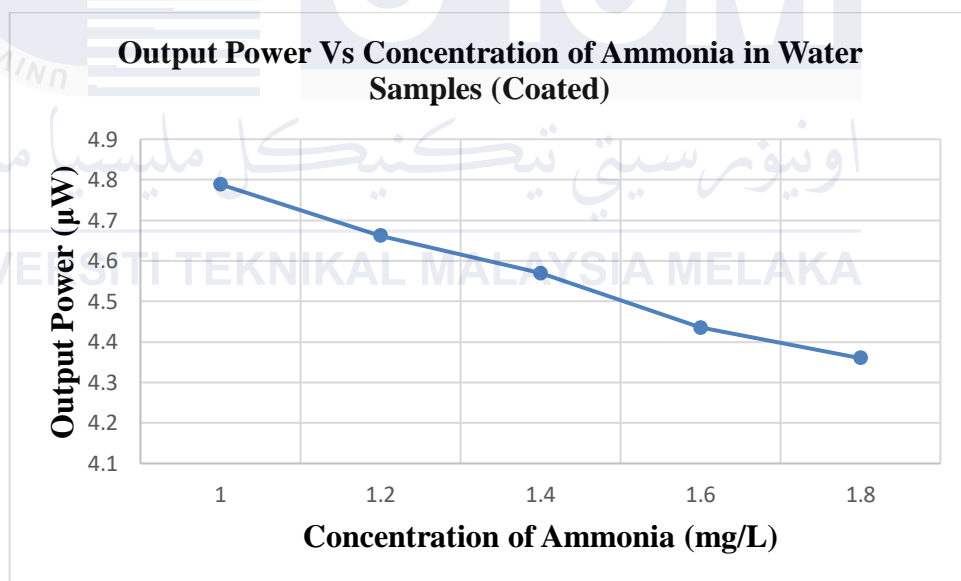


Figure 4.6: The graph of Output Power against Concentration of Ammonia (Coated)

4.1.5 Output Power of water sample with the Variation of PH Values (Uncoated and Coated POF)

From Table 4.4, it can be examined that as the PH levels increase, the output power is decreased. The table shows the power output measured in μW for uncoated and zinc oxide coated POF, respectively. Subsequently, 5 water samples were prepared to get better accuracy, containing 5, 6, 7, 8 and 9 of PH levels. The output power of uncoated POF decreases from $3.3868 \mu\text{W}$ to $2.8247 \mu\text{W}$ while coated zinc oxide POF decreases from $3.4968 \mu\text{W}$ to $2.8398 \mu\text{W}$, as the refractive index increases, as plotted in Figure 4.7 and Figure 4.8.

Table 4.4: PH Levels and Output Power (Uncoated and Coated)

Water Sample No	PH Levels	Output Power (μW)	
		Uncoated	Coated
1	5	3.3868	3.4968
2	6	3.2176	3.2676
3	7	3.1393	3.1893
4	8	2.9016	2.9916
5	9	2.8247	2.8398

According to both graphs, the amount of output power produced steadily decreases as the PH levels of water sample increases. The results can be related to previous research by [27], showing similar trends where the power value decreased as the pH raised. As the pH level increases, indicating a shift towards alkalinity or basicity, it triggers modifications in the optical properties of the surrounding environment. These

changes influence the propagation of light through the optical fiber, ultimately affecting the intensity of light reaching the sensor's photodetector and the resulting output power.

One primary mechanism through which this interaction occurs is through changes in the absorption properties of the medium. Certain pH-sensitive compounds or ions may absorb light at specific wavelengths, attenuating the intensity of light reaching the sensor's photodetector. This absorption effect leads to a reduction in the electrical signal generated by the photodetector, resulting in a decrease in the output power of the sensor as pH levels increase.

Additionally, alterations in pH levels can also impact the refractive index of the medium, affecting the propagation of light within the optical fiber. As pH levels increase, leading to higher alkalinity, the refractive index of the medium undergoes corresponding variations. Changes in refractive index can further modify the distribution of light reaching the photodetector and contribute to variations in the sensor's output power. In general, an increase in pH concentration leading to increased alkalinity can result in a decrease in the output power of the sensor.

As a result of this analysis, the output power measured by the coated POF was higher than uncoated POF. It is possible to deduce that the coated ZnO POF sensor will have a higher degree of sensitivity in situations in which there is less energy being lost to the water sample. Other than that, ZnO was able to increase the sensitivity of the optical sensor. In a nutshell, the output power produced by the water sample will be lower in proportion to the pH levels that is present in the sample.

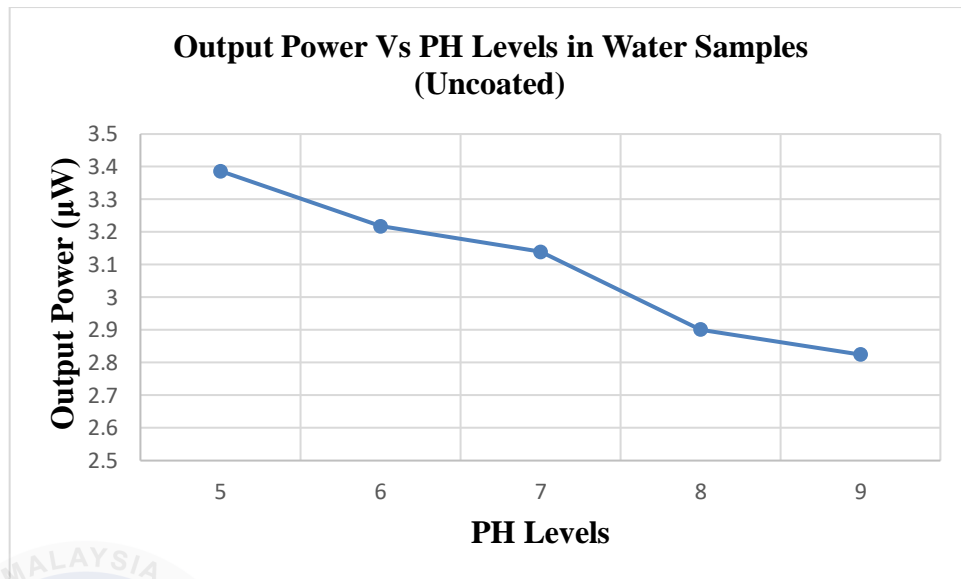


Figure 4.7: The graph of Output Power against PH Levels (Uncoated)

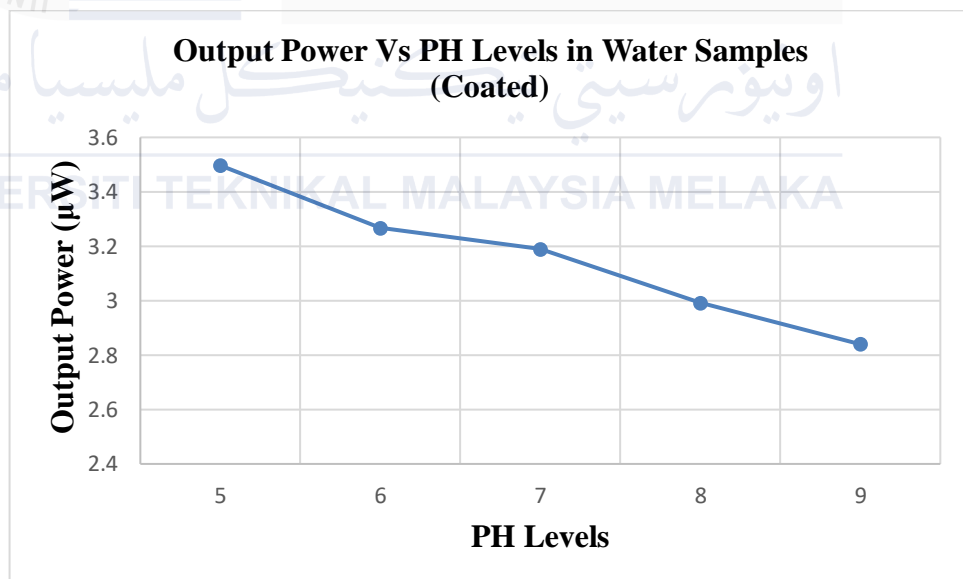


Figure 4.8: The graph of Output Power against PH Levels (Coated)

4.2 ELECTRICAL CHARACTERIZATION

For electrical characterization, the input source of light of red LED with wavelength 650nm was supplied to the polymer optical as input whilst the tip end of uncoated POF and coated zinc oxide POF was attached to a receiver circuit, which consists of a photodiode and an amplifier for output voltage measurement.

4.2.1 Output Voltage of Water Samples with the Variation of Ammonia Concentration

Table 4.5 shows the voltage of water samples with different concentrations of ammonia for both zinc oxide coated and non-coated. This voltage is produced because of the angle of refraction of the light source passing through the POF sensor. Referring to Table 4.5, the output voltage in voltage decreases progressively as the concentration of ammonia increases. When the POF sensor is immersed in various water samples, the rate at which the light source passes through the POF sensor will vary. Consequently, as the concentration of ammonia increases, it introduces additional molecules into the surrounding environment. These ammonia molecules can interact with the light propagating through the optical fiber, leading to changes in its properties. In brief, as the concentration of ammonia increases, the output voltage produced by the water sample will decrease.

Table 4.5: Concentration of Ammonia and Output Voltage (Uncoated and Coated)

Water Sample No	Concentration of Ammonia (mg/L)	Output Voltage (V)	
		Uncoated	Coated
1	1	1.3983	1.4563
2	1.2	1.2324	1.2924
3	1.4	1.1493	1.1893
4	1.6	0.9264	0.9964
5	1.8	0.8698	0.9198

From the graph of output voltage for uncoated POF as shown in Figure 4.9 and coated POF with Zinc Oxide as shown in Figure 4.10, it is shown that the voltage decreases proportion to the concentration of ammonia. The results can be related to previous research by [31], showing similar trends where the voltage value decreased as the concentration of ammonia raised. One primary mechanism through which this interaction occurs is through changes in the absorption properties of the medium. Ammonia molecules have specific absorption bands in the ultraviolet or visible regions of the electromagnetic spectrum. When light encounters these molecules, it can be absorbed, attenuating the intensity of light reaching the sensor's photodetector. This absorption effect results in a reduction in the electrical signal generated by the photodetector, leading to a decrease in the output voltage of the sensor as the concentration of ammonia increases.

Additionally, alterations in ammonia concentration can also influence the refractive index of the medium, affecting the propagation of light within the optical fiber.

Changes in refractive index can further modify the distribution of light reaching the photodetector and contribute to variations in the sensor's electrical output.

Besides that, the coated POF has a higher voltage sensing than the uncoated POF. The nanoparticles from the ZnO successfully changed the optical nature of the plastic optical fiber and enhanced the sensitivity of sensing the voltage of the water sample.

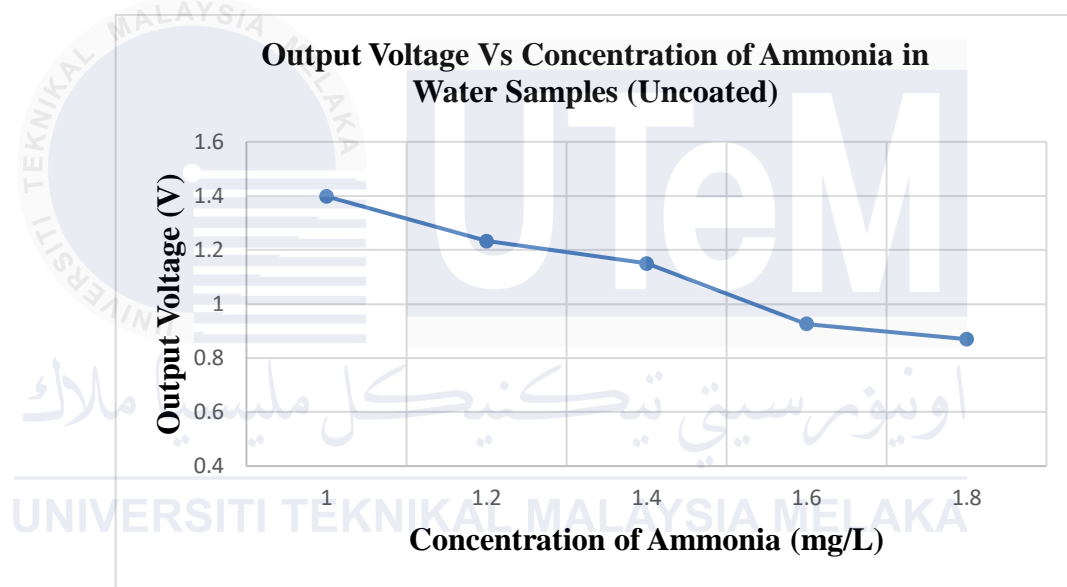


Figure 4.9: The graph of Output Voltage against Concentration of Ammonia (Uncoated)

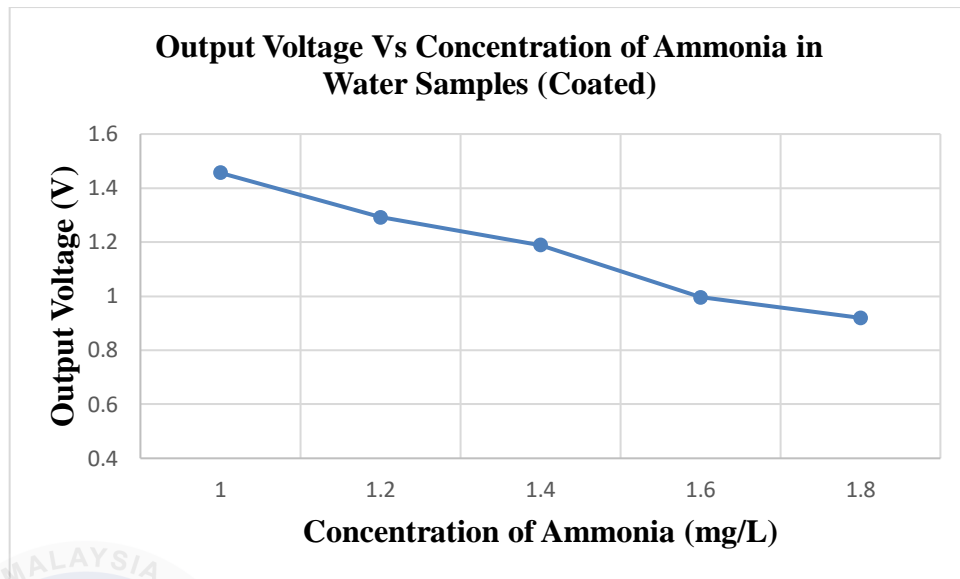


Figure 4.10: The graph of Output Voltage against Concentration of Ammonia (Coated)

4.2.2 Output Voltage of Water Samples with the Variation of PH Levels

Table 4.6 shows the voltage of water samples with different pH levels for both zinc oxide coated and non-coated. This voltage is produced because of the angle of refraction of the light source passing through the POF sensor. Referring to Table 4.6, the output voltage in voltage decreases progressively as the pH levels increase. When the POF sensor is immersed in various water samples, the rate at which the light source passes through the POF sensor will vary. Consequently, as the pH levels increases, it introduces additional molecules into the surrounding environment. These pH molecules can interact with the light propagating through the optical fiber, leading to changes in its properties. In brief, as the pH levels increase, the output voltage produced by the water sample will decrease.

Table 4.6: PH Levels and Output Voltage (Uncoated and Coated)

Water Sample No	PH Levels	Output Voltage (V)	
		Uncoated	Coated
1	5	1.2886	1.3663
2	6	1.1324	1.2328
3	7	1.0493	1.1596
4	8	0.8964	0.9864
5	9	0.7798	0.8698

From the graph of output voltage for uncoated POF as shown in Figure 4.11 and coated POF with Zinc Oxide as shown in Figure 4.12, it is shown that the voltage decreases proportion to the pH levels. The results can be related to previous research by [28], showing similar trends where the voltage value decreased as the pH raised.

As the pH level increases, signifying a shift towards alkalinity or basicity, it initiates modifications in the optical properties of the surrounding environment. These changes influence the amount of light reaching the sensor's photodetector and subsequently affect the electrical output of the sensor. One primary mechanism through which this interaction occurs is through changes in the absorption properties of the medium. Certain pH-sensitive compounds or ions may absorb light at specific wavelengths, attenuating the intensity of light reaching the sensor's photodetector. This absorption effect leads to a reduction in the electrical signal generated by the photodetector, resulting in a decrease in the output voltage of the sensor as pH levels increase.

Additionally, alterations in pH levels can also impact the refractive index of the medium, affecting the propagation of light within the optical fiber. Changes in

refractive index can further modify the distribution of light reaching the photodetector and contribute to variations in the sensor's electrical output. In general, an increase in pH concentration leading to increased alkalinity can result in a decrease in the output voltage of the sensor.

Besides that, the coated POF has a higher voltage sensing than the uncoated POF. The nanoparticles from the ZnO successfully changed the optical nature of the plastic optical fiber and enhanced the sensitivity of sensing the voltage of the water sample.

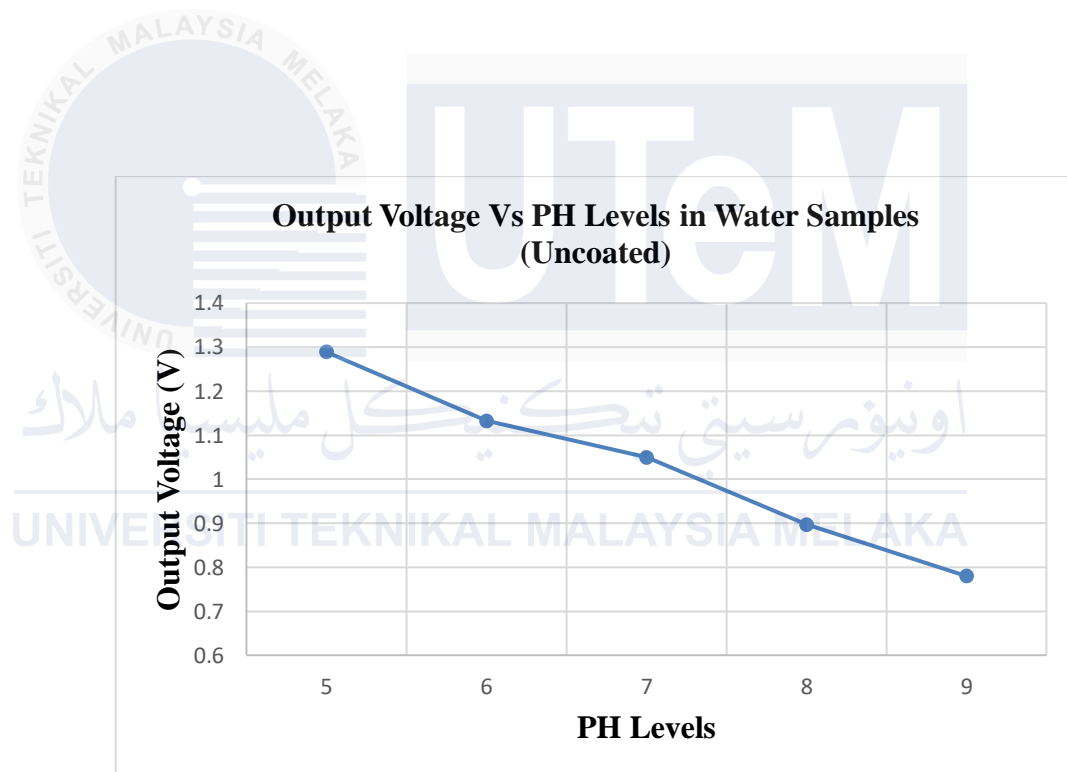


Figure 4.11: The graph of Output Voltage against PH levels (Uncoated)

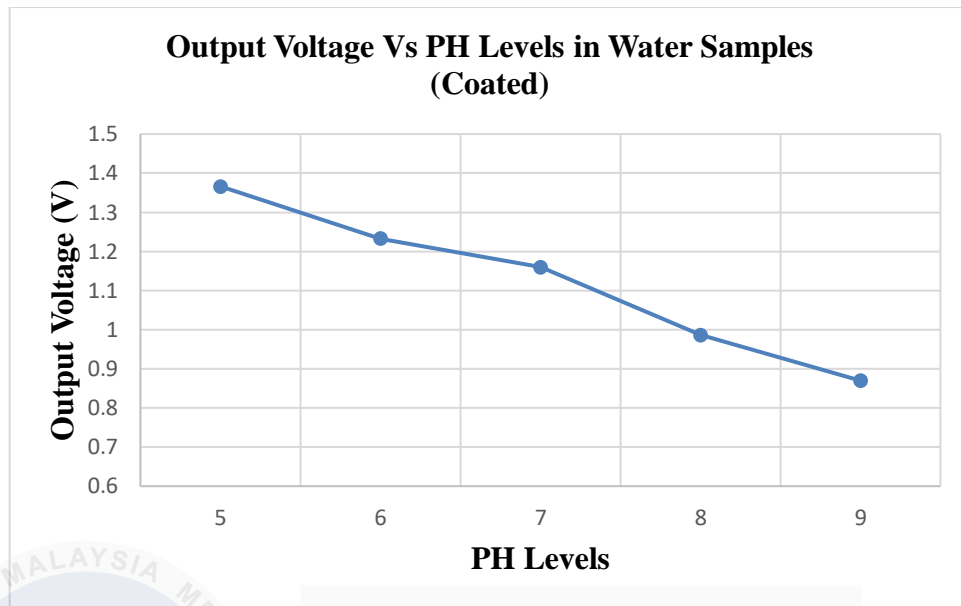


Figure 4.12: The graph of Output Voltage against PH Levels (Coated)

4.3 Sensitivity and Linearity Comparison of Uncoated POF and Coated POF

Sensitivity and linearity between uncoated POF and coated POF based on the output voltage can be observed for both coated and uncoated POF. From the analysis, the output voltage shown by the coated POF has a better sensitivity and linearity than the uncoated POF.

This circumstance contributes to the negative slope that represents the sensitivity of the sensor. From the graph, the mathematical expression to estimate the sensor performance that relates the output voltage and concentration of ammonia /pH levels can be formulated as:

$$y = mx + c \quad Eq(4.1)$$

where:

y = Output voltage

x = Concentration of ammonia / pH levels

c = y-intercept in line graph

The equation represents the y as the output voltage, x as the concentration of ammonia and pH levels in water samples and c as the y-intercept in the line graph. From mathematical modelling, the sensitivity of the polymer optical fiber sensor can be determined by the gradient of the graph.

4.3.1 Sensitivity and Linearity of Uncoated and Coated ZnO POF with the Variation of Ammonia Concentration

Figure 4.13 shows the sensor sensitivity and linearity for Uncoated POF and Coated ZnO POF. Based on Figure 4.13, the Coated ZnO POF produces the higher sensitivity of $-0.0128 \text{ V/mg}L^{-1}$ with linearity of 0.9861. While Uncoated POF produces the sensitivity of $-0.0085 \text{ V/mg}L^{-1}$ with linearity of 0.9731. Moreover, it is clear from Figure 4.13 that the output voltage decreases as the ammonia concentration increases.

The sensitivity was calculated from the analysis from the value of output voltage divided by the concentration of ammonia. Moreover, Using the Beer-Lambert law, the concentration of the ammonia can be determined by measuring the absorbance. By comparing the sample's absorbance to known concentrations of ammonia, it is possible to construct a calibration curve that allows for the estimation of the ammonia concentration in a water sample.

$$I = I_0 e^{(-ax)} \quad \text{Eq (4.2)}$$

I Represent the intensity of the light emitted at a specific distance x from the source in this expression. I_0 represents the incident or initial light intensity, whereas a represents the absorption coefficient of the medium. x represents the distance light has travelled within a medium. As light passes through an absorbing medium, its intensity decreases exponentially, as represented by the equation. Attenuation or intensity diminution caused by absorption is described by the exponential term $e^{(-ax)}$. The adsorption coefficient measures the intensity with which a medium absorbs light at a specific wavelength. It depends on variables such as the properties of the medium, the concentration of the absorbing species, and the wavelength of the light. This equation defines the light attenuation caused by absorption, whereas the Beer-Lambert law explains the relationship between the concentration of an absorbing substance and light absorption.

As aforementioned, concentration of ammonia caused RI changes at the sensing region, thus increasing the numerical aperture at the sensing region. Increasing of numerical aperture causes more light loss to the surrounding medium. This condition creates an evanescence field around the sensing region within the surrounding medium where analyte in the surrounding medium absorbs the light used for the transmission. Therefore, as the amount of ammonia increases, more light is absorbed, and it causes decreasing of light detected (negative slope) [31]. The output voltage for straight fiber optic sensor increases linearly with the ammonia concentration as shown in Figure 4.13. This is because straight sensor has uniform RI at the sensing area, resulting in the refractive index on the core remains constant. In theory, as ammonia concentration increases, the refractive index of the sample also increases. Due to this circumstance, when the ammonia concentration increases, the difference between the refractive index of water sample and the refractive index of

fiber core will decrease. This condition contributes to higher light loss, causing a decrease in the output voltage [32]. The zinc oxide-coated optical sensor offers a sensitive and selective method for detecting contaminants in water samples.

Table 4.7: Sensitivity and Linearity of Uncoated and Coated ZnO POF with Variation Ammonia Concentration

POF	Output Voltage (V)	
	Sensitivity	Linearity, R^2
Uncoated	-0.0085	0.9731
Coated ZnO	-0.0128	0.9861

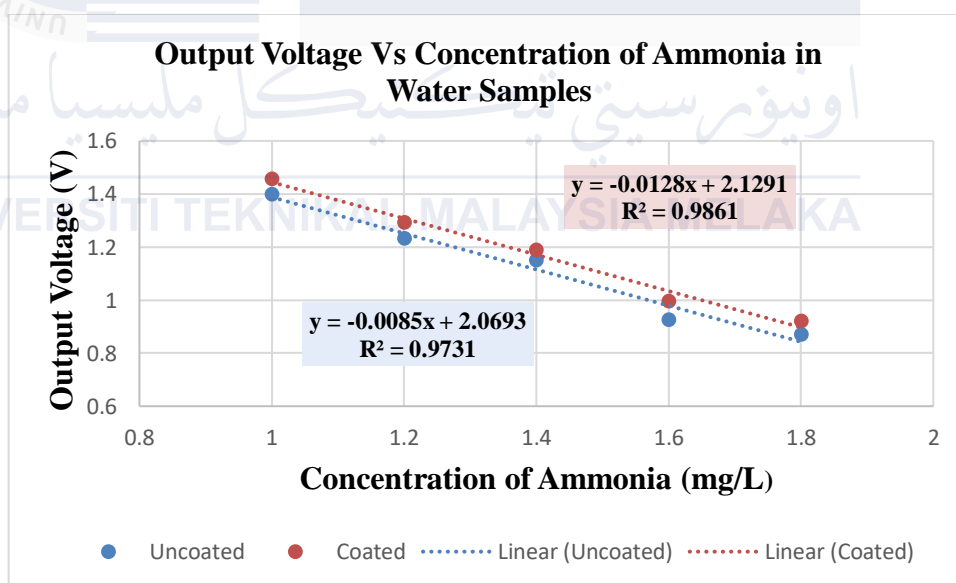


Figure 4.13: Sensitivity and Linearity of Uncoated and Coated ZnO POF with Variation Ammonia Concentration

4.3.2 Sensitivity of Uncoated and Coated ZnO POF with the Variation of pH Levels

The results of measurement are used to determine sensor characteristics. Characteristic values of pH based on POF include determining the value of the output voltage range, sensitivity, and linearity. Based on Figure 4.14 the Coated ZnO POF produces the higher sensitivity of -0.0419 V/pH with linearity of 0.9887. While Uncoated POF produces the sensitivity of -0.0384 V/pH with linearity of 0.9735. Moreover, it is clear from Figure 4.14 that the output voltage decreases as the PH levels increase.

The sensitivity was calculated from the analysis. The difference value between the maximum output voltage toward the minimum output voltage, namely range (ΔV). Sensitivity level of quantity sensor measured, namely sensitivity (S). While, the smallest value of a quantity measured, namely resolution (R). They are calculated by using the equations below:

$$\Delta V = V_{max} - V_{min}$$
$$S = \frac{V_{max} - V_{min}}{pH_{max} - pH_{min}}$$

Where V_{max} is the maximum output voltage and V_{min} is the minimum output voltage. The pH_{max} as maximum pH value and pH_{min} as the minimum pH value.

In Figure 4.14 shows that the coated ZnO affects the characteristics values of the sensor. The best measurement result is shown in POF sensor type of Coated ZnO, i.e. sensitivity -0.0419 V/pH and linearity 0.9887. This shows that Coated ZnO POF sensor, the more power losses contained in POF. Increased power losses are also

caused by the type of sensor peel. The sensor type of Coated ZnO has a greater power loss compared to the type of with Uncoated. In addition, the power losses resulted from the measurement of pH based on POF sensor are also affected by the pH solution refractive index. The refractive index of the pH solution increases will affect the refractive index around on the POF sensor causes the power losses increasing. It causes a decreasing of output voltage and output power, so the range and sensitivity of sensor are also greater. This research has suitability with previous research about POF as pH sensor that increasing the pH range results cause higher sensitivity [28]. Another suitability of the research is the higher refractive index of the solution measured using a POF sensor causes the sensor output voltage to decrease [29]. Measurement of the pH value based on POF as sensor is suitable for use with advantages such as have a simple measurement process and high sensitivity.

Table 4.8: Sensitivity and Linearity of Uncoated and Coated ZnO POF with Variation of PH Levels

POF	Output Voltage (V)	
	Sensitivity	Linearity, R^2
Uncoated	-0.0384	0.9735
Coated ZnO	-0.0419	0.9887

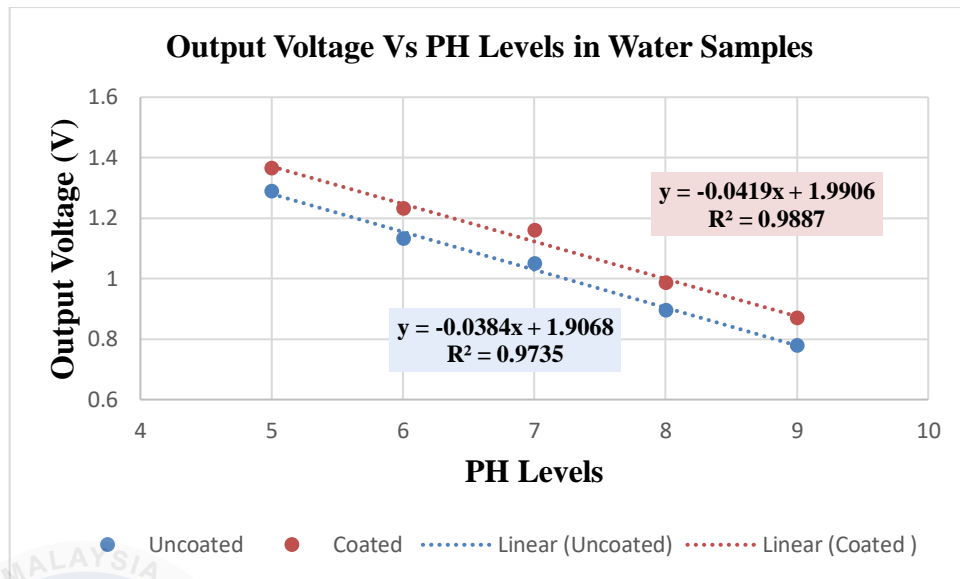


Figure 4.14: Sensitivity and Linearity of Uncoated and Coated ZnO POF with variation of PH Levels

4.4 Importance of Zinc oxide in Sensitivity of POF

The nanoparticles from the ZnO successfully increase the sensing, optoelectronics, energy storage of the plastic optical fiber. Their unique qualities, like a high surface area, a bandgap that can be changed, and good photocatalytic activity. As a result, the ZnO was a suitable chemical substance to enhance the potential of the plastic optical fiber to function as sensor in this project. Zinc oxide is well-known for its sensing properties and ability to interact with substances. Incorporating a zinc oxide-coated optical sensor enables the detection and quantification of adulterants based on changes in absorbance. The interaction of the sensor's surface with the adulterant molecules alters the quantity of light absorbed by the sensor.

There have been significant numbers of studies on optical sensors based on nanostructure materials such as zinc oxide (ZnO) [6], tungsten disulfide (WS₂) [7], tin

oxide (SnO₂) [8], titanium dioxide (TiO₂) [9], polyethyleneimine (PEI), and graphene oxide (GO) [10]. Among them, ZnO has been widely used for sensing as it is a high refractive index (RI) material (RI = 2.008), in which the surface adsorption of water molecules onto the ZnO leads to changes in the optical properties of ZnO [22]. By using an optical fiber for sensing, the complex RI can be modified by coating the optical fiber with the nanostructure material [23]. ZnO has distinctive optical and electrical features such as thermal stability, good electrical conductivity with a high exciting binding energy (60 meV), a large bandgap energy (3.37 eV), and reactive surfaces for chemisorption of molecular water at ambient temperature. One of the main features of ZnO nanorods is that their effective RI changes during exposure to water, causing higher light scattering loss via the nanorods' structure. This effect contributes to changes in light transmission and increases the sensitivity to water samples.

— As mentioned previously, in order to be used as a POF sensor, one of the most important components is the sensitive layer that changes its properties in response to the presence of a particular analyte. Characteristics such as sensitivity or response time are highly dependent on the performance and characteristics of the sensitivity layer. Zinc Oxide are ideal candidates due to their characteristics like absorption, emission, charge transfer, and complexing properties due to the rod structure. In this project increased the sensitivity of the sensor by coating the optical fiber with ZnO.

4.5 Adoptability of Glass Fiber Optic

The main technical challenge for a glass fiber-based nephelometer is the small core sizes of glass fibers. Typical core sizes of glass fibers range from 10 μm to 200 μm in diameter, which are markedly smaller than the core sizes of plastic fibers (typically > 1 mm). As a result, the amount of scattered light that can be collected by a glass fiber is orders-of-magnitude lower than a plastic fiber due to the much smaller light-collecting area of the glass fiber. With lower collected optical power, glass-fiber turbidity sensors are projected to have poor signal-to-noise ratios (SNR) and hence reduced turbidity sensitivity. This is why polymer optical fibers (POF) have been widely studied for water quality measurement while little research has been reported on glass fiber-based nephelometers.

4.6 Comparative with Previous Study

In this project, employed a hydrothermal zinc oxide (ZnO) process integrated with polymer optical fibers (POF) to develop an advanced fiber optic sensor for water quality monitoring. This innovative approach is compared to previous studies that have utilized various materials and methods for similar purposes. Previous research often focused on different nanomaterials and fabrication techniques to enhance the sensitivity and accuracy of fiber optic sensors. However, many of these studies faced challenges such as high production costs, complex manufacturing processes, and limited sensitivity to certain contaminants.

In contrast, the hydrothermal ZnO process offers a cost-effective, environmentally friendly method to produce high-purity, well-crystallized ZnO nanostructures. These

structures, when combined with POF, significantly improve the sensor's interaction with light and its sensitivity to changes in water quality, particularly in detecting contaminants such as ammonia and pH levels. This project aims to build on the strengths and address the weaknesses of previous research by providing a more reliable, efficient, and sensitive water quality monitoring solution.

4.6.1 Comparison of Previous Developments for Detection of Concentration Ammonia in Water Samples

Table 4.9 shows the performance comparison of the previous developments for detection of concentration ammonia in water samples. The performance of each sensor is compared into two performance parameters: Sensitivity and linearity. Based on Table 4.9, the performances of this coated ZnO are comparable competitive with respect to others. It can be observed that the sensor with the coated ZnO shows better performance in terms of sensor sensitivity and linearity i.e. sensitivity $0.0128 \text{ V/mgL}^{-1}$ and linearity 0.9861. This proves that Coated ZnO POF sensor improves the performance of sensor in detecting different ammonia concentration.

In other words, this indicates that a coated ZnO POF sensor experiences increased power losses, influenced by the type of sensor peel. The POF sensor type of coated ZnO has a greater power loss compared to the type with uncoated POF sensor. These sensors experience higher power losses due to the coating, which introduces additional scattering and absorption. The refractive index of the concentration ammonia impacts the refractive index around the POF sensor, influencing power losses. These losses can lead to decreased output voltage and power. Despite the increased power losses, the coated ZnO POF sensors may still exhibit higher sensitivity compared to their uncoated counterparts. This higher sensitivity arises from the improved optical

properties conferred by the coating, which enhances the sensor's ability to detect subtle changes in concentration ammonia. This research has suitability with previous research about POF as water monitoring sensor that increasing the concentration of ammonia results cause higher sensitivity [30]. Another suitability of the research is the higher refractive index of the solution measured using a POF sensor causes the sensor output power decreases [31]. Measurement of the ammonia concentration based on POF as sensor is suitable for use with advantages such as have a simple measurement process and high sensitivity. These findings underscore the importance of considering coating materials and solution properties in POF sensor design and application.

Table 4.9: Performance comparison of the Previous Developments for Detection of Concentration Ammonia in Water Samples.

Types of POF	Sensitivity, V/mgL^{-1}	Linearity, R^2
U-shaped Bent [30]	0.0020	0.9099
Balloon-like Bent [31]	0.0060	0.9154
Coated ZnO [This Work]	0.0128	0.9861
Uncoated ZnO	0.0085	0.9731

4.6.2 Comparison of Previous Developments for Detection of pH Levels in Water Samples

Table 4.10 shows the performance comparison of the previous developments for detection of pH levels in water samples. From Table 4.10 shows that the different types of POF used affects the characteristics values of the sensor. The best

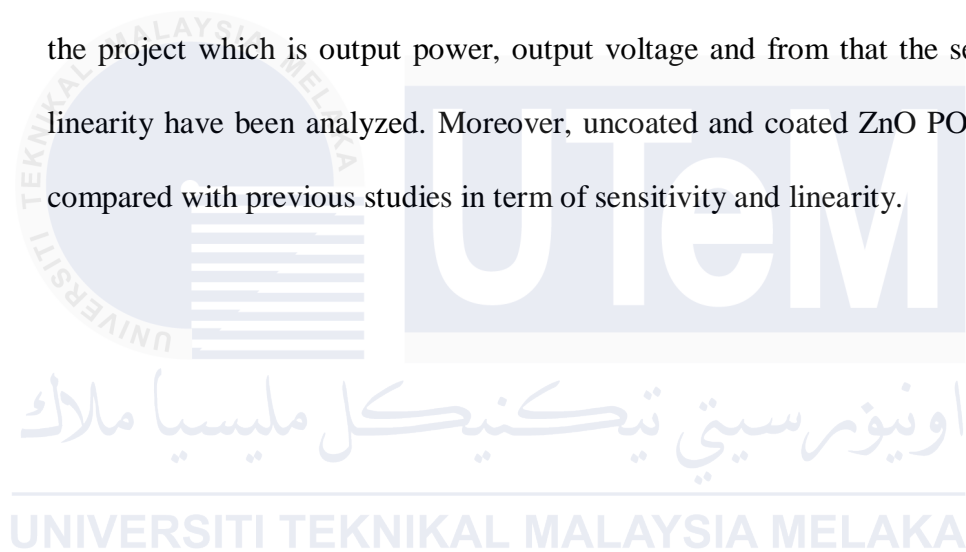
measurement result is shown in sensor type of Coated ZnO i.e. sensitivity 0.0419 V/pH and linearity 0.9887. However, these sensors may experience higher power losses due to the coating, which introduces additional scattering and absorption. The refractive index of the pH solution impacts the refractive index around the POF sensor, influencing power losses. These losses can lead to decreased output voltage and power. Despite the increased power losses, the coated ZnO POF sensors may still exhibit higher sensitivity compared to their uncoated counterparts. This higher sensitivity arises from the improved optical properties conferred by the coating, which enhances the sensor's ability to detect subtle changes in pH levels. Therefore, the overall performance of ZnO-coated POF sensors in pH measurement is a delicate balance between their improved sensitivity and the accompanying increase in power losses. This research has suitability with previous research about POF as pH sensor that increasing the pH range results cause higher sensitivity [29]. Another suitability of the research is the higher refractive index of the solution measured using a POF sensor causes the sensor output power decreases [33]. Measurement of the pH value based on POF as sensor is suitable for use with advantages such as have a simple measurement process and high sensitivity.

Table 4.10: Performance comparison of the Previous Developments for Detection of PH Levels in Water Samples.

Types of POF	Sensitivity, V/pH	Linearity, R^2
Coated Sol-Gel [27]	0.0103	0.9544
4 loops without Cladding [28]	0.0350	0.9354
Coated ZnO [This Work]	0.0419	0.9887
Uncoated ZnO	0.0384	0.9735

4.7 Summary of Chapter 4

This chapter assembles the project's findings and discussions. The characterization process is divided into two parts: Optical Characterization and Electrical Characterization. It involves acquiring data on samples containing varying proportions of water quality samples, as well as their respective refractive index values. The water quality was based on the concentration of ammonia and pH levels in water samples. Additionally, this chapter also discusses the data analysis that has been collected from the project which is output power, output voltage and from that the sensitivity and linearity have been analyzed. Moreover, uncoated and coated ZnO POF sensor also compared with previous studies in term of sensitivity and linearity.



CHAPTER 5

CONCLUSION AND FUTURE WORKS



This chapter concludes the overall project, including a discussion on the achievement of the objectives and the overall working of the project. At the end of this chapter, a future recommendation is given to further improve on this project.

5.1 CONCLUSION

In the last decade, FOEW POF sensors have experienced rapid development because of their unique characteristics of microstructure, long-distance transmission with low loss, corrosion resistance, distributed measurements, and lack of electromagnetic interference. FOEW POF sensors have been successfully used in the detection of a large number of water quality parameters including pH, temperature, turbidity, oxygen, RI, ions, organic and inorganic compounds, and microorganisms.

In this project, a simple and highly sensitive water quality monitoring sensor based on fibre-optic technology has been developed and experimentally verified with good results. Besides, this project contains two parts which are optical characterization and electrical characterization. For this project, all the two objectives of the project were achieved. For the first objective, zinc oxide coated and uncoated polymer optical fiber (POF) sensor capable of measuring multiple water quality parameters, including PH, and Ammonia were successfully designed and developed. The fabrication can be done by integrating Zinc Oxide (ZnO) coating using a hydrothermal approach was also achieved. The hydrothermal method is capable of growth the zinc oxide at the exposed area of the POF. The SEM analysis also shows the successful coating of zinc dioxide at the exposed area region. The EDX analysis also proves the presence of the ZnO element in the POF layer. The POF produces significant sensing performances toward the ammonia and pH liquid concentration level.

Next, for the second objective, the sensing response of the sensor towards the water quality in term of output power, output voltage and sensitivity were successfully analyzed and monitored using IoT Cloud via Nodemcu microcontroller. The water samples will generate output voltage which will be sensed by the POF sensor then will

be transmitted to the photodiode. The photodiode will convert current to voltage which will be displayed on the lcd display and IoT.

Coated ZnO POF and Uncoated POF sensor with the integration to the IoT technology have been successfully tested for the sensor's responses towards concentration of ammonia and pH value. The outputs show a linear response of output power and voltage to the changes in concentration of ammonia and pH values. It was concluded that as the concentration of ammonia and pH values increased, the lower the output power and output voltage of the fibre optic sensor. Upon completion, it was discovered that the Coated ZnO POF sensor is more sensitive to concentration of ammonia and pH changes in the ranges of 1-1.8 mg/L for ammonia and 5 to 9 for pH value. The Coated ZnO POF sensor has the sensitivity and linearity $0.0128 \text{ V/mgL}^{-1}$ and 0.9861 for ammonia measurement and 0.0419 V/pH and linearity 0.9987 for pH measurement.

The project sustainability and impact are divided into three categories which are economic, social, and environmental. First, it saves money by not requiring daily maintenance and has a longer lifespan than a traditional electronic sensor. As a result, maintenance costs will be drastically reduced. In terms of social safety, the optical fiber sensor is completely safe for any living creature because it does not consume a large amount of energy, which could be harmful. Finally, optical fiber is environmentally friendly because it produces no chemical or hazardous substances and consumes less energy than a traditional electronic sensor.

5.2 FUTURE WORK

For further investigation, the Coated ZnO POF sensor with a bending radius of 1.5 cm is tested using water samples gathered in the vicinity of Batu Pahat, Johor, Malaysia. The water samples are first tested using Ammonia High Range Portable Photometer (HI96733) purchased from Hanna Instrument and the concentration obtained are 1.5mg /L, 4.5 mg /L, 7.5 mg /L , 10.5 mg /L and 13.5 mg /L. As the reference, the ammonia concentration of DI water is also measured with the commercial photometer which gives the reading and record. The water samples are then tested using the proposed fiber optic sensor and the result comparable performance.

Other than that, expanding multiplexed detection capability of fiber optic sensor. It is well known that water quality is affected by many factors such as physics, chemistry, biology, hydraulics, and human activities, which means that water quality parameters are complicated, nonlinear, and vary over time because of their interactions. This means that interference may surround target detection parameters of water quality. In the first strategy, wavelength-division multiplexing technology is used to couple multiple detection principles in a sensing region to obtain water quality parameters, as shown in Figure 5.1. An alternative approach is to use an FG unit to perform multi-parameter detection. FOEW sensors based on an FG unit for the simultaneous detection of two or three parameters in water have been demonstrated. In the second strategy, different FOEW sensors are bundled together to quantitatively analyze multiple parameters of water quality. This strategy is feasible because optical fibers are small size and show good compatibility when integrated. Besides optical fiber bundles, optical fibers with multiple cores can also achieve the same outcome by

interaction of the EWs of different fiber cores. These results indicate that FOEW sensors have great potential for real-time multiparameter monitoring of water quality.

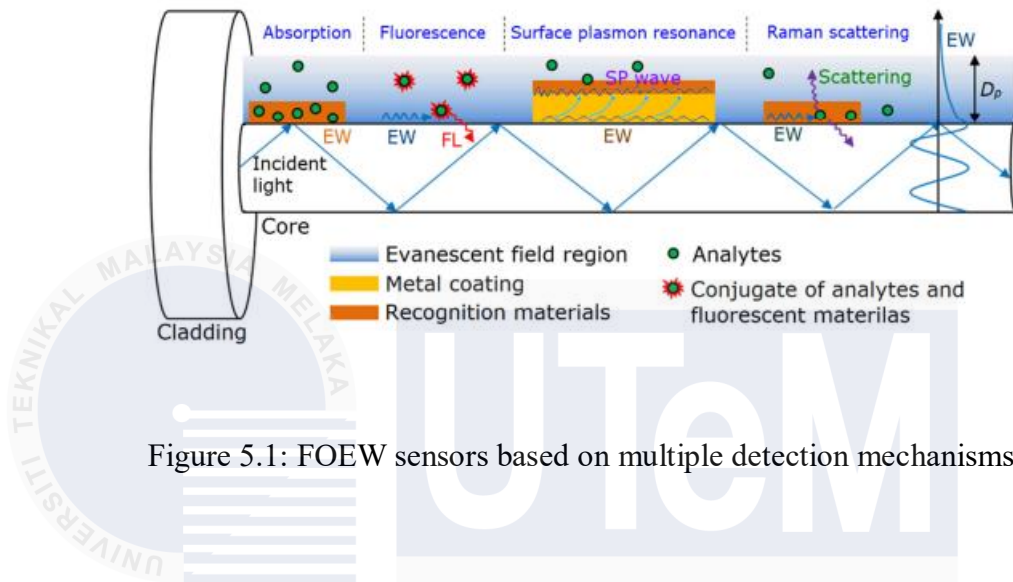


Figure 5.1: FOEW sensors based on multiple detection mechanisms.

REFERENCES

[1] Taru, Y.K.; Karwankar, A. Water monitoring system using arduino with labview. In Proceedings of the 2017 International Conference on Computing Methodologies and Communication (ICCMC), Erode, India, 18–19 July 2017; pp. 416–419.

[2] Rahman, H.A. Water Issues in Malaysia. *Int. J. Acad. Res. Bus. Soc. Sci.* 2021, 11, 860–875. *Journal of Environment*

[3] World Health Organization. Drinking Water; World Health Organization: Geneva, Switzerland, 2020; Available online: <https://www.who.int/news-room/fact-sheets/detail/drinking-water> (accessed on 18 July 2020).

[4] Leizi Jiao, Nianbing Zhong, Xiande Zhao. Recent advances in fiber-optic evanescent wave sensors for monitoring organic and inorganic pollutants in water. *TrAC Trends in Analytical Chemistry* Volume 127, June 2020, 115892.

[5] Zubel, M., Sobaszek, M., Koba, M., & Baran, M. (2017). Fiber-optic sensors in environmental monitoring. *Sensors*, 17(9), 2017.

[6] Homola, J., Yee, S. S., & Gauglitz, G. (2018). Surface plasmon resonance sensors: review. *Sensors and Actuators B: Chemical*, 54(1-2), 3-15.

[7] Yu, Y., Zhang, X., Shao, J., & Zhang, S. (2018). A multi-parameter fiber optic sensor for water quality monitoring. *Sensors and Actuators B: Chemical*, 255(2), 2225-2230.

[8] Weston, D. P. (2017). The ecological effects of pesticides on stream communities. US Geological Survey, Reston, Virginia, USA. [USGS Scientific Investigations Report 2006-5012]

[9] Gravina, M. A. S., & Ferreira, J. F. (2021). Cost-benefit analysis applied to water quality monitoring technology. In *International Conference on Industrial Engineering and Operations Management (IEOM)* (pp. 871-877).

[10] Ben-David, T., & Oron, G. (2021). Integrating real-time data into water quality monitoring and decision-making. *Environmental Modeling & Assessment*, 26(2), 205-218.

[11] Yasser Chiniforooshan, Jianjun Ma, Wojtek J. Bock (2018). Evanescent-Wave Fiber-Optic Sensor: On Power Transfer from Core-Cladding Interface to Fiber End-Face. *Journal of Lightwave Technology*.

[12] Zubia, J., & Arrue, J. (2001). Plastic optical fibers: An introduction to their technological processes and applications. *Optical fiber technology*, 7(2), 101- 140.

[13] M. López-López, J. C. Alonso-Álvarez, L. M. Mateos-Gil, L. M. Lechuga, and C. López-Higuera (2019). Characterization of a Fiber-Optic Evanescent Wave Absorbance Sensor for Nonpolar Organic Compounds. *IEEE Sensors Journal. Optics Express*

[14] M. López-López, J. C. Alonso-Álvarez, L. M. Mateos-Gil, L. M. Lechuga, and C. López-Higuera (2021). Fiber-optic sensor based on evanescent wave absorbance around 2.7 μm for determining water content in polar organic solvents.

[15] R. Fitzpatrick, 2018, 'Total Internal Reflection in Polymer Optical Fiber', University of Texas at Austin, accessed 14 March 2018.

[16] Sultanova, N.; Kasarova, S.; Nikolov, I. (October 2009). 'Dispersion Properties of Optical Polymers Fiber'. *Acta Physica Polonica A*. **116** (4): 585–587

[17] Siswanto, N. T. Rochman, and P. R. Akwalia (2017), "Fabrication and characterization of Zinc Oxide (ZnO) nanoparticle by sol-gel method," in *Journal of Physics: 57 Conference Series*, Institute of Physics Publishing, Jun. 2017. doi: 10.1088/1742-6596/853/1/012041

[18] A. G. Leal-Junior, C. Marques, A. Frizera, and M. J. Pontes (2018), "Dynamic Mechanical Analysis on a PolyMethyl Methacrylate (PMMA) Polymer Optical Fiber,"

IEEE Sens J, vol. 18, no. 6, pp. 2353–2361, Mar. 2018, doi: 10.1109/JSEN.2018.2797086.

[19] Osman, D. A. M., & Mustafa, M. A. (2017). Synthesis and characterization of zinc oxide nanoparticles using zinc acetate dihydrate and sodium hydroxide. J. Nanosci. Nanoeng, 1(4), 248-251.

[20] A. R. A. Rashid, N. A. F. Shamsuri, A. H. Surani, A. A. N. Hakim, and K. Ismail (2017), “Zinc oxide coated polymer optical fiber for measuring uric acid concentrations.”

[21] Verbič A, Gorjanc M, Simončič B(2019). Zinc Oxide for Functional Textile Coatings: Recent Advances. Coatings. 2019; 9(9):550. 70

[22] Hazli Rafis Abdul Rahim, Hazli Rafis Abdul Rahim, Siddharth Thokchom, Waleed S. Mohammed, Joydeep Dutta, Sulaiman Wadi Harun (2020). Chapter 11 - Optical fiber coated with zinc oxide nanorods toward light side coupling for sensing application, Editor(s).

[23] A. S. Prasanth, Sukadev Meher, Z. C. Alex (2022). Zinc Oxide Thin films coated Evanescent Wave based Fiber Optic sensor. Journal Article.

[24] Tavernier, Filip and Steyaert, Michiel (2011) *High-Speed Optical Receivers with Integrated Photodiode in Nanoscale CMOS*. Springer. Chapter 3 *From Light to Electric Current – The Photodiode*

[25] Kenza Azil, Kouider Ferria, Said Bouzid (2020). Cladless optical fiber sensor based on evanescent wave absorption for monitoring methylene blue induced water pollution. Journal of The Optical Society of America B-optical Physics.

[26] Mohamad Afi Abdul Hisam (2022). Tapered plastic optical fiber loop coated with ZnO nanorods using multiple channels for relative water quality sensing. Journal Article.

[27] Tiago B. Marinho, Victor G. M. Almeida, Waleska F. de Oliveira, Joao I. S. Miranda, Marcos E. R. da Silva, Auzuir R. de Alexandriak, Glendo de F. Guimaraes. (2021) "Development of evanescent field optical fiber sensor for pH measurement using sol-gel technology". Instituto Federal do Ceara - IFCE, Fortaleza, Brasil <https://orcid.org/0000-0002-1470-5859>.

[28] A Arifin, Hardianti, M Yunus and S Dewang. "Application of plastic optical fiber material as pH measurement sensor using loop configuration". IOP Conf. Series: Journal of Physics: Conf. Series 1317 (2020) 012047 IOP Publishing doi:10.1088/1742-6596/1317/1/012047.

[29] Gu B, Yin M, Zhang A P, Qian J and He S 2021 Biocompatible Fiber Optic pH Sensor Based on Modal interferometer Self Assembled with Sodium Alginate/Polythelimine Coating IEEE Sensors Journal 5 1-6

[30] A.S. Rajamani, D. M, V.V.R. Sai, "Plastic fiber optic sensor for continuous ammonia liquid monitoring using U-bent shape", Sens. Actuators A Phys. 296 (2022) 192–199, <https://doi.org/10.1016/j.sna.2022.07.021>.

[31] Nurfatihah Che Abd Rashid, Noran Azizan Cholan, Kim Gaik Tay, Azra Munirah Mat Daud, Nurul Atika Nabila Jaharudin, Nazrah Ilyana Sulaiman, Nor Hafizah Ngajikin. "Ammonia detection in water using balloon-like fiber optic sensor". Optik - International Journal for Light and Electron Optics 301 (2024) 171677

[32] Kim Gaik Tay¹, Azra Munirah Mat Daud, Nurul Atika Nabila Jaharudin, Nazrah Ilyana Sulaiman and Nor Hafizah Ngajikin. "Ammonia detection in water with balloon-like plastic optical fiber sensor". Eng. Res. Express 5 (2023) 025080 <https://doi.org/10.1088/2631-8695/acdfbb>.

[33] Rovati L, Fabbri P, Ferrari L and Pilati F 2021 Plastic Optical Fiber pH Sensor Using a Sol-Gel Sensing Matrix Fiber Optic Sensor 416-438.

APPENDICES



Dual/Quad Rail-to-Rail Output, Picoamp Input Precision Op Amps

FEATURES

- **Offset Voltage: 50 μ V Max (LT1884A)**
- **Input Bias Current: 400pA Max (LT1884A)**
- **Offset Voltage Drift: 0.8 μ V/ $^{\circ}$ C Max**
- **Rail-to-Rail Output Swing**
- Operates with Single or Split Supplies
- Open-Loop Voltage Gain: 1 Million Min
- 1mA Maximum Supply Current Per Amplifier
- Slew Rate: 1V/ μ s
- Standard Pinouts

APPLICATIONS

- Thermocouple Amplifiers
- Bridge Transducer Conditioners
- Instrumentation Amplifiers
- Battery-Powered Systems
- Photo Current Amplifiers
- Precision Integrators
- Precision Current Sources

DESCRIPTION

The LT[®]1884/LT1885 op amps bring high accuracy input performance to amplifiers with rail-to-rail output swing while providing faster response than other precision amplifiers. Input offset voltage is trimmed to less than 50 μ V and the low drift maintains this accuracy over the operating temperature range. Input bias currents are an ultralow 400pA maximum.

The amplifiers work on any total power supply voltage between 2.7V and 36V (fully specified from 5V to \pm 15V). Output voltage swings to within 40mV of the negative supply and 220mV of the positive supply make these amplifiers good choices for low voltage single supply operation.

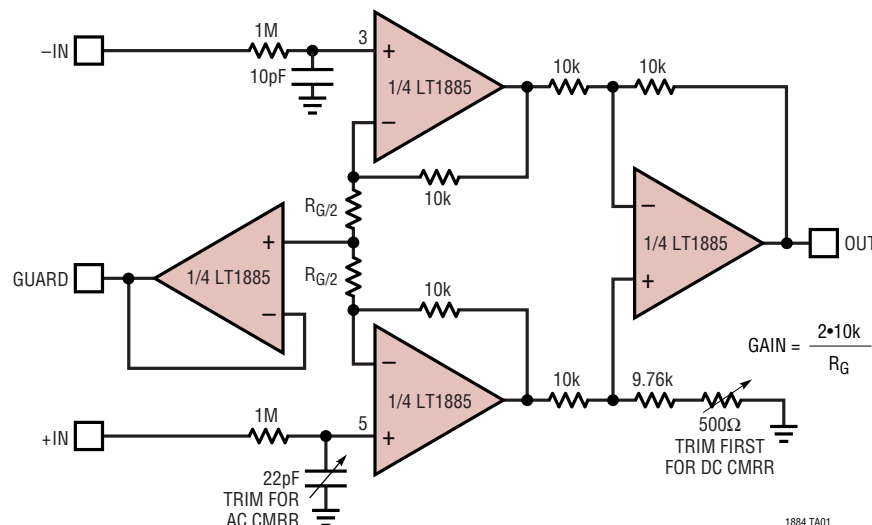
Slew rates of 1V/ μ s with a supply current of less than 1mA per amplifier give superior response and settling time performance in a low power precision amplifier.

The dual LT1884 is available with standard pinouts in 8-pin SO and PDIP packages. The quad LT1885 is also in the standard pinout 14-pin SO package.

LT, LTC and LT are registered trademarks of Linear Technology Corporation.

TYPICAL APPLICATION

Input Fault Protected Instrumentation Amplifier



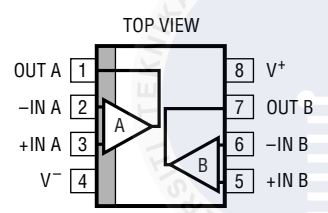
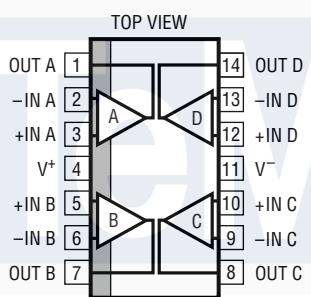
1884 TA01

LT1884/LT1885

ABSOLUTE MAXIMUM RATINGS (Note 1)

Supply Voltage (V^+ to V^-)	40V	Operating Temperature Range (Note 4) ..	-40°C to 85°C
Differential Input Voltage (Note 2)	$\pm 10\text{V}$	Specified Temperature Range (Note 5) ...	-40°C to 85°C
Input Voltage	V^+ to V^-	Maximum Junction Temperature	150°C
Input Current (Note 2)	$\pm 10\text{mA}$	Storage Temperature Range	-65°C to 150°C
Output Short-Circuit Duration (Note 3)	Indefinite	Lead Temperature (Soldering, 10 sec)	300°C

PACKAGE/ORDER INFORMATION

 <p>TOP VIEW</p> <p>N8 PACKAGE 8-LEAD PDIP</p> <p>S8 PACKAGE 8-LEAD PLASTIC SO</p> <p>$T_{JMAX} = 150^{\circ}\text{C}$, $\theta_{JA} = 130^{\circ}\text{C/W}$ (N8) $T_{JMAX} = 150^{\circ}\text{C}$, $\theta_{JA} = 190^{\circ}\text{C/W}$ (S8)</p>	ORDER PART NUMBER	 <p>TOP VIEW</p> <p>S PACKAGE 14-LEAD PLASTIC SO</p> <p>$T_{JMAX} = 150^{\circ}\text{C}$, $\theta_{JA} = 110^{\circ}\text{C/W}$</p>	ORDER PART NUMBER
	LT1884CN8 LT1884CS8 LT1884ACN8 LT1884ACS8 LT1884IN8 LT1884IS8 LT1884AIN8 LT1884AIS8		LT1885CS LT1885IS
	S8 PART MARKING		
	1884 1884I 1884A 1884AI		

Consult factory for Military grade parts.

ELECTRICAL CHARACTERISTICS

The ● denotes the specifications which apply over the full operating temperature range, otherwise specifications are at $T_A = 25^{\circ}\text{C}$.
 Single supply operation $V_{EE} = 0$, $V_{CC} = 5\text{V}$; $V_{CM} = V_{CC}/2$ unless otherwise noted. (Note 5)

SYMBOL	PARAMETER	CONDITIONS	MIN	TYP	MAX	UNITS
V_{OS}	Input Offset Voltage (LT1884A)	$0^{\circ}\text{C} < T_A < 70^{\circ}\text{C}$		25	50	μV
		$-40^{\circ}\text{C} < T_A < 85^{\circ}\text{C}$			85	μV
					110	μV
	Input Offset Voltage (LT1884/LT1885)	$0^{\circ}\text{C} < T_A < 70^{\circ}\text{C}$		30	80	μV
		$-40^{\circ}\text{C} < T_A < 85^{\circ}\text{C}$			125	μV
					150	μV
	Input Offset Voltage Drift (Note 6)	$0^{\circ}\text{C} < T_A < 70^{\circ}\text{C}$		0.3	0.8	$\mu\text{V}/^{\circ}\text{C}$
		$-40^{\circ}\text{C} < T_A < 85^{\circ}\text{C}$		0.3	0.8	$\mu\text{V}/^{\circ}\text{C}$
I_{OS}	Input Offset Current (LT1884A)	$0^{\circ}\text{C} < T_A < 70^{\circ}\text{C}$		100	300	pA
		$-40^{\circ}\text{C} < T_A < 85^{\circ}\text{C}$			400	pA
					500	pA
	Input Offset Current (LT1884/LT1885)	$0^{\circ}\text{C} < T_A < 70^{\circ}\text{C}$		150	900	pA
		$-40^{\circ}\text{C} < T_A < 85^{\circ}\text{C}$			1200	pA
					1400	pA

ELECTRICAL CHARACTERISTICS

The ● denotes the specifications which apply over the full operating temperature range, otherwise specifications are at $T_A = 25^\circ\text{C}$.
Single supply operation $V_{EE} = 0$, $V_{CC} = 5\text{V}$; $V_{CM} = V_{CC}/2$ unless otherwise noted. (Note 5)

SYMBOL	PARAMETER	CONDITIONS	MIN	TYP	MAX	UNITS
I_B	Input Bias Current (LT1884A)	$0^\circ\text{C} < T_A < 70^\circ\text{C}$	●	100	400	pA
		$-40^\circ\text{C} < T_A < 85^\circ\text{C}$	●		500	pA
					600	pA
	Input Bias Current (LT1884/LT1885)	$0^\circ\text{C} < T_A < 70^\circ\text{C}$	●	150	900	pA
		$-40^\circ\text{C} < T_A < 85^\circ\text{C}$	●		1200	pA
					1400	pA
	Input Noise Voltage	0.1Hz to 10Hz		0.4		μV_{P-P}
e_n	Input Noise Voltage Density	$f = 1\text{kHz}$		9.5		$\text{nV}/\sqrt{\text{Hz}}$
i_n	Input Noise Current Density	$f = 1\text{kHz}$		0.05		$\text{pA}/\sqrt{\text{Hz}}$
V_{CM}	Input Voltage Range		●	$V_{EE} + 1.0$	$V_{CC} - 1.0$	V
				$V_{EE} + 1.2$	$V_{CC} - 1.2$	V
CMRR	Common Mode Rejection Ratio	$1\text{V} < V_{CM} < 4\text{V}$	●	108	128	dB
		$1.2\text{V} < V_{CM} < 3.8\text{V}$	●	106		dB
PSRR	Power Supply Rejection Ratio	$V_{EE} = 0$, $V_{CM} = 1.5\text{V}$	●	108	132	dB
		$0^\circ\text{C} < T_A < 85^\circ\text{C}$, $2.7\text{V} < V_{CC} < 32\text{V}$	●	108	132	dB
		$T_A = -40^\circ\text{C}$, $3\text{V} < V_{CC} < 32\text{V}$	●			dB
	Minimum Operating Supply Voltage		●	2.4	2.7	V
A_{VOL}	Large-Signal Voltage Gain	$R_L = 10\text{k}$; $1\text{V} < V_{OUT} < 4\text{V}$	●	500	1600	V/mV
			●	350		V/mV
		$R_L = 2\text{k}$; $1\text{V} < V_{OUT} < 4\text{V}$	●	400	800	V/mV
			●	300		V/mV
V_{OL}	Output Voltage Swing Low	$R_L = 1\text{k}$; $1\text{V} < V_{OUT} < 4\text{V}$	●	300	400	V/mV
			●	200		V/mV
		No Load	●	20	40	mV
		$I_{SINK} = 100\mu\text{A}$	●	25	50	mV
V_{OH}	Output Voltage Swing High (Referred to V_{CC})	$I_{SINK} = 1\text{mA}$	●	70	150	mV
		$I_{SINK} = 5\text{mA}$	●	270	600	mV
		No Load	●	120	220	mV
		$I_{SOURCE} = 100\mu\text{A}$	●	130	230	mV
I_S	Supply Current per Amplifier	$I_{SOURCE} = 1\text{mA}$	●	180	300	mV
		$I_{SOURCE} = 5\text{mA}$	●	360	600	mV
		$V_{CC} = 3\text{V}$	●	0.45	0.65	0.85
						1.30
		$V_{CC} = 5\text{V}$	●	0.50	0.65	0.9
						1.4
		$V_{CC} = 12\text{V}$	●	0.50	0.70	1.0
I_{SC}	Short-Circuit Current				1.5	mA
		V_{OUT} Short to GND	●	15	30	mA
GBW	Gain-Bandwidth Product	V_{OUT} Short to V_{CC}	●	15	30	mA
GBW	Gain-Bandwidth Product	$f = 20\text{kHz}$		1.2	2	MHz
t_S	Settling Time	0.01%, $V_{OUT} = 1.5\text{V}$ to 3.5V , $A_V = -1$, $R_L = 2\text{k}$		10		μs
SR^+	Positive Slew Rate	$A_V = -1$	●	0.45	0.9	V/ μs
			●	0.36		V/ μs
SR^-	Negative Slew Rate	$A_V = -1$	●	0.35	0.7	V/ μs
			●	0.25		V/ μs

ELECTRICAL CHARACTERISTICS

The ● denotes the specifications which apply over the full operating temperature range, otherwise specifications are at $T_A = 25^\circ\text{C}$.
Single supply operation $V_{EE} = 0$, $V_{CC} = 5\text{V}$; $V_{CM} = V_{CC}/2$ unless otherwise noted. (Note 5)

SYMBOL	PARAMETER	CONDITIONS	MIN	TYP	MAX	UNITS
ΔV_{OS}	Offset Voltage Match (LT1884A)	$0^\circ\text{C} < T_A < 70^\circ\text{C}$		30	70	μV
		$-40^\circ\text{C} < T_A < 85^\circ\text{C}$			125	μV
					160	μV
	Offset Voltage Match (LT1884/LT1885)	(Note 7)		35	125	μV
		$0^\circ\text{C} < T_A < 70^\circ\text{C}$			195	μV
		$-40^\circ\text{C} < T_A < 85^\circ\text{C}$			235	μV
	Offset Voltage Match Drift	(Notes 6, 7)		0.4	1.2	$\mu\text{V}/^\circ\text{C}$
ΔI_{B+}	Noninverting Bias Current Match (LT1884A)	$0^\circ\text{C} < T_A < 70^\circ\text{C}$		200	600	pA
		$-40^\circ\text{C} < T_A < 85^\circ\text{C}$			700	pA
					850	pA
	Noninverting Bias Current Match (LT1884/LT1885)	(Notes 7, 9)		250	1200	pA
		$0^\circ\text{C} < T_A < 70^\circ\text{C}$			1600	pA
		$-40^\circ\text{C} < T_A < 85^\circ\text{C}$			1900	pA
ΔCMRR	Common Mode Rejection Match	(Notes 7, 9)	104	125		dB
ΔPSRR	Positive Power Supply Rejection Match (Notes 7, 9)	$V_{EE} = 0$, $V_{CM} = 1.5\text{V}$				
		$0^\circ\text{C} < T_A < 85^\circ\text{C}$, $2.7\text{V} < V_{CC} < 32\text{V}$	104	126		dB
		$T_A = -40^\circ\text{C}$, $3\text{V} < V_{CC} < 32\text{V}$	104	126		dB

The ● denotes the specifications which apply over the full operating temperature range, otherwise specifications are at $T_A = 25^\circ\text{C}$.
Split supply operation $V_S = \pm 15\text{V}$; $V_{CM} = 0\text{V}$ unless otherwise noted. (Note 5)

SYMBOL	PARAMETER	CONDITIONS	MIN	TYP	MAX	UNITS
V_{OS}	Input Offset Voltage (LT1884A)	$0^\circ\text{C} < T_A < 70^\circ\text{C}$		25	50	μV
		$-40^\circ\text{C} < T_A < 85^\circ\text{C}$			85	μV
					110	μV
	Input Offset Voltage (LT1884/LT1885)	$0^\circ\text{C} < T_A < 70^\circ\text{C}$		30	80	μV
		$-40^\circ\text{C} < T_A < 85^\circ\text{C}$			125	μV
					150	μV
	Input Offset Voltage Drift (Note 6)	$0^\circ\text{C} < T_A < 70^\circ\text{C}$		0.3	0.8	$\mu\text{V}/^\circ\text{C}$
		$-40^\circ\text{C} < T_A < 85^\circ\text{C}$		0.3	0.8	$\mu\text{V}/^\circ\text{C}$
I_{OS}	Input Offset Current (LT1884A)	$0^\circ\text{C} < T_A < 70^\circ\text{C}$		150	300	pA
		$-40^\circ\text{C} < T_A < 85^\circ\text{C}$			400	pA
					500	pA
	Input Offset Current (LT1884/LT1885)	$0^\circ\text{C} < T_A < 70^\circ\text{C}$		150	900	pA
		$-40^\circ\text{C} < T_A < 85^\circ\text{C}$			1200	pA
					1400	pA
I_B	Input Bias Current (LT1884A)	$0^\circ\text{C} < T_A < 70^\circ\text{C}$		150	400	pA
		$-40^\circ\text{C} < T_A < 85^\circ\text{C}$			500	pA
					600	pA
	Input Bias Current (LT1884/LT1885)	$0^\circ\text{C} < T_A < 70^\circ\text{C}$		150	900	pA
		$-40^\circ\text{C} < T_A < 85^\circ\text{C}$			1200	pA
					1400	pA
	Input Noise Voltage	0.1Hz to 10Hz		0.4		μV_{P-P}
e_n	Input Noise Voltage Density	$f = 1\text{kHz}$		9.5		$\text{nV}/\sqrt{\text{Hz}}$
i_n	Input Noise Current Density	$f = 1\text{kHz}$		0.05		$\text{pA}/\sqrt{\text{Hz}}$
V_{CM}	Input Voltage Range		$V_{EE} + 1.0$		$V_{CC} - 1.0$	V
			$V_{EE} + 1.2$		$V_{CC} - 1.2$	V
CMRR	Common Mode Rejection Ratio	$-13.5\text{V} < V_{CM} < 13.5\text{V}$	114	130		dB

ELECTRICAL CHARACTERISTICS

The ● denotes the specifications which apply over the full operating temperature range, otherwise specifications are at $T_A = 25^\circ\text{C}$. Split supply operation $V_S = \pm 15\text{V}$; $V_{CM} = 0\text{V}$ unless otherwise noted. (Note 5)

SYMBOL	PARAMETER	CONDITIONS		MIN	TYP	MAX	UNITS
+PSRR	Positive Power Supply Rejection Ratio	$V_{EE} = -15\text{V}$, $V_{CM} = 0\text{V}$; $1.5\text{V} < V_{CC} < 18\text{V}$	●	114	132		dB
–PSRR	Negative Power Supply Rejection Ratio	$V_{CC} = 15\text{V}$, $V_{CM} = 0\text{V}$; $-1.5\text{V} < V_{EE} < -18\text{V}$	●	106	132		dB
	Minimum Operating Supply Voltage		●		± 1.2	± 1.35	V
A_{VOL}	Large-Signal Voltage Gain	$R_L = 10\text{k}\Omega$; $-13.5\text{V} < V_{OUT} < 13.5\text{V}$	●	1000	1600		V/mV
			●	700			V/mV
		$R_L = 2\text{k}\Omega$; $-13.5\text{V} < V_{OUT} < 13.5\text{V}$	●	250	420		V/mV
			●	175			V/mV
		$R_L = 1\text{k}\Omega$; $-12\text{V} < V_{OUT} < 12\text{V}$	●	100	230		V/mV
			●	75			V/mV
V_{OL}	Output Voltage Swing Low (Referred to V_{EE})	No Load	●		20	40	mV
		$I_{SINK} = 100\mu\text{A}$	●		25	50	mV
		$I_{SINK} = 1\text{mA}$	●		70	150	mV
		$I_{SINK} = 5\text{mA}$	●		270	600	mV
V_{OH}	Output Voltage Swing High (Referred to V_{CC})	No Load	●		160	220	mV
		$I_{SOURCE} = 100\mu\text{A}$	●		160	230	mV
		$I_{SOURCE} = 1\text{mA}$	●		180	300	mV
		$I_{SOURCE} = 5\text{mA}$	●		360	600	mV
I_S	Supply Current Per Amplifier	$V_S = \pm 15\text{V}$	●		0.85	1.1 1.6	mA mA
I_{SC}	Short-Circuit Current	V_{OUT} Short to V_{EE}	●	15	50		mA
		V_{OUT} Short to V_{CC}	●	15	30		mA
GBW	Gain-Bandwidth Product	$f = 20\text{kHz}$		1.5	2.2		MHz
t_S	Settling Time	0.01%, $V_{OUT} = -5\text{V}$ to 5V , $A_V = -1$, $R_L = 2\text{k}\Omega$			17		μs
SR^+	Positive Slew Rate	$A_V = -1$	●	0.5 0.4	1.0		V/ μs V/ μs
SR^-	Negative Slew Rate	$A_V = -1$	●	0.40 0.26	0.7		V/ μs V/ μs
ΔV_{OS}	Offset Voltage Match (LT1884A)	(Note 7)			35	70	μV
		$0^\circ\text{C} < T_A < 70^\circ\text{C}$	●			125	μV
		$-40^\circ\text{C} < T_A < 85^\circ\text{C}$	●			160	μV
	Offset Voltage Match (LT1884/LT1885)	(Note 7)			35	125	μV
		$0^\circ\text{C} < T_A < 70^\circ\text{C}$	●			175	μV
		$-40^\circ\text{C} < T_A < 85^\circ\text{C}$	●			235	μV
	Offset Voltage Match Drift	(Note 6, 7)	●		0.4	1.1	$\mu\text{V}/^\circ\text{C}$
ΔI_B^+	Noninverting Bias Current Match (LT1884A)	(Notes 7, 8)			200	600	pA
		$0^\circ\text{C} < T_A < 70^\circ\text{C}$	●			700	pA
		$-40^\circ\text{C} < T_A < 85^\circ\text{C}$	●			850	pA
	Noninverting Bias Current Match (LT1884/LT1885)	(Notes 7, 8)			240	1200	pA
		$0^\circ\text{C} < T_A < 70^\circ\text{C}$	●			1600	pA
		$-40^\circ\text{C} < T_A < 85^\circ\text{C}$	●			1900	pA
ΔCMRR	Common Mode Rejection Match	(Notes 7, 9)	●	106	125		dB
$\Delta +\text{PSRR}$	Positive Power Supply Rejection Match	$V_{EE} = -15\text{V}$, $V_{CM} = 0\text{V}$, $1.5\text{V} < V_{CC} < 18\text{V}$, (Notes 7, 9)	●	108	124		dB
$\Delta -\text{PSRR}$	Negative Power Supply Rejection Match	$V_{CC} = 15\text{V}$, $V_{CM} = 0\text{V}$, $-1.5\text{V} < V_{EE} < -18\text{V}$, (Notes 7, 9)	●	102	132		dB

ELECTRICAL CHARACTERISTICS

Note 1: Absolute Maximum Ratings are those values beyond which the life of the device may be impaired.

Note 2: The inputs are protected by back-to-back diodes. If the differential input voltage exceeds 0.7V, the input current should be limited to less than 10mA.

Note 3: A heat sink may be required to keep the junction temperature below absolute maximum.

Note 4: The LT1884C/LT1885C and LT1884I/LT1885I are guaranteed functional over the operating temperature range of -40°C to 85°C .

Note 5: The LT1884C/LT1885C are designed, characterized and expected to meet specified performance from -40°C to 85°C but are not tested or QA sampled at these temperatures. LT1884I is guaranteed to meet specified performance from -40°C to 85°C .

Note 6: This parameter is not 100% tested.

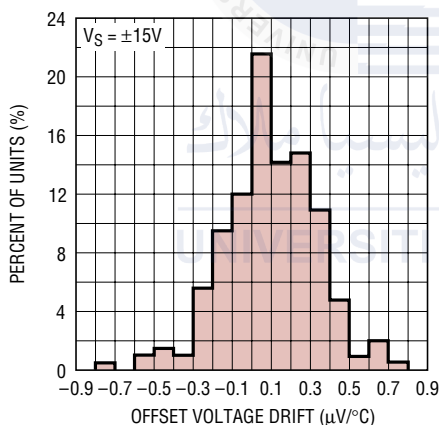
Note 7: Matching parameters are the difference between amplifiers A and B in the LT1884 and between amplifiers A and D and B and C in the LT1885.

Note 8: This parameter is the difference between the two noninverting input bias currents.

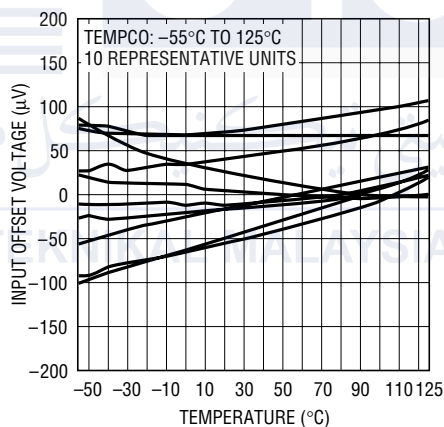
Note 9: ΔCMRR and ΔPSRR are defined as follows: CMRR and PSRR are measured in $\mu\text{V/V}$ on each amplifier. The difference is calculated in $\mu\text{V/V}$ and then converted to dB.

TYPICAL PERFORMANCE CHARACTERISTICS

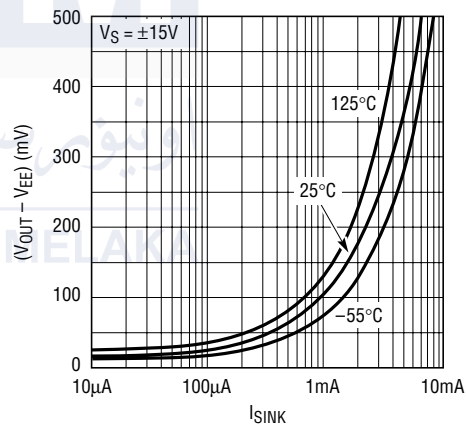
Distribution of Offset Voltage Drift



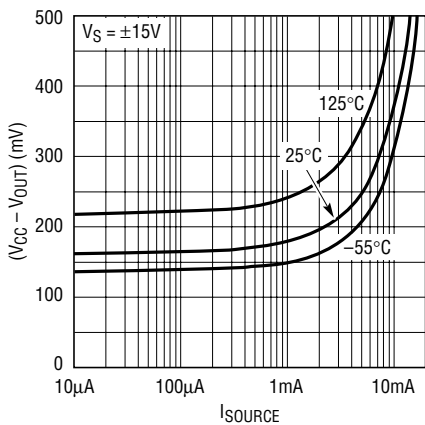
Input Offset Voltage vs Temperature



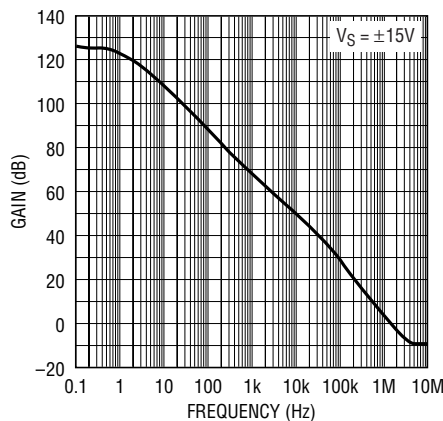
V_{OUT} vs I_{SINK}



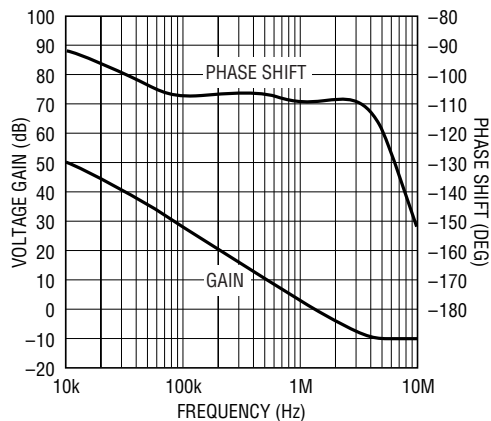
V_{OUT} vs I_{SOURCE}



Gain vs Frequency

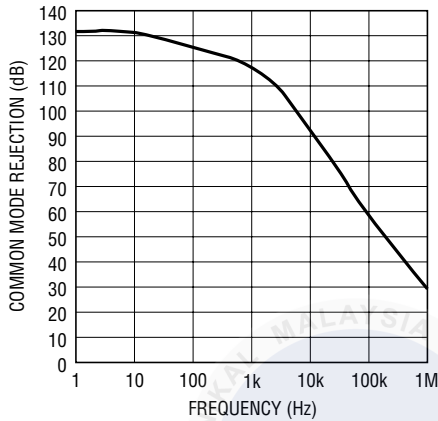


Gain, Phase Shift vs Frequency

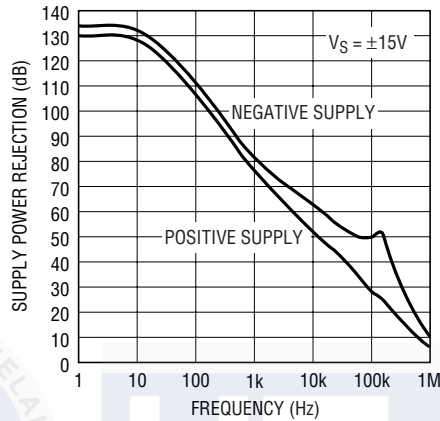


TYPICAL PERFORMANCE CHARACTERISTICS

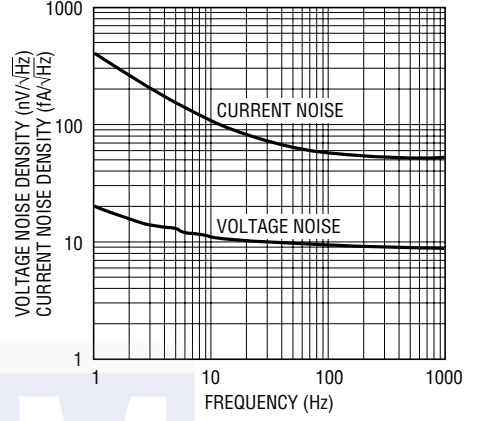
CMRR vs Frequency



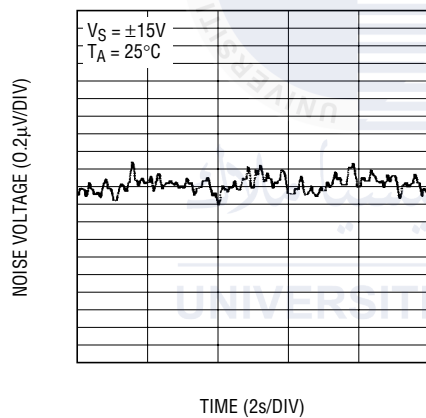
PSRR vs Frequency



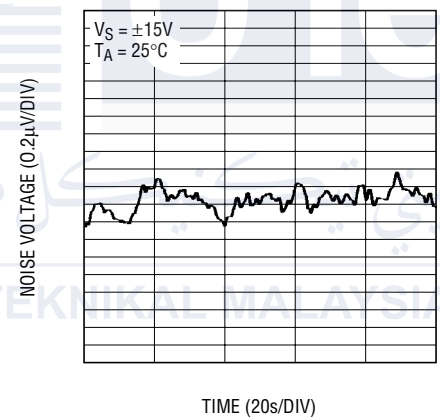
V_n, I_n vs Frequency



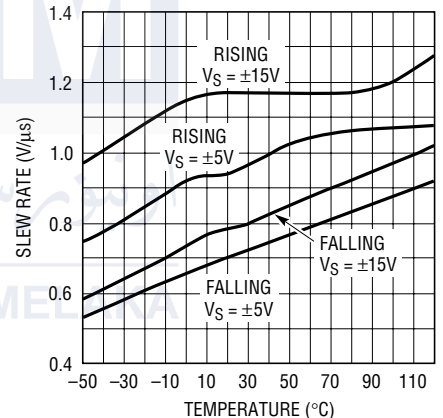
0.1Hz to 10Hz Noise



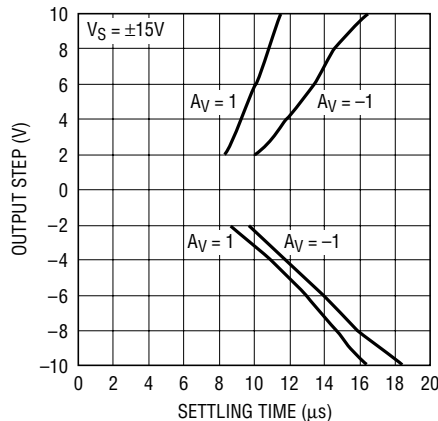
0.01Hz to 1Hz Noise



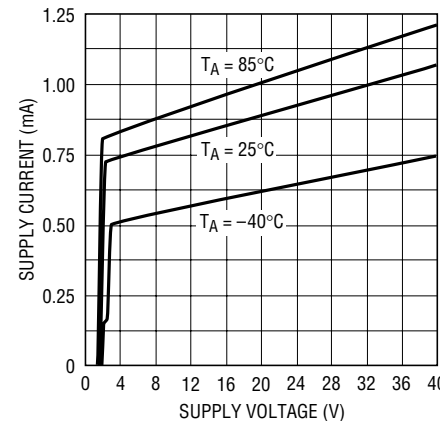
Slew Rate vs Temperature



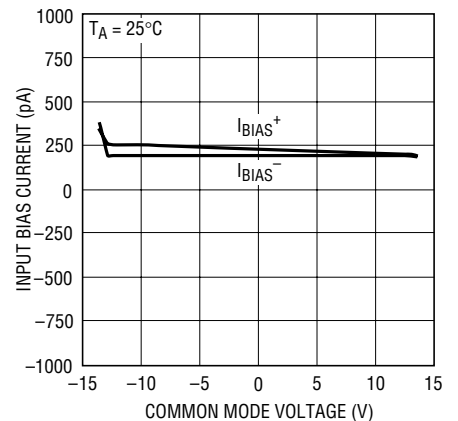
Settling Time to 0.01% vs Output Step



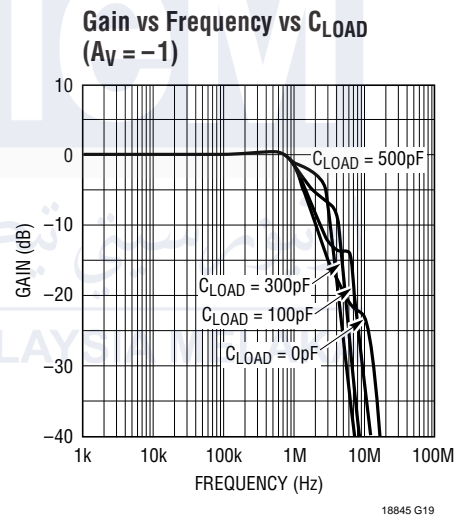
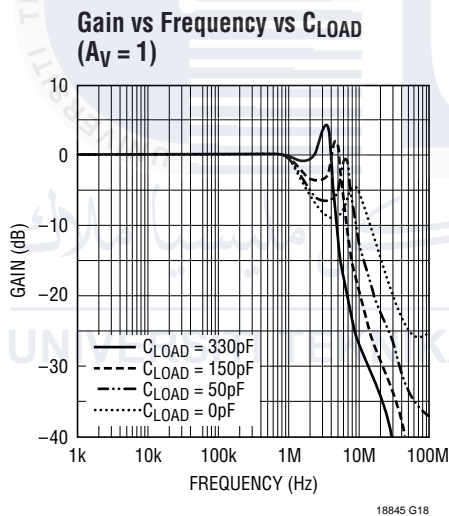
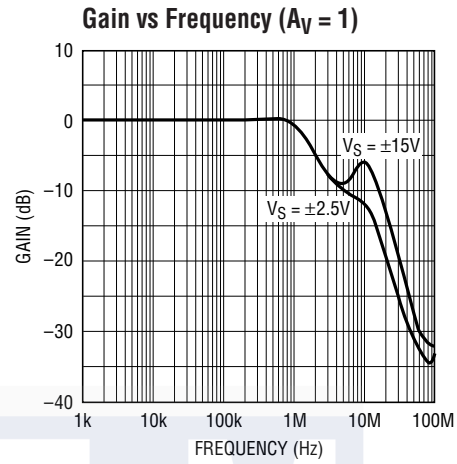
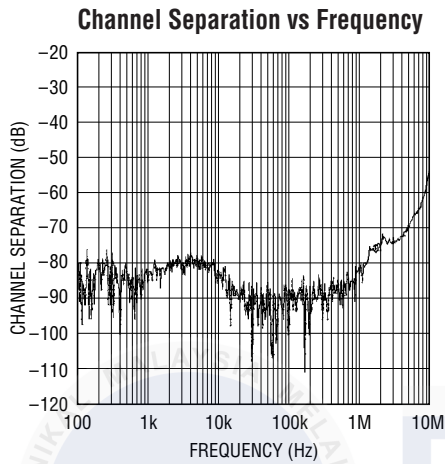
Supply Current per Amplifier vs Supply Voltage



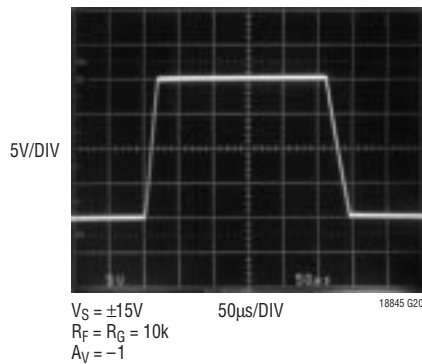
Input Bias Current vs Common Mode Voltage



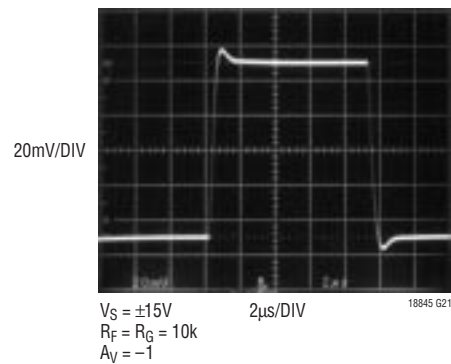
TYPICAL PERFORMANCE CHARACTERISTICS



Large-Signal Response



Small-Signal Response



APPLICATIONS INFORMATION

The LT1884/LT1885 dual op amp features exceptional input precision with rail-to-rail output swing. Slew rate and small-signal bandwidth are superior to other amplifiers with comparable input precision. These characteristics make the LT1884/LT1885 a convenient choice for precision low voltage systems and for improved AC performance in higher voltage precision systems. Maintaining the advantage of the precision inherent in the amplifier depends upon proper applications circuit design and board layout.

Preserving Input Precision

Preserving the input voltage accuracy of the LT1884/LT1885 requires that the applications circuit and PC board layout do not introduce errors comparable to or greater than the 30 μ V offset. Temperature differentials across the input connections can generate thermocouple voltages of 10s of microvolts. PC board layouts should keep connections to the amplifier's input pins close together and away from heat dissipating components. Air currents across the board can also generate temperature differentials.

The extremely low input bias currents, 100pA, allow high accuracy to be maintained with high impedance sources and feedback networks. The LT1884/LT1885's low input bias currents are obtained by using a cancellation circuit on-chip. This causes the resulting I_{BIAS}^+ and I_{BIAS}^- to be uncorrelated, as implied by the I_{OS} specification being comparable to the I_{BIAS} . The user should not try to balance the input resistances in each input lead, as is commonly recommended with most amplifiers. The impedance at either input should be kept as small as possible to minimize total circuit error.

PC board layout is important to ensure that leakage currents do not corrupt the low I_{BIAS} of the amplifier. In high precision, high impedance circuits, the input pins should be surrounded by a guard ring of PC board

interconnect, with the guard driven to the same common mode voltage as the amplifier inputs.

Input Common Mode Range

The LT1884/LT1885 output is able to swing close to each power supply rail, but the input stage is limited to operating between $V_{EE} + 0.8V$ and $V_{CC} - 0.9V$. Exceeding this common mode range will cause the gain to drop to zero; however, no gain reversal will occur.

Input Protection

The inverting and noninverting input pins of the LT1884/LT1885 have limited on-chip protection. ESD protection is provided to prevent damage during handling. The input transistors have voltage clamping and limiting resistors to protect against input differentials up to 10V. Short transients above this level will also be tolerated. If the input pins may be subject to a sustained differential voltage above 10V, external limiting resistors should be used to prevent damage to the amplifier. A 1k resistor in each input lead will provide protection against a 30V differential voltage.

Capacitive Loads

The LT1884/LT1885 can drive capacitive loads up to 300pF when configured for unity gain. The capacitive load driving capability increases as the amplifier is used in higher gain configurations. Capacitive load driving may also be increased by decoupling the capacitance from the output with a small resistance.

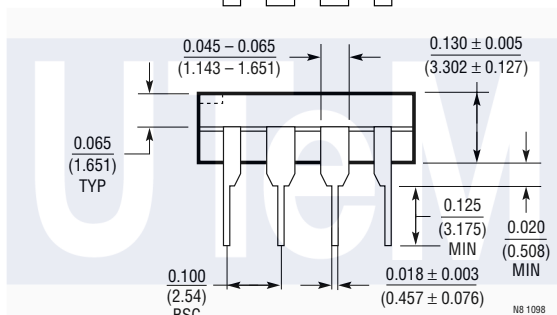
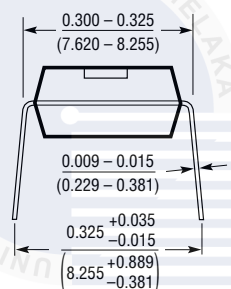
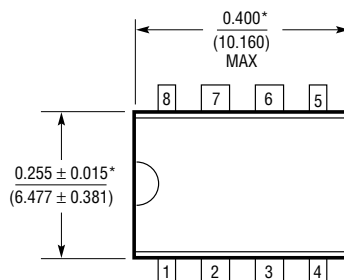
Input Bias Currents

While it may be tempting to seek out a JFET amplifier for low input bias current, remember that bipolar devices improve with temperature while JFETs degrade.

PACKAGE DESCRIPTION

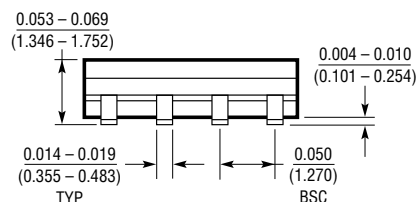
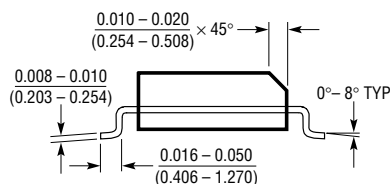
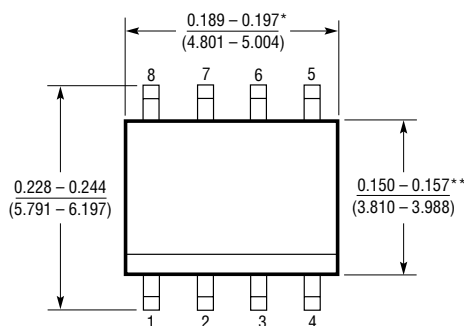
Dimensions in inches (millimeters) unless otherwise noted.

N8 Package 8-Lead PDIP (Narrow 0.300) (LTC DWG # 05-08-1510)



*THESE DIMENSIONS DO NOT INCLUDE MOLD FLASH OR PROTRUSIONS.
MOLD FLASH OR PROTRUSIONS SHALL NOT EXCEED 0.010 INCH (0.254mm)

S8 Package 8-Lead Plastic Small Outline (Narrow 0.150) (LTC DWG # 05-08-1610)



* DIMENSION DOES NOT INCLUDE MOLD FLASH. MOLD FLASH SHALL NOT EXCEED 0.006" (0.152mm) PER SIDE

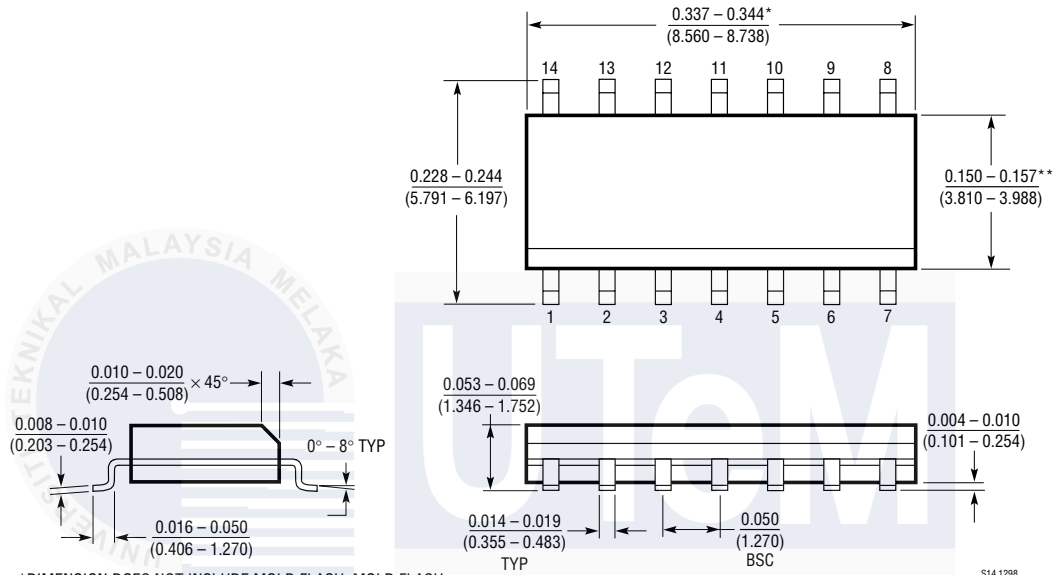
** DIMENSION DOES NOT INCLUDE INTERLEAD FLASH. INTERLEAD FLASH SHALL NOT EXCEED 0.010" (0.254mm) PER SIDE

S08 1298

PACKAGE DESCRIPTION

Dimensions in inches (millimeters) unless otherwise noted.

S Package
14-Lead Plastic Small Outline (Narrow 0.150)
 (LTC DWG # 05-08-1610)

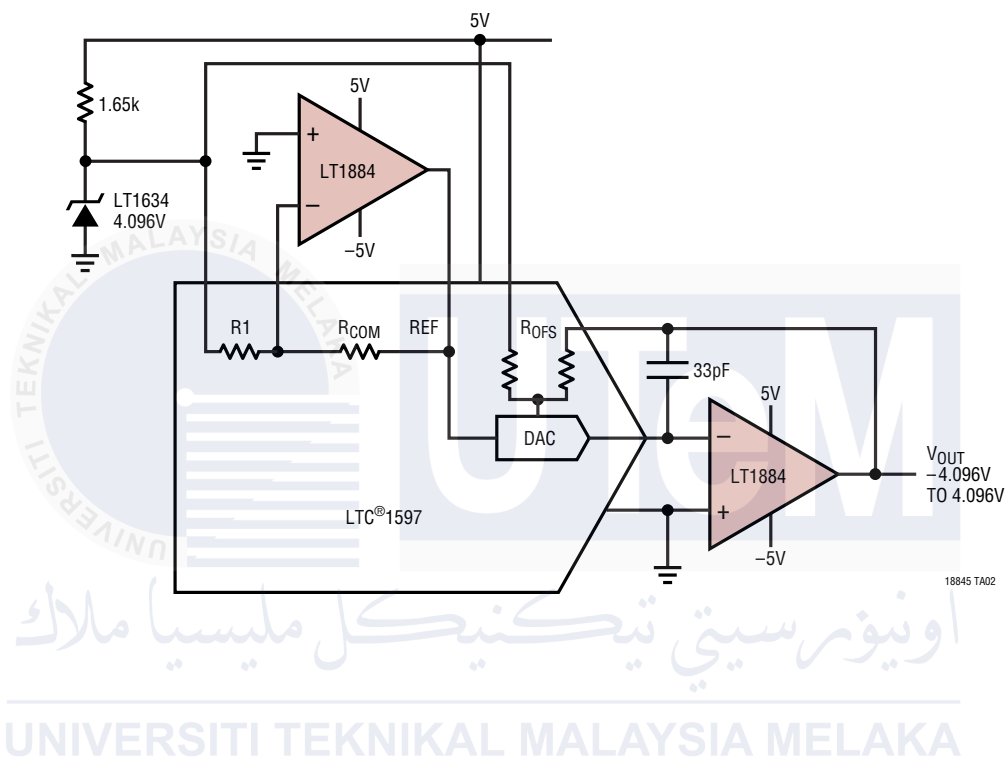


S14 1298

UNIVERSITI TEKNIKAL MALAYSIA MELAKA

TYPICAL APPLICATION

16-Bit Voltage Output DAC on ±5V Supply



RELATED PARTS

PART NUMBER	DESCRIPTION	COMMENTS
LT1112	Dual Picoamp Input Op Amp	$V_{OS} = 60\mu V$ Max
LT1114	Quad Picoamp Input Op Amp	$V_{OS} = 60\mu V$ Max
LT1167	Gain Programmable Instrumentation Amp	Gain Error = 0.08% Max
LT1490	Micropower Rail-to-Rail Input and Output Op Amp	Over-The-Top™ Common Mode Range
LT1793	Low Noise JFET Op Amp	$I_B = 10pA$ Max
LT1881/LT1882	Picoamp Input Rail-to-Rail Output Op Amp	Lower Input Bias Currents Than LT1884/LT1885
LTC2050	Zero Drift Op Amp in SOT-23	$V_{OS} = 3\mu V$ Max, Rail-to-Rail Output

Over-The-Top is a trademark of Linear Technology Corporation.